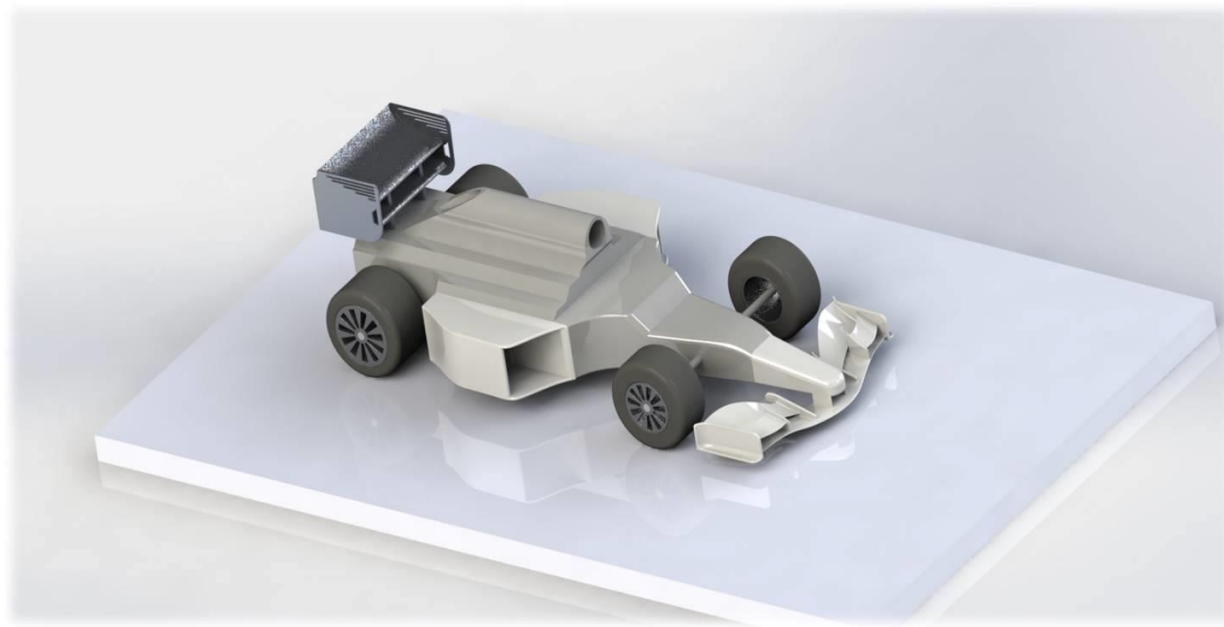


MecE 468

Final Project

Design of a Formula 1 Race Car for Aerodynamic Performance, Structural Integrity, and Heat Transfer Using Numerical Simulation



Team 5	
Name	Project
Erik Hartikainen	P1
Alexander Lin	P2
Anthony Tang	P3
Mellissa Gomez	P4
Daniel Guenter	P5
Toya Okeke	P6

December 8, 2017

Executive Summary

On November 21, 2017 Nobes Inc. requested F1VE Engineering Ltd. to complete a design of a Formula 1 race car using numerical simulation. The task was broken down into six projects including aerodynamic, structural, and heat transfer simulation analysis for different components of the car. F1VE determined design objectives for each project and designed the race car using numerical simulation tools in SOLIDWORKS for submission to Nobes Inc. on December 8, 2017. Basic models were created to gain an understanding of what the various aerodynamic, structural, and heat transfer results produce under simplified conditions. An iterative design process was then carried out to optimize the design of components to meet the objectives pertaining to their functions.

The first project involved aerodynamic design of the front wing with the primary goals of managing airflow to the rest of the car and achieving a downforce 3.5 times the weight of the final design. After validating the initial base simulation with analytical estimates and convergence analysis, three iterations of design led to a final downforce of 2307 N. Since the final weight of the wing was 400 N, the downforce goal was accomplished. Additionally, geometry was optimized to control turbulent vortices around the front wheels to effectively direct air to the rest of the car. While the design goals were accomplished, further analysis should be completed regarding the effect of ground and determining stall angles of the airfoils used for the wing. These tasks are computationally expensive to run in SOLIDWORKS under the provided time constraints to adequately capture the effect of boundary layers. Next, the second project included structural design of the front wing. The structural team worked closely with the aerodynamic team in the initial phase of design. The structural goals for the front wing were to minimize weight and maximize safety factor. Through an iterative design study, the final mass of the front wing was 23.3 kg with a factor of safety of 8.5. Further consideration is needed for the directionality of the carbon fiber material since it was assumed to have bulk material properties in this analysis. Additionally, further consultation with the aerodynamics team would be required to determine how a changing pressure field would affect, and be affected by deflection. To continue, the rear wing also involved aerodynamic and structural projects. For aerodynamics of the rear wing, the goals were to maximize downforce and minimize drag. To design the rear wing, a 4-digit NACA Airfoil profile was optimized by analyzing the lift-drag tradeoff during 2-dimensional flow simulations as various parameters were changed. The resultant profile was subsequently subjected to simulations at different angles of attack and speeds. An angle of attack of 20 degrees was selected, and the lift-drag relationship was shown to change negligibly at different speeds. A 3D model was put together using two identical airfoil profiles previously determined, and subjected to further flow simulations, whose results were used to test for yielding by the structural team. Further improvements were studied, namely the relative orientations of the airfoils, and additional features/changes to the end plates, which minimize and direct the vortices. Structural analysis was conducted on the rear wing by implementing the forces obtained by the aerodynamic team to run finite element analysis simulations. Similar to the structure goals of the front wing, the design was optimized to reduce the mass of the rear wing and ensure it would not yield in operation. The final rear wing design had a mass of 62 kg and a factor of safety of 27.8. The aerodynamics and heat transfer of the side pod goals included designing a heat exchanger that could effectively dissipate the heat from the engine. This meant determining realistic engine parameters that would simulate real life and then designing a side pod that would dissipate the heat as well as reduce the overall drag on the side pod. The maximum final temperatures of the radiator and exit air (at max engine power and speed) were determined to be 719.5 K and 385.2 K, respectively. The overall drag at these temperatures on each side pod was found to be 143.4 N. After each component was completed, a simulation of the whole car was done. The drag to lift ratio for the whole vehicle had local maxima at 150 and 250 km/h. The drag and lift at these speeds were 4 and 400 N, and 6.5 and 1300 N respectively.

Furthermore, the project demonstrated the interactions that would take place among engineers in a design team environment and demonstrated the level of dependence that the results of one team's work could have with others. This is primarily shown in the interaction between the aerodynamic and structural teams, and in the interaction of all teams with the full model simulation team. The limited time interval to complete the project also stressed the importance of recognizing the key aspects required to achieve the goal and leave some auxiliary aspects to be completed for future improvements.

Table of Contents

Executive Summary	i
List of Figures.....	iv
List of Tables	v
1 Aerodynamics of the Front Wing	1
1.1 Introduction	1
1.2 Initial Design Iteration.....	2
1.3 Second Design Iteration	3
1.4 Final Design Iteration	4
1.5 Conclusions & Recommendations.....	5
2 Structural Design of the Front Wing	6
2.1 Introduction	6
2.2 Initial Design Iteration.....	7
2.3 Second Design Iteration	8
2.4 Final Design Iteration	9
2.5 Conclusions & Recommendations.....	10
3 Aerodynamics of the Rear Wing	12
3.1 Introduction	12
3.2 Initial Design Iteration.....	13
3.3 Second Design Iteration	14
3.4 Final Design Iteration	15
3.5 Conclusions & Recommendations.....	16
4 Structural Design of the Rear Wing.....	17
4.1 Introduction	18
4.2 Initial Design Iteration.....	19
4.3 Second Design Iteration	20
4.4 Final Design Iteration	21
4.5 Conclusions & Recommendations.....	22
5 Aerodynamics and Heat Transfer in the Side Pod	23
5.1 Introduction	24
5.2 Initial Design Iteration.....	25
5.3 Second Design Iteration	26
5.4 Final Design Iteration	26
5.5 Conclusions & Recommendations.....	28
6 Aerodynamics of the Whole Car	29
6.1 Introduction	30
6.2 Initial Design Iteration.....	31
6.3 Second Design Iteration	32

6.4	Third Design Iteration	33
6.5	Final Design Iteration	34
6.6	Conclusions & Recommendations.....	35
7	References	36
8	Appendices.....	37
8.1	Appendix A: Aerodynamics of the Front Wing.....	39
8.1.1	Simple Airfoil.....	39
8.1.2	2D Convergence Analysis for Simple Airfoil	39
8.1.3	Analytical Calculation of Lift for Model Validation	40
8.1.4	NACA 0009 Design Plots	41
8.1.5	3D Convergence Analysis for Design Iteration 1.....	41
8.1.6	NACA 6406 Deflector Plate Design Plots	42
8.1.7	Final Design.....	43
8.2	Appendix B: Structural of the Front Wing	45
8.2.1	Initial Design Iteration	45
8.2.2	Second Design Iteration.....	49
8.2.3	Final Design Iteration.....	52
8.3	Appendix C: Aerodynamics of the Rear Wing	54
8.3.1	Initial Design Iteration	54
8.3.2	Second Design Iteration.....	57
8.3.3	Final Design Iteration.....	59
8.4	Appendix D: Structural Analysis of the Rear Wing	61
8.4.1	Initial Design Iteration	61
8.4.2	Second Design Iteration.....	63
8.4.3	Third Design Iteration	65
8.5	Appendix E: Aerodynamics and Heat Transfer of the Side Pod	68
8.5.1	Initial Design Iteration	68
8.5.2	Second Design Iteration.....	76
8.5.3	Final Design Iteration.....	78
8.6	Appendix F: Aerodynamics of the Whole Car	81
8.6.1	Initial Design Iteration	81
8.6.2	Second Design Iteration.....	86
8.6.3	Third Design Iteration	91
8.6.4	Final Design Iteration	96
8.7	Appendix G: Engineering Drawings	103

List of Figures

Figure 1 Two plots of (a) surface pressure and flow trajectory and (b) force on the front wing for a range of vehicle speeds in the initial design iteration.	2
Figure 2 A labelled flow trajectory plot for design iteration 2 indicating direction of flow around tires.	3
Figure 3 Two plots of (a) lift and drag characteristics for vehicle speeds of 0 to 300 km/h and (b) a velocity cut plot located on a plane tangent to the back face of the tire.	4
Figure 4 A plot of changes to lift and drag characteristics over consecutive design iterations at 300 km/h.	4
Figure 5 A rendered image of the final aerodynamic front wing design with key functional features labelled.	5
Figure 6 FBD and demonstration of the cross-sectional area of the airfoil. Modelled as a cantilever with a uniform pressure field. Note from cross-sectional view that the centroid is not located in the center of the beam. a) FBD, b) Cross-Sectional Area.....	7
Figure 7 Mesh dependency of cantilevered airfoil simulation. Stress does not converge due to sharp edge. Note that while the displacement appears to diverge due to the deviation between values, in terms of its magnitude, it deviates by less than 1 %.....	7
Figure 8 a) The stress concentration caused by a concentrated point load. This can be safely ignored as the true pressure field is not concentrated into a single point as it is in this simulation. b) Detail of the yield regions experienced when using aluminum 6061 alloy	8
Figure 9 Depiction of final configuration of the half model of the front wing	9
Figure 10 Design study of front wing degree of hollowness. This plot demonstrates the easy choice of a 2 mm shell in order to maximize FOS and minimize mass.....	9
Figure 11 a) Stress distribution over the front wing based on the two point loads. Note significantly higher stresses in the support struts than elsewhere in the model. b) Displacement distribution of the front wing from two point loads	10
Figure 12 Render of final configuration of the front wing with nose cone attached	10
Figure 13 Velocity cut plots for first design iteration at angles of attack of 20 and 40 degrees	13
Figure 14 Design plots for lift/drag versus. angle of attack and speed for first design iteration	13
Figure 15: Airfoil configuration and resultant 3D model for second design iteration	14
Figure 16 Velocity cut plot for second design iteration at a speed of 300 km/h.....	14
Figure 17 Airfoil configurations for optimization of final design iteration and final 3Dmodel.....	15
Figure 18 (a) Loading conditions of the simulation of a 15° inclined, flat plate subjected to 300 km/h air that is acting as a point load, and (b) the associated stress distribution plot	19
Figure 19 Graph comparing maximum von Mises stress and maximum deflection between different simulation styles for increasing angles of attack at an air velocity of 300 km/h.....	19
Figure 20 Stress distribution plot for the (a) initial design and (b) the optimized design of the rear wing.....	20
Figure 21 Isometric views of (a) airfoils of the rear wing, and (b) final design of the rear wing in order to display the design changes made from iteration 2 to iteration 3.....	21
Figure 22 Graph of car speed versus required radiator heat dissipation	25
Figure 23 Model of first iteration side pod with boundary conditions.....	26
Figure 24 Graph of speed versus maximum radiator temperature.....	26
Figure 25 Graph of the drag force and max radiator temperature for each iteration	27
Figure 26 Final rendering of the right side pod model	27
Figure 27 Mesh used for the wedge. 30 047 total/fluid cells were used with 3618 fluid cells contacting wedge.....	31
Figure 28 Drag and lift for half the wedge as velocity increases	31
Figure 29 Mesh of the vehicle used for the second iteration. 49021 total/fluid cells were used with 5129 cells contacting the vehicle	32
Figure 30 drag and lift of the vehicle as its speed increases.	32
Figure 31 Mesh of the vehicle used for the third iteration. 29612 total/fluid cells were used with 5764 contacting the vehicle	33
Figure 32 Drag and lift of the vehicle on the road as its speed increases	33
Figure 33 Mesh of the vehicle used for the final design. 59644 total cells and 44349 fluid cells were used with 15295 fluid cells contacting the vehicle.....	34
Figure 34 Drag and lift of the vehicle on the road as its speed increases	34

List of Tables

Table 1 A comparison of lift and drag coefficients regarding the effect of ground.....	2
Table 2 Comparison of structurally modified design to the completed second aerodynamic design iteration.....	3
Table 3 Summary of values tested to approximate the pressure field obtained from the aerodynamic team as two discrete point loads	8
Table 4 Summary of parameter values as a result of the design studies	9
Table 5 Summary of lift to drag ratios for different airfoil configurations	15
Table 6 Summary of design study parameters and values optimized, where coloured values are the values chosen as a result of the optimization.....	20
Table 7 Comparison of important parameters for different designs of the rear wing	21

1 Aerodynamics of the Front Wing



Completed by Erik Hartikainen

1.1 Introduction

The front wing of the formula 1 race car was designed for aerodynamic performance by considering two major functions of the component. First, the management of airflow around the front tires is crucial to prevent turbulent vortices from disturbing airflow under the car. Second, large downforce is required to ensure the car remains on the ground when cornering at high speeds. Considering these key functions, design of the front wing was carried out with goals of directing airflow around the tires and achieving a downforce of at least 3.5 times the final weight of the component. This was selected as a minimum criterion for downforce because a modern Formula 1 car can develop 3.5 times its weight in downforce [1]. Therefore, it was assumed the front wing should have this capability at a minimum. To complete this project, three aerodynamic design iterations were completed using modelling and simulation tools in SOLIDWORKS. First, a basic airfoil was analyzed for its performance characteristics as a baseline of comparison to further design work. Then, design commenced with each iteration addressing specific targets related to downforce and flow control while also consulting the structural team to ensure aerodynamic features had structural integrity. These three design iterations are presented in this section for aerodynamic design of the front wing.

Some key assumptions regarding the trade-off between lift and drag and general flow parameters were made for initializing the study. These include:

- Flow velocity is in one direction only. There is no wind or out of plane flow to consider.
- Standard air conditions of 1 atm, 20°C ambient temperature, and air density of 1.204 kg/m³ apply [2].
- Airflow management around the front tires is more crucial than maximizing downforce because uncontrolled turbulent vortices can deteriorate performance of other car components.
- Flow speed of 300 km/h with laminar and turbulent effects on the body was initialized in the simulation to represent the high-end speed limit of the vehicle for standard racing conditions.
- Increasing downforce has more value than minimizing drag. While the lift-drag trade off was considered, downforce and flow control were prioritized as primary functions; especially for tracks with many turns.

Considering these assumptions, mesh convergence analysis and validation was completed as seen in Appendix A to begin design of the front wing for the mentioned objectives.

1.2 Initial Design Iteration

The main purpose of the initial design iteration was to maximize downforce, and examine the recirculation of flow around the front wing. To establish an initial design, simple NACA airfoils were considered as a basis for comparison of lift and drag characteristics. Through a comparison of airfoils discussed in Appendix A, a NACA 0009 airfoil was selected as a base component for its high lift-drag ratio and a NACA 6406 airfoil was selected for the deflector plate. This airfoil was found to achieve high downforce due to its cambered profile. Convergence analyses and validation for the 2D domain of airfoils and 3D domain of design iteration 1 were completed and are presented in Appendix A.

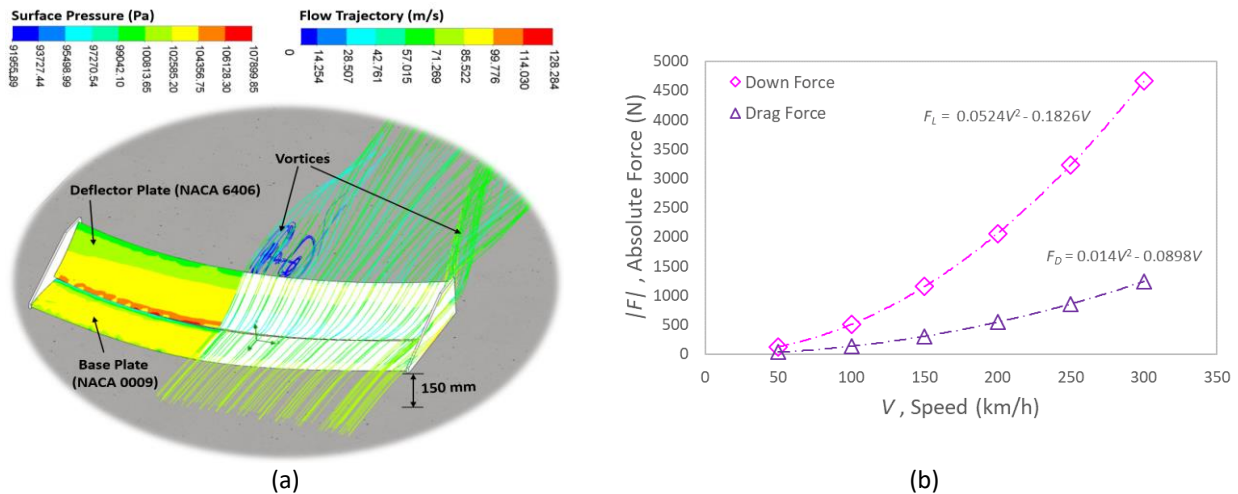


Figure 1 Two plots of (a) surface pressure and flow trajectory and (b) force on the front wing for a range of vehicle speeds in the initial design iteration.

Shown in Figure 1 are design plots for the first design iteration of the front wing. In Figure 1(a), the front wing is illustrated with the NACA airfoil profiles discussed previously at a vertical distance of 150 mm from the ground. The surface plot of pressure distribution on the left half of the wing indicates higher pressure on the top of the wing and lower pressure on the bottom which creates the required downforce. Additionally, the flow trajectory plot on the right half of the wing indicates strong vortices created by the side plates and the effect of the ground. The forces on the front wing are illustrated in Figure 1(b) for different speeds of the race car. Both the down force and drag increase quadratically with speed. This result agrees with the theoretical prediction since the lift and drag forces are proportional to the square of velocity as seen in Equation A3 of Appendix A. As well, the results shown in this plot are desirable because greater downforce is required for higher speeds so that the car can travel faster around turns on the track. Overall, the initial design increased down force to 4665 N over the 2714 N provided by the basic airfoil used as a base case in Appendix A.

Table 1 A comparison of lift and drag coefficients regarding the effect of ground.

Parameter	Neglecting Ground Effect	Considering Ground Effect	Deviation
Lift Coefficient	-2.03	-0.563	72%
Drag Coefficient	0.300	0.297	1%

From Table 1, the effect of running simulation with the ground included had minimal effect on drag; however, a substantial impact on the lift coefficient was observed. These results suggest the ground significantly reduces downforce on the front wing. It was unexpected the ground would significantly reduce. A reason for the large discrepancy is that flow simulation fails to handle boundary layer flow on the bottom surface of the wing. For this reason, the remaining design iterations considered comparison of downforce neglecting the effect of ground, but considering the flow trajectories and vortices induced by the ground. Future design should focus on establishing simulation studies which capture ground effect with greater confidence

1.3 Second Design Iteration

In the initial design iteration, the downforce was maximized with comparison to the case of the simple airfoil. From review of the results of design iteration 1, it was apparent that the wake of air recirculation induced by the front wing needed to be addressed to ensure vortices of turbulent air were directed around the tires and prevented from disturbing airflow under the car. After receiving modifications from the structural team to strengthen the front wing and account for regulation sizes as per the 2018 F1 technical regulations, the second design iteration commenced with the primary goal of directing air circulation and a secondary goal of increasing downforce due to the changes.

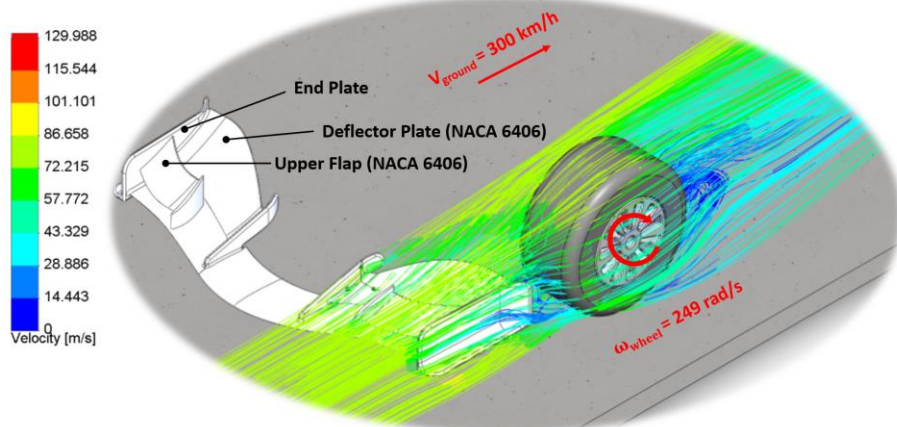


Figure 2 A labelled flow trajectory plot for design iteration 2 indicating direction of flow around tires.

Illustrated in Figure 2 is the revised aerodynamic design which includes key changes of optimized endplates and the addition of upper flaps. The simulation was initialized with the same 3D computational domain and mesh control that was applied to the initial design iteration. If given more time, convergence analysis would be completed for every design iteration; however, the initial 3D convergence analysis and mesh conditions were decided to be adequate due to relatively minor changes to geometry. Additionally, boundary conditions were established to capture the flow adequately. The ground plate shown was initialized with a linear velocity of 300 km/h and the wheel given an angular velocity of 249 rad/s. These conditions allowed a reasonable flow trajectory because they represent actual conditions of the vehicle travelling at 300 km/h. Considering design features, end plates were modelled to direct flow around the outside of the tires and upper flaps were implemented to increase flow over the tires and generate more downforce. These flaps were designed based on NACA 6406 airfoil profiles like the deflector plate and implemented because more downforce needed to be generated since the structural team removed the middle portion of the deflector plate to strengthen the wing and account for nose cone assembly. Therefore, upper flaps increase the surface area for more down force. In addition, the flow trajectory plot indicates how this design iteration accomplished the goal of directing the vortex at the end plates around the tire. Overall, flow induced by the front wing was directed in a controlled manner to avoid disturbing air downstream.

Table 2 Comparison of structurally modified design to the completed second aerodynamic design iteration.

Parameter	Structural Team Modified Design	Completed Design Iteration 2	% Change
Drag Force (N)	640	685	+7.03%
Lift Force (N)	-1997	-2132	+6.76%

The structural team made modifications to the initial design to account for weight and strength goals. This design was aerodynamically optimized to yield the result shown in Figure 2. As seen in Table 2 above, the down force was increased by 6.76%. This was accomplished while also controlling flow vortices around the tires at the expense of a minor 7.03% increase in drag. Thus, the second goal for design iteration 2 of improving downforce was accomplished.

1.4 Final Design Iteration

A final design iteration was completed to account for the addition of the nose cone. The purpose of this phase of design was to implement a nose cone which maintained flow and down force characteristics achieved in previous iterations.

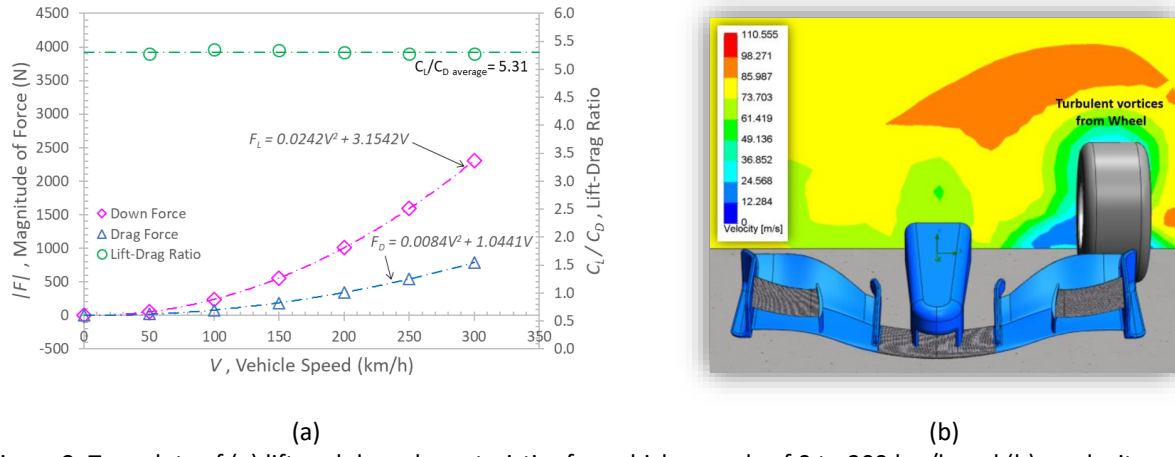


Figure 3 Two plots of (a) lift and drag characteristics for vehicle speeds of 0 to 300 km/h and (b) a velocity cut plot located on a plane tangent to the back face of the tire.

Shown in Figure 3 are design plots for the final design of the front wing. The lift and drag plots in (a) agree with theoretical predictions that force is proportional to the square of velocity as presented by Çengel (2014) [2]. The average lift-drag ratio over the range of vehicle speeds was found to be 5.31. While lift was primarily investigated in this design study, the final design also provided a reasonable trade-off between lift and drag. Additionally, the velocity cut plot in (b) indicates how flow vortices downstream are largely a result of the turbulent wake caused by the tire as seen from the annotated region. Thus, the wake of air circulation from the front wing was managed to avoid disturbing flow downstream.

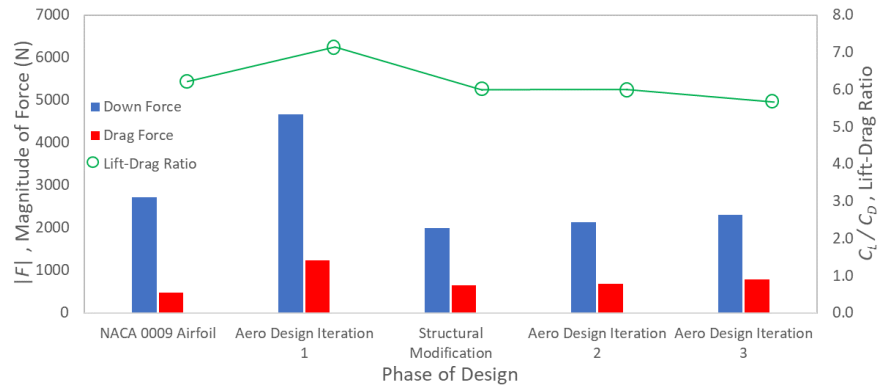


Figure 4 A plot of changes to lift and drag characteristics over consecutive design iterations at 300 km/h.

In Figure 4 the lift and drag characteristics are illustrated for each design iteration for a vehicle speed of 300 km/h. The large decrease in down force between aerodynamic design iteration 1 and the structural team's modification was due to the addition of struts and separating the deflector into two parts to account for the nose cone as per 2018 F1 regulations. Remaining iterations focused on airflow management with moderate increases to downforce. Additionally, the ratio of lift to drag remained relatively consistent throughout the process for a range of 5.31 - 7.25. The final weight of the front wing with the nose cone attached was 400 N with the carbon fiber composite selected by the structural team. Thus, since the final down force achieved of 2307 N is greater than 3.5 times the weight of the wing, the design goal for down force was achieved.

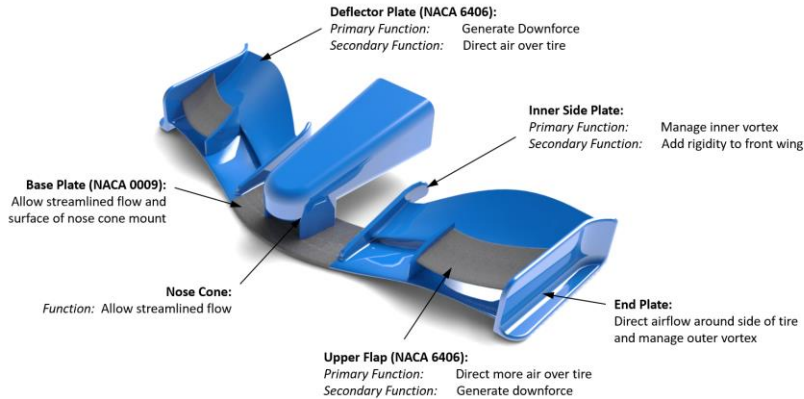


Figure 5 A rendered image of the final aerodynamic front wing design with key functional features labelled.

Illustrated in Figure 5 is a rendered image of the final aerodynamic design with key functional features identified. For managing airflow around the tires, key features are the end plates, inner side plates, upper flaps, and deflector plates. These were designed to direct vortices around tires and prevent disruption of flow under the car. Additionally, the largest contributors to down force are the deflector plates and upper flaps. Together, these features accomplished the design goals of managing airflow and achieving greater than 3.5 times the weight of the wing.

1.5 Conclusions & Recommendations

The front wing for the formula 1 race car was designed for aerodynamics considering a main goal of managing airflow around the front tires and a second goal of achieving downforce at least three times larger than the final weight of the wing. These objectives were accomplished through three design iterations and collaboration with the structural team. Prior to beginning analysis, basic airfoil profiles were examined from existing NACA tables [3] to determine desirable characteristics for the wing design. A NACA 0009 profile was considered for its symmetric profile to establish a basis from which to compare design results. Next, the initial design was developed which consisted of a NACA 0009 baseplate and a NACA 6406 deflector plate. The objective for the first design iteration was to select a deflector plate which maximized downforce to hand off a worst-case loading scenario to the structural team. The NACA 6406 profile was selected because its camber allowed for high downforce of 4665 N. Next, the second design iteration focused on managing airflow around the tires. This was accomplished by modelling endplates, inner side plates, and upper flaps as seen in Figure 5 which all contributed to directing air around the tires and avoiding disturbance of downstream air. Finally, the last design iteration included the nose cone assembly. The objective was to maintain the down force and airflow from the previous iteration while including new geometry. By modelling a streamlined nose cone to create pressure on the top face, additional down force was achieved. The final down force of 2307 N was produced and considering the final weight of the wing was 400 N, the goal of having a downforce at least 3.5 times larger than the weight of the wing was achieved.

While the objectives of this project were accomplished, there are areas which require further study to ensure adequate results. Through a simulation including the effect of ground it was found that down force significantly reduced to 1295 N from 4665 N in the first design iteration. It was unexpected that the ground would reduce downforce so substantially. Further analysis should consider how to best simulate the effect of boundary layers under the wing to obtain reasonable results. This was neglected in this study due to time constraints. In addition, simulations for the NACA airfoils at different angles of attack were completed to obtain design plots for the two airfoils examined. Further analysis is required to determine the stall point of the airfoils since the boundary layer separation that occurs at higher angles of attack was neglected in simulation. Anderson (2016) [4] attributes the parabolic nature of drag coefficient to this boundary layer separation due to induced pressure drag. This effect was inadequately captured in the simulations carried out.

2 Structural Design of the Front Wing



Completed by: Alexander Lin

2.1 Introduction

The purpose of this section of the project is to optimize the front wing structurally in terms of minimum weight and maximum factor of safety. In the first iteration, the methodology of analysis was verified through the comparison of a simulation model with an analytical solution. Once the model was validated, a 3D model and associated pressure field was obtained from the aerodynamic team. After an initial simulation, it was noticed that a significant amount of air was shown to have been directed into the end plate causing yielding at the end plate and the base airfoil. Modifications were performed in order to accommodate space for the front nose and to stiffen the wing by dividing the deflection plate into two sections and adding additional plates in the center. This modified model was given to the aerodynamics team who adjusted the angle of the end plates to avoid similar complications as what occurred in the initial model. After approximating the pressure field as two discrete point loads, a series of design studies was performed in order to optimize the front wing in terms of minimum mass and high factor of safety. The final iteration involved adding the front nose, and ensuring that the change in the point of attachment induced no complications in terms of stress concentrations in the front wing.

2.2 Initial Design Iteration

The purpose of this iteration is to determine a valid means of analysis. Analysis began with modelling the front wing as a uniform airfoil with an angle of attack of 15 degrees above the horizontal. Half of the total length was modelled in order to take advantage of symmetry in the airfoil. A calculation of the negative lift force was performed using an assumed maximum Formula One car speed of 413 km/h based on the maximum achieved speed achieved by the Formula One Bar Honda [5]. This calculation can be found in Appendix B. The airfoil is constrained symmetrically in order to reduce computational load. As shown in Figure 6, the half section was assumed to be supported in a cantilever-like fashion and a uniform pressure field was applied in order to simulate the worst case. Aluminum 6061 Alloy was selected as the initial test material. Modelling the airfoil as a cantilever allows for calculations to be performed based on known beam deflection properties as shown in Appendix B, which resulted in a calculated value of 6.6 mm.

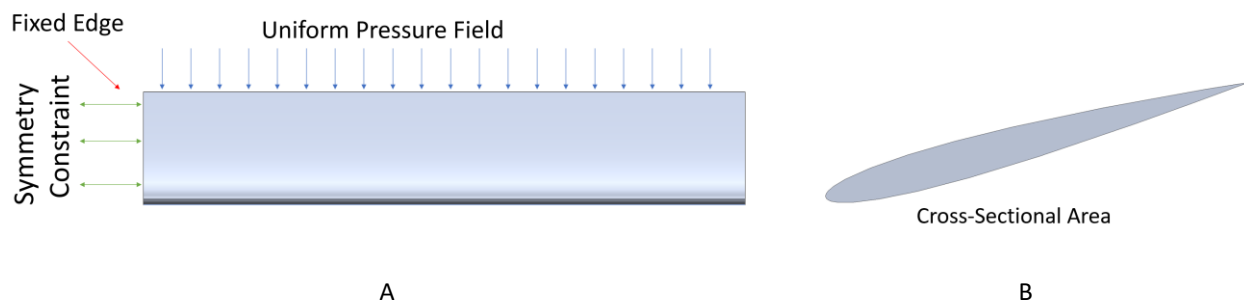


Figure 6 FBD and demonstration of the cross-sectional area of the airfoil. Modelled as a cantilever with a uniform pressure field. Note from cross-sectional view that the centroid is not located in the center of the beam. a) FBD, b) Cross-Sectional Area

The stress and displacement distributions can be found in Appendix B. A mesh convergence analysis was also performed in order to confirm the initial findings of the simulation as shown in Figure 7. The displacement converged fairly quickly however, the max stress diverges. This was determined to have been caused by a sharp edge in the model which distorts the stress distribution results.

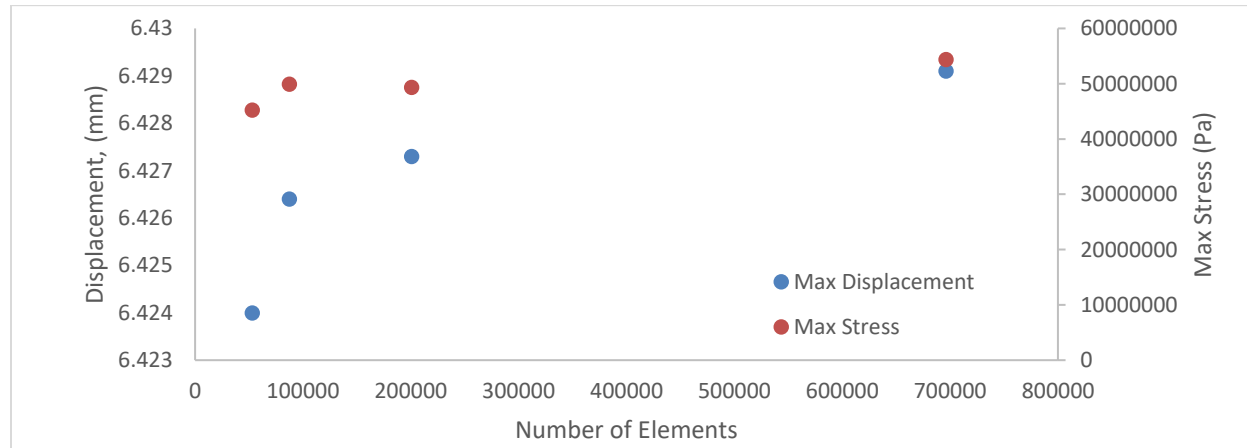


Figure 7 Mesh dependency of cantilevered airfoil simulation. Stress does not converge due to sharp edge. Note that while the displacement appears to diverge due to the deviation between values, in terms of its magnitude, it deviates by less than 1 %.

A value of 6.43 mm was determined by the simulation. The simulation and analytical solutions deviate by 2.8 % which was taken to be within acceptable limits. Thus, the simulation model was considered to be sufficiently validated by the analytical solution.

2.3 Second Design Iteration

The initial model obtained from the aerodynamic team was first analyzed with the simulated air field. However, the initial model was shown to have failed in several regions using aluminum 6061 alloy. The stress distribution is shown in Appendix B. After addressing some concerns with the airflow, it was decided that the model was to be optimized for minimum weight and maximizing factor of safety (FOS). In order to efficiently perform the design study, the pressure field obtained from the aerodynamic team was approximated as two discrete point loads. The point loads were gradually varied until the maximum stress generated by the point loads closely approximated the pressure field.

Table 3 Summary of values tested to approximate the pressure field obtained from the aerodynamic team as two discrete point loads

Applied Point Load (N)	Maximum Stress from Point Load Simulation (MPa)	Maximum Stress from Pressure Field (MPa)	Percent Deviation from Pressure Field (%)
450	2.79E+08	2.33E+08	19.61
400	2.52E+08	2.33E+08	8.33
350	2.26E+08	2.33E+08	-2.96
375	2.39E+08	2.33E+08	2.69

A load of 375 N was selected in spite of being virtually identical in terms of deviation as the 350 N point load as it is preferred that the estimate be conservative. The front wing was shown to experience significant yielding when using aluminum 6061 alloy as shown in Figure 8. Of note is the strict usage of curved elements in order to successfully mesh the split lines necessary to perform the simulations and account for the various curvatures of the model.

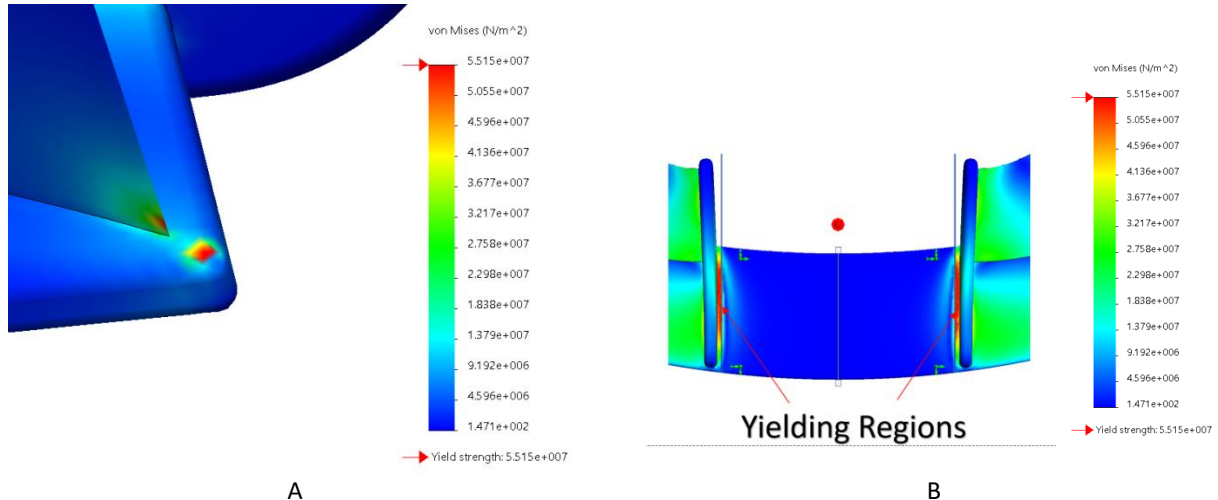


Figure 8 a) The stress concentration caused by a concentrated point load. This can be safely ignored as the true pressure field is not concentrated into a single point as it is in this simulation. b) Detail of the yield regions experienced when using aluminum 6061 alloy

To address the significant yielding issues observed in previous iterations, the material was changed to HM carbon fiber (material properties based on [6]). Furthermore, changing the material to carbon fiber decreased the overall weight of the design. In contrast to the roughly 45 kg of the aluminum mode, the HM carbon fiber weighed approximately 30 kg. A large design study was undertaken in order to narrow the range of potential parameters to vary. It was found that the results obtained from the available material data showed that the base airfoil could support a large cavity thereby reducing the weight significantly. This study was also used to narrow the parameters to examine in greater detail. A further design study was undertaken to determine the optimal configuration of the

support struts. The results of the optimization results can be found in greater detail in Appendix B. A summary of the parameters obtained as a result of the studies can be found in Table 4, with the final result being depicted in Figure 9. Mesh analysis of the final result can be found in Appendix B.

Table 4 Summary of parameter values as a result of the design studies

Strut Diameter (mm)	Strut Spacing (mm)	Number of Struts	Strut Height Position (mm)	Strut Position Depth (mm)	Elliptical Cavity Height (mm)	Elliptical Cavity Width (mm)
5	30	2	30	250	15	172

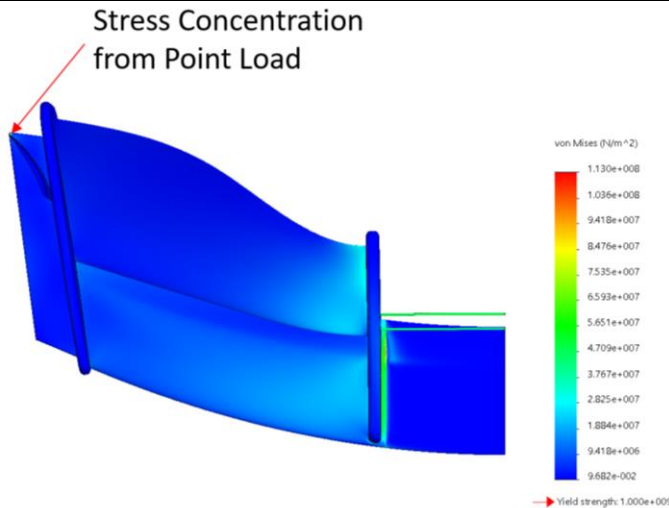


Figure 9 Depiction of final configuration of the half model of the front wing

2.4 Final Design Iteration

This design iteration focused on the addition of the nose cone and ensuring that the means of attachment introduced no additional stress concentrations or failures. The opportunity was also taken in order to minimize the weight of the nose cone. A design study was performed in order to determine to what degree to shell the nose in order to remove as much material as possible while maintaining structural stability which, as shown in Figure 10, results in a 2 mm shell.

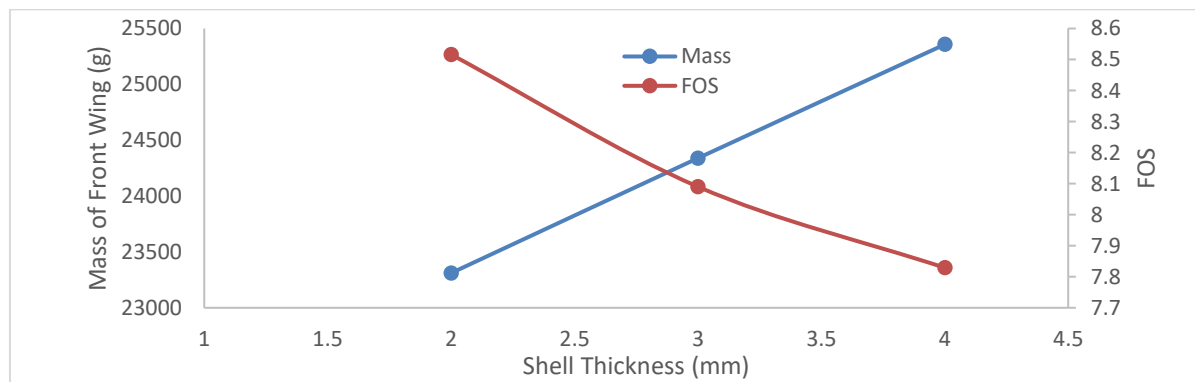


Figure 10 Design study of front wing degree of hollowness. This plot demonstrates the easy choice of a 2 mm shell in order to maximize FOS and minimize mass

The result was the model shown in Figure 11 and Figure 12. Analysis of the loading conditions show that the thin struts take a significant amount of load, but at a low enough magnitude that it retains a high safety factor. However, as a result, the wing itself experiences a significantly lower load in the regions noted in the second

iteration. The struts can therefore act as a wear or sacrificial part, being simpler and cheaper relative to the rest of the front wing. As a result of the design studies, the front wing has a total mass of 23.3 kg with an FOS of 8.5.

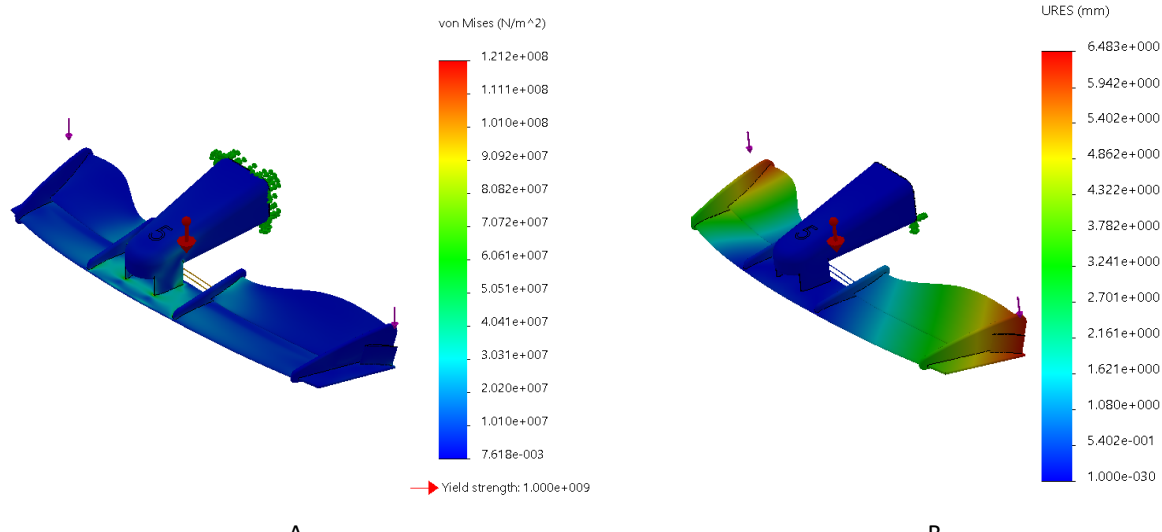


Figure 11 a) Stress distribution over the front wing based on the two point loads. Note significantly higher stresses in the support struts than elsewhere in the model. b) Displacement distribution of the front wing from two point loads

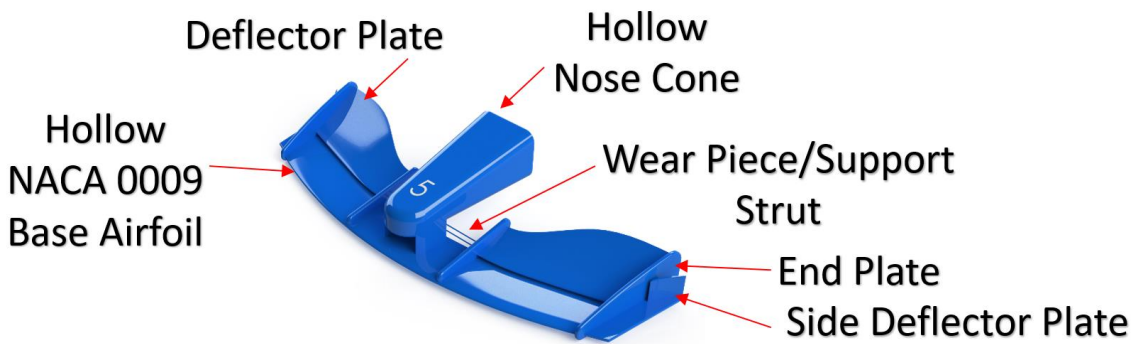


Figure 12 Render of final configuration of the front wing with nose cone attached

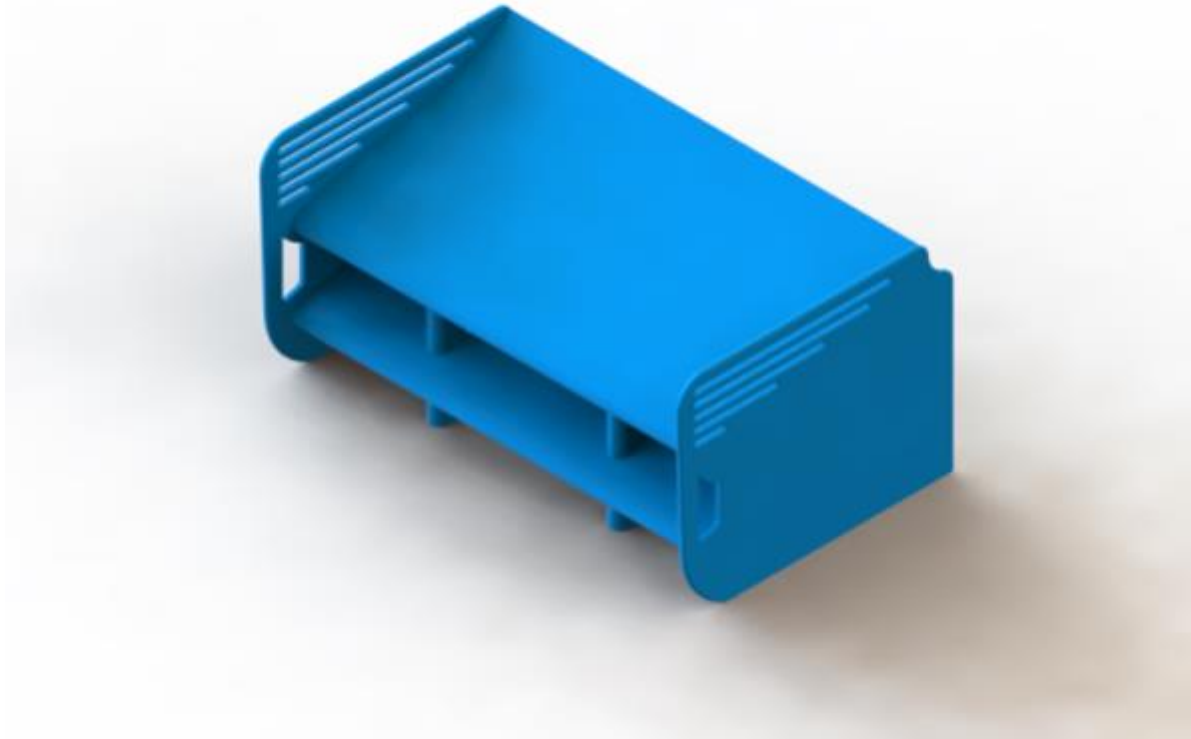
2.5 Conclusions & Recommendations

Thus, the front wing was designed by first determining a valid simulation method. This was done by modeling the airfoil as a cantilevered beam and applying a calculated constant pressure. The deflection as a result of the pressure was compared to an analytical solution. After collaborating and establishing a common model with the aerodynamic team, the pressure field obtained from the aerodynamic team was approximated as two point loads. A series of design studies was then performed in order to optimize the front wing in terms of minimum weight and maximum FOS. Finally, the nose cone was added and a final design study performed in order to minimize the weight contribution of the nose. The final mass of the front wing is 23.3 kg with a FOS of 8.5.

Due to the limited time allotted to the project, there are several points of improvement that can be made. The first is to take into account the directionality of the material in the carbon fiber. The current model assumes bulk material properties which is what was feasible within the allotted time, however it is inaccurate relative to actual

material behavior. Another improvement would be the reduction of finite and sharp edge as they are impossible to manufacture and cause unnecessary stress concentrations. Loading conditions assumed point loads, however it does not take into account the pressure effects on the nose of the front wing. Structural supports would normally be present within the nose, however due to the lack of a pressure field there was insufficient time to properly analyze this configuration and approximate the pressure field in this region. Furthermore, the wing experiences significant bending, it is conceivable that this may become an issue as the car would be changing speeds regularly depending on the course, thus inducing a variable pressure field and consequently a varying load experienced by the front wing. Fatigue loads should therefore also be considered if a more complete solution is desired. The last two recommendations would be best considered in conjunction with the aerodynamic team as they would be able to simulate and provide the changing pressure flow fields. They would also be able to determine if the deflection seen by the wing would induce significant airflow changes and thereby change the aerodynamic properties.

3 Aerodynamics of the Rear Wing



Completed by Anthony Tang

3.1 Introduction

The following chapter will describe the methodology used to iteratively design a rear wing for a F1 race car whose primary design goals are to maximize negative lift and minimize drag. Increased negative lift results in greater normal forces on the race car's wheels which result in greater traction/friction which increases vehicle speed. Conversely, drag directly opposes the vehicle's motion, reducing its speed. For the initial design iteration, 2-dimensional flow simulations were used on various 4-digit NACA Airfoils to gauge the performance changes which result from different geometries. For all flow simulations, the flow was assumed to be in the x-direction only. The results were used to produce an optimized airfoil profile which was subjected to more 2-dimensional flow simulations at various angles of attack and speeds. In the second design iteration, two of the optimized airfoil profiles, at the selected angle of attack, based on the results, were used to model a rear wing in three dimensions. This iteration of the design was subjected to flow simulations, whose resultant loads were used by the structural team to observe whether the model would yield. For the final design iteration, the relative positions and orientations of the two airfoil profiles were modified to make different rear wing models, which were then subjected to flow simulations and the performance changes were observed. Ultimately a final design was reached in collaboration with the structural team, which used the airfoil configuration from the second design iteration, with additional features on the end plates. Topics such as mesh convergence analysis and validation of the lift and drag forces were also explored.

3.2 Initial Design Iteration

The rear wing design was planned to be based on the interaction of two geometrically similar 4-digit NACA Airfoils. In order to select parameters which would optimize the airfoils' performance, airfoils with varying parameters were examined in 2-dimensions. Plots for this process are shown in Appendix C. The resultant airfoil was subjected to further flow simulations, to determine the best angle of attack, again while considering lift and drag tradeoff, and to observe how the lift and drag tradeoff changes over different speeds. Mesh convergence analysis was performed to verify that the mesh used yielded a sufficiently accurate solution, shown in Appendix C. The velocity cut plots for angles of attack (counterclockwise with respect to the x-axis) of 20 and 40 degrees are shown in Figure 13. It can be observed that at an angle of attack of 20 degrees, the top and bottom flow boundary layers follow the same path as each other as they cross the airfoil's surface. However, at some angle of attack between 20 and 40, the boundary layers separate entirely, which creates a large region of low pressure beyond the airfoil, which greatly reduces lift and increases drag, which is greatly detrimental to the design.

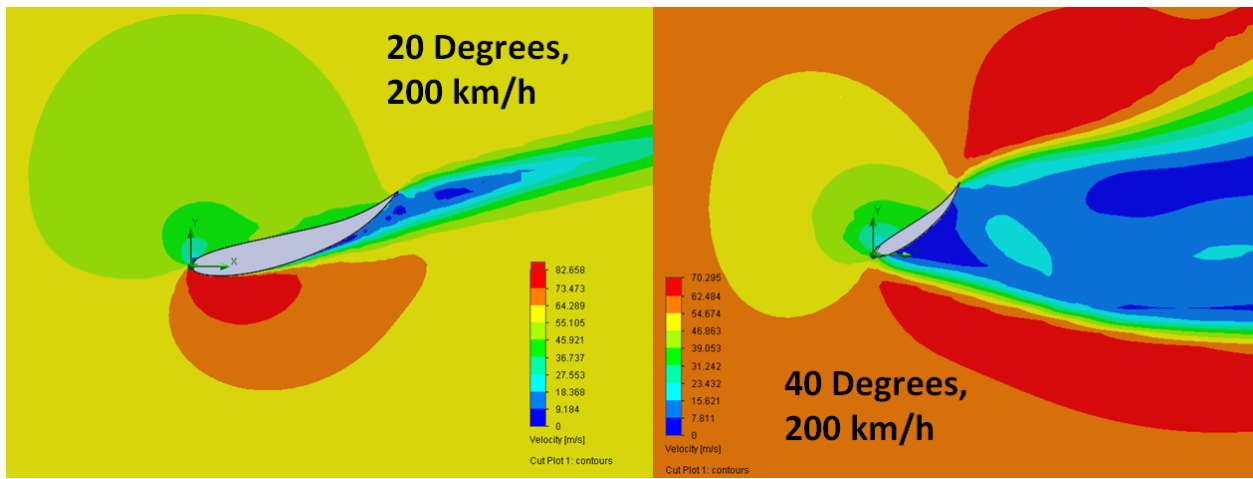


Figure 13 Velocity cut plots for first design iteration at angles of attack of 20 and 40 degrees

The design plots for the effects on the Negative Lift:Drag ratio due to changes in angle of attack and speed is shown in Figure 14. The design plot reflects the flow separation phenomenon described earlier, as the Negative Lift:Drag ratio decreases rapidly for increasing angles of attack. Although the best ratio occurred at 10 degrees, 20 degrees was selected since it yielded the highest value of negative lift, and the tradeoff was deemed satisfactory. The Negative Lift:Drag ratio was observed to change negligibly.

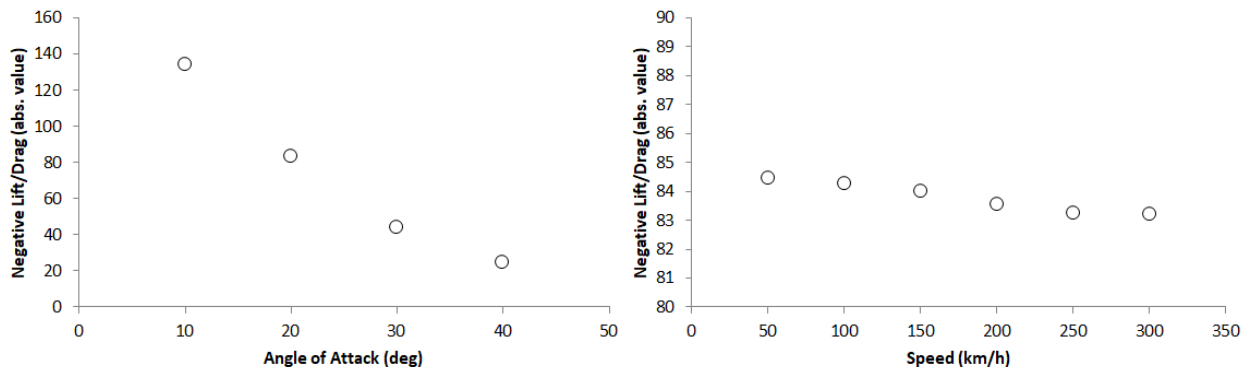


Figure 14 Design plots for lift/drag versus. angle of attack and speed for first design iteration

3.3 Second Design Iteration

The second design iteration served as the first 3-dimensional flow simulation, whose results could be exported and analyzed by the structural team to observe whether the rear wing yields and fulfills certain weight requirements. To model the rear wing, the airfoil profile (and orientation) determined in the first design iteration was scaled in all directions by a factor of 3.45 about the origin so that its chord length was approximately 520 mm, approximated by known F1 Guidelines. It was then duplicated and oriented an arbitrary distance above the first profile. The two profiles were extruded and end plates were added as well as a single, filleted support near the nose end. The profiles' dimensions were purposely left under-constrained so they could be easily modified later on, shown in Figure 15 along with the resultant 3D Model. In order to simulate the most extreme loading scenario, a flow simulation at the maximum specified speed of 300 km/h was performed. Mesh convergence analysis was performed to verify that the mesh used yielded a sufficiently accurate solution, shown in Appendix C. The velocity cut plot for this flow simulation is shown in Figure 16. It can be observed that although low pressure regions formed beyond each airfoil, the overall boundary layers do not separate. At 300 km/h the entire model generated negative lift and drag of approximately **3880 N** and **1200 N** respectively.

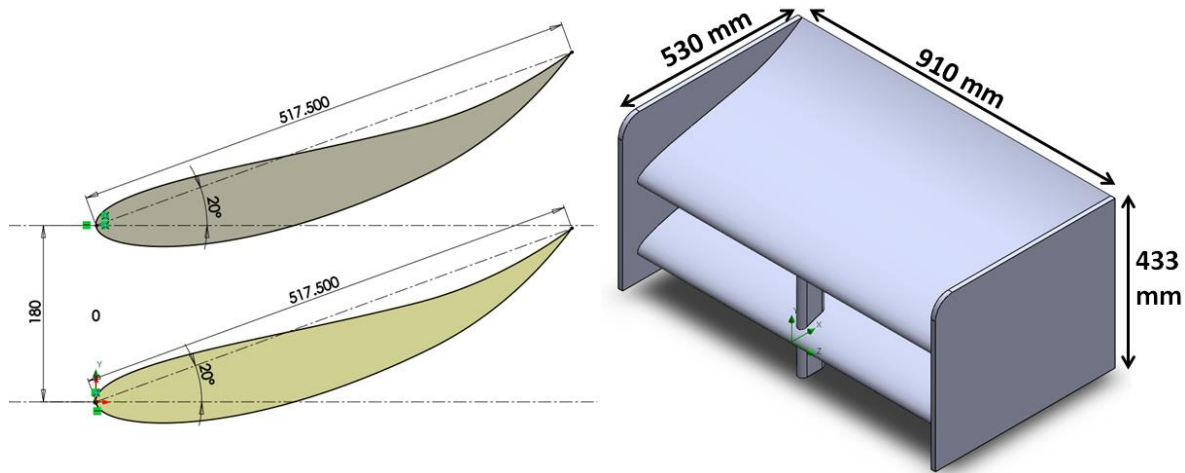


Figure 15: Airfoil configuration and resultant 3D model for second design iteration

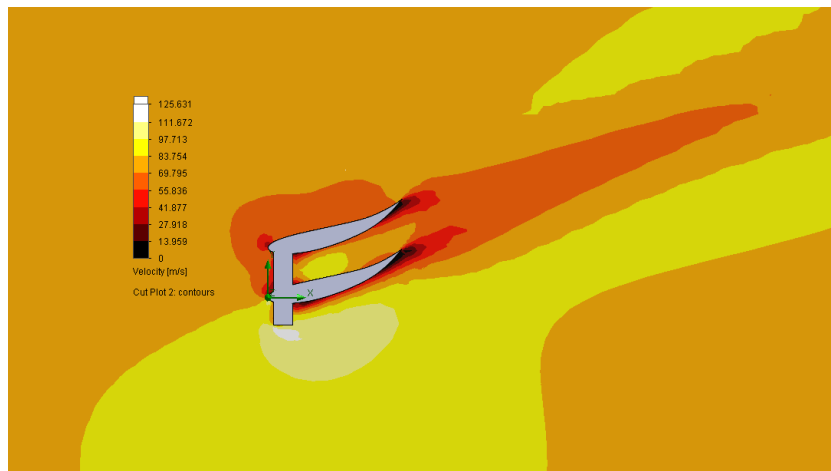


Figure 16 Velocity cut plot for second design iteration at a speed of 300 km/h

3.4 Final Design Iteration

For the final design iteration, different airfoil configurations and the addition of more complex features/modifications were considered for implementation in the final design. For the different airfoil configurations, the top airfoil's position and angle were adjusted, and for each configuration the end plates, which serve to reduce the vortices which form beyond the rear wing, were resized to fit. The flow simulation with the same settings as before were run on each of the configurations shown in Figure 17, this time using surface goals to determine the lift and drag on each airfoil. Lift:Drag ratio was again used to gauge each configuration's performance and the results are summarized in Table 5. While Configuration D yielded the best Lift:Drag ratio, the Final Configuration, whose results are also summarized in Table 5 was ultimately used as the final design due to time constraints. Through collaboration with the structural team, the final model was hollowed out, and holes were removed from the end plates to further reduce the overall weight, and to help streamline flow/reduce vortices. It should be noted that for the flow simulations run on Configurations A through D, the models did not have supports, but the Final Configuration's simulation included the supports, which is the reason the lift and drag are reduced substantially compared to the results from the second design iteration.

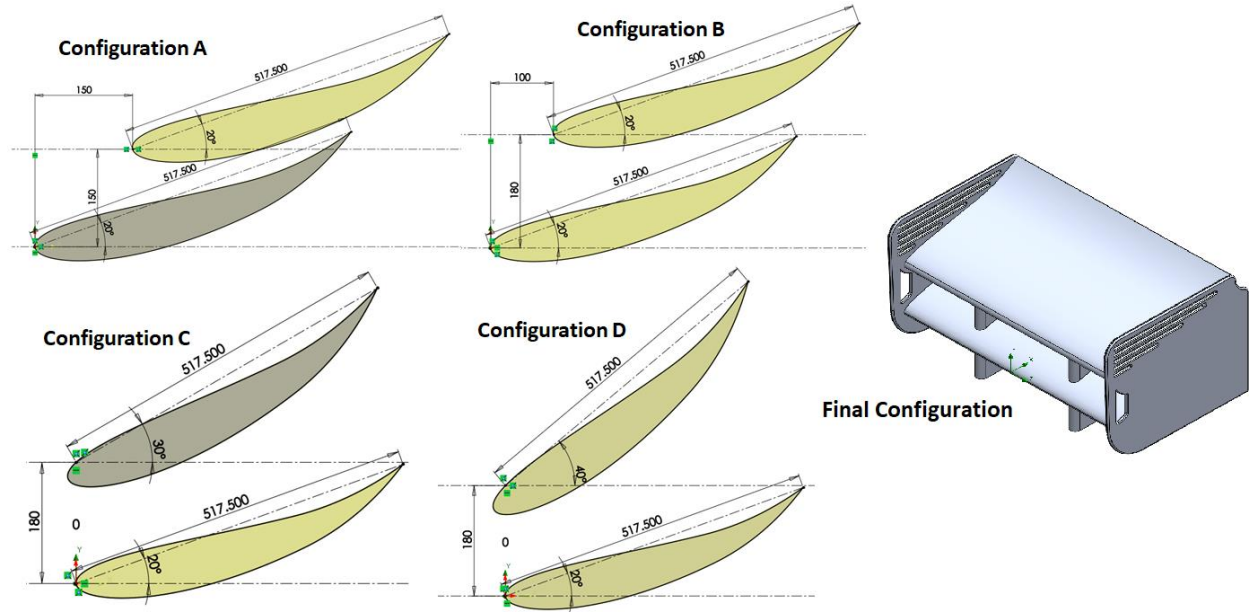


Figure 17 Airfoil configurations for optimization of final design iteration and final 3Dmodel

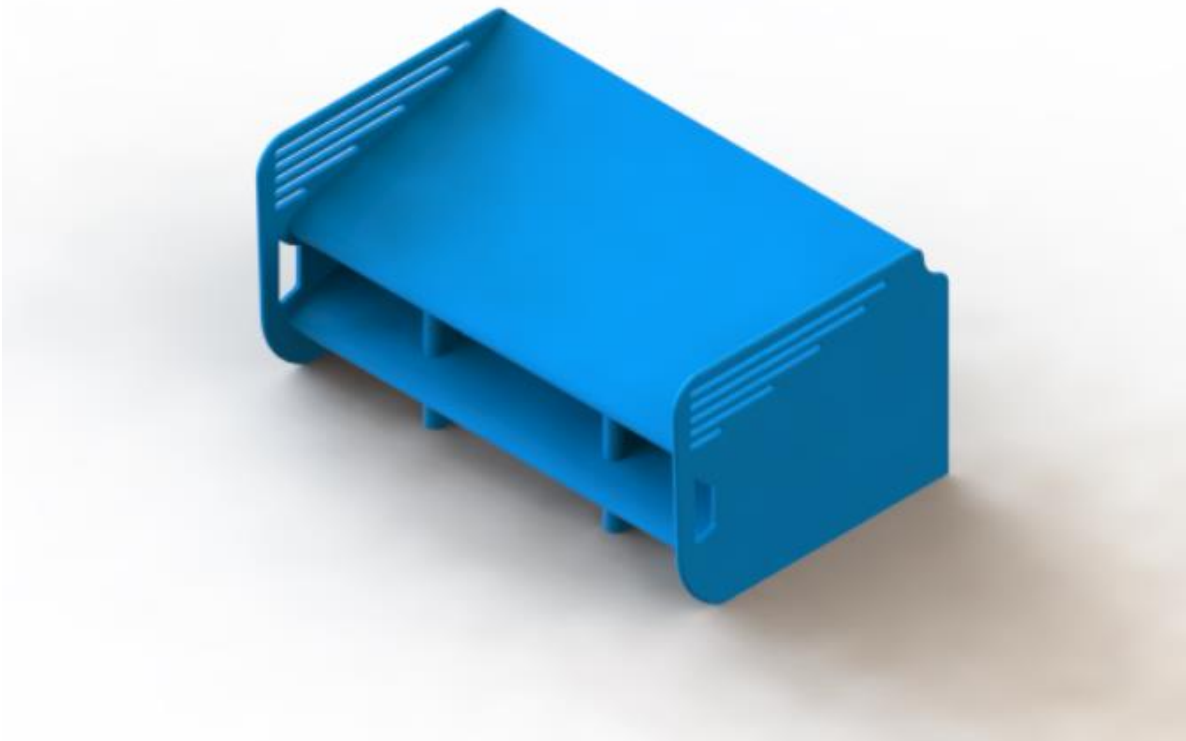
Table 5 Summary of lift to drag ratios for different airfoil configurations

Configuration	Drag on Top Airfoil (N)	Lift on Top Airfoil (N)	Drag on Bottom Airfoil (N)	Lift on Bottom Airfoil (N)	Lift:Drag Ratio (abs. value)
A	680.04	-2065.14	462.01	-1772.35	3.36
B	179.95	319.17	522.97	-2028.09	2.43
C	840.37	-1568.61	509.80	-1929.67	2.59
D	1188.50	-2790.94	430.70	-2954.77	3.55
Final	750.61	-2002.75	291.10	-1237.38	3.11

3.5 Conclusions & Recommendations

A rear wing for an F1 race car was iteratively designed while primarily considering the aerodynamic performance characteristics of each design. Specifically, the primary goal for each design was to maximize negative lift and minimize drag, and the ratio between these values on the airfoils was generally used to compare design parameters. The final design was reached with collaboration with the structural team. In the initial design iteration, the effects of changing parameters on an (upside-down) 4-digit NACA Airfoil were analyzed by performing 2-Dimensional flow simulations on different profiles of an airfoil. Optimal parameters for the airfoil were subsequently selected and the resultant profile was subjected to further 2-Dimensional flow simulations at different angles of attack and speeds. The angles of attack tested included 10, 20, 30, and 40 and it was observed that the ratio between negative lift and drag decreased rapidly as the angle of attack increased; an angle of attack of 20 degrees was selected. The lift:drag ratio changed negligibly at different speeds. For the second design iteration, a 3D-model for a rear wing using two of the airfoils designed previously was made, and subjected to flow simulation to determine the lift and drag experienced by the model at maximum speed (300 km/h). The simulation loads were exported and used by the structural team to determine if the rear wing would yield. For the final design iteration, further rear wing configurations, using different relative positions and orientations between the two airfoils were subjected to flow simulations in order to further improve the lift:drag ratio. It was observed that moving the top airfoil backwards relative to the bottom airfoil rapidly reduced the negative lift on the top airfoil. This is likely due to the top flow boundary layer from the bottom airfoil pushing upwards on the top airfoil in those cases. It was also observed that increasing the angle of attack of the top airfoil rapidly increases both negative lift and drag experienced by that airfoil, so greater angles of attack may be desirable, but the actual effects of these changes on the speed of the vehicle should be considered in more detail. The design criteria of maximizing negative lift and minimizing drag was used to simplify this design process. In a real design scenario, the upper bounds for the drag or lower bounds for the negative lift should likely be considered. Perhaps a way to weigh the importance of negative lift versus drag could be used. Due to time constraints, the configurations studied in the final design iteration assumed that the two airfoils are identical. Future optimization of this design would likely benefit from scaling the top airfoil down, moving it backwards, and increasing its angle of attack. This way, a better tradeoff of increased negative lift and increased drag should be possible.

4 Structural Design of the Rear Wing



Completed by Mellissa Gomez

4.1 Introduction

This chapter will discuss the design process of the F1 car's rear wing, with respect to structural considerations. This section was completed in conjunction with the aerodynamic rear wing design team. The rear wing must not fail during the F1 car's race, that is, the rear wing must not fall apart when subjected to relative air speeds of 300 km/h. In addition, the design is optimized in order to minimize the deflection that the rear wing will experience, as well as minimize the weight of the rear wing. Design was accomplished by running structural simulations on generated 3D models using SOLIDWORKS' finite element analysis (FEA) simulation package.

The first iteration focused on how to approach the basic setup of the problem. An inclined flat plate was subjected to a vertical negative lift force and a horizontal drag force to simulate the actual loading conditions due to air flow. The forces were analyzed as a point load, a line load, and a distributed load in order to determine which value would most accurately describe the conditions. A simple hand calculation was completed to determine the validity of the simulation.

The second iteration used a relatively simple double airfoil apparatus as an initial rear wing design. The aerodynamic team provided forces that the rear wing would be subjected to provide a starting point for design optimization. Design studies were completed on during this iteration to ensure that the rear wing would not fail during operation.

The third iteration focused on weight reduction in the rear wing. A weight-reduced model of the rear wing was generated and given to the aerodynamic team. The aerodynamic team then conducted CFD simulations to provide the forces that would be acting on the newest revision of the rear wing. A final simulation was conducted with these forces to confirm that the final design of the rear wing would not fail during operation within some factor of safety (FOS).

A mesh analysis was run for each iteration in order to ensure value convergence. Iteration 1 and 2 were analyzed via a manual mesh convergence whereas Iteration 3 utilized an h-adaptive method. Mesh analysis figures and additional relevant information regarding the structural design of the rear wing can be found in Appendix D.

The following general assumptions were made for the simulation:

- Flow velocity is in one direction only, there is no wind or out of plane flow to consider
- Only forces due to the wind are considered relevant
- Negative lift force acted downwards only
- Drag force acted perpendicular to the lift force, in the direction of the flow velocity
- Material properties are constant, there is no work hardening
- The flow velocity of the air is constant

4.2 Initial Design Iteration

The first iteration of the rear wing focused on determining the best way to apply the loading conditions. To this end, an inclined flat plate was modelled that would mimic an air foil. Assuming an air flow velocity of 300 km/h, lift force and drag force acting on the plate were determined for different angles of attack, that is, different angles of inclination. Three ways of applying these forces on the plate were considered: as a point load, as a line load, and as a distributed load. Figure 18 displays the loading conditions for a point load simulation, as well as the results of the simulation. Similar simulations were conducted for the other two cases, where all three cases were run for different angles of attack.

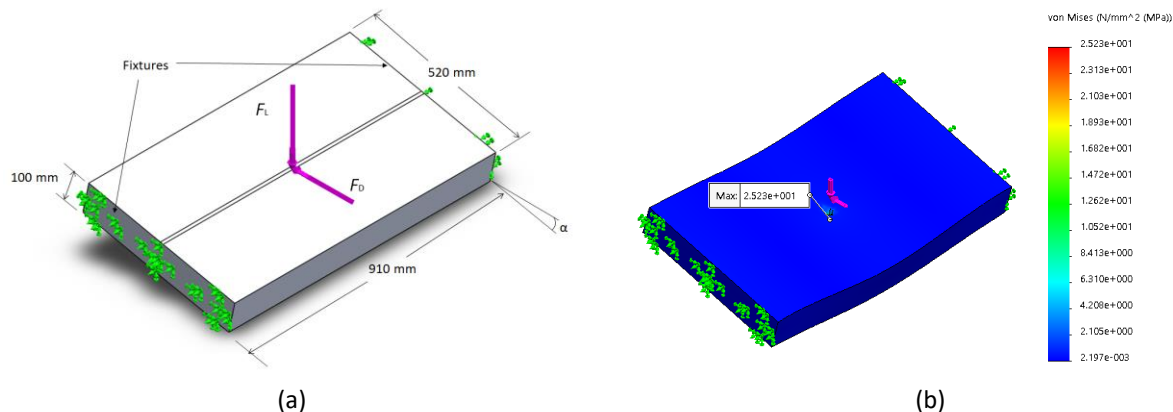


Figure 18 (a) Loading conditions of the simulation of a 15° inclined, flat plate subjected to 300 km/h air that is acting as a point load, and (b) the associated stress distribution plot

A comparison of the results of the different simulation styles is shown in Figure 19. It is apparent that using a point load will greatly overestimate the deflection and stress results as compared to the distributed load or the line load. Though the line load and distributed load results appear to be close, they are not within 10% of each other, meaning the error is significant. As such, it was determined that a distributed load would be the most accurate simulation style and thus would be used for the structural simulation of later iterations.

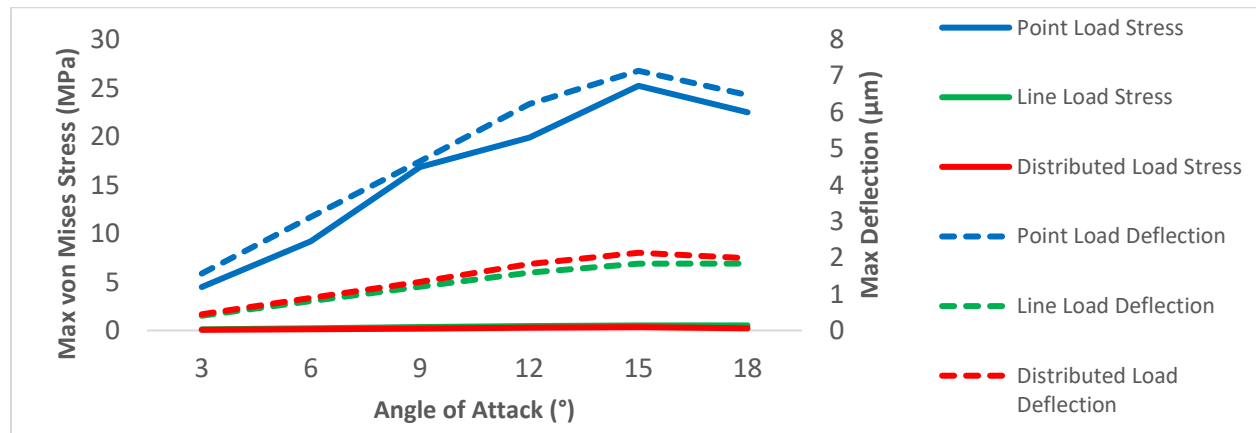


Figure 19 Graph comparing maximum von Mises stress and maximum deflection between different simulation styles for increasing angles of attack at an air velocity of 300 km/h

For a distributed load, maximum deflection is simulated to be 2.1 micron. Hand calculations, shown in Appendix A, calculate the maximum deflection as 1.8 micron. The small deviance in values is likely due to the small scale of deflection. As such, we would consider the simulation to be validated.

4.3 Second Design Iteration

A simple initial design consisting two airfoils overtop one another was modelled, where the profile was determined by the aerodynamic team's first design iteration. Simple side plates were used to connect the airfoils, and a single strut added as a support beam. The material used 1060 aluminum alloy. This model was given to the aerodynamic team in order to begin aerodynamic analysis of the rear wing. From the values provided by aerodynamic team, an FEA simulation was conducted on this design where the strut would be fixed and the rear wing was subjected to a negative lift force of 2810.8 N and a drag force of 985.5 N. Simulation results are shown in Figure 20 (a). It is evident that the rear wing would yield at the support, as such a second strut was considered.

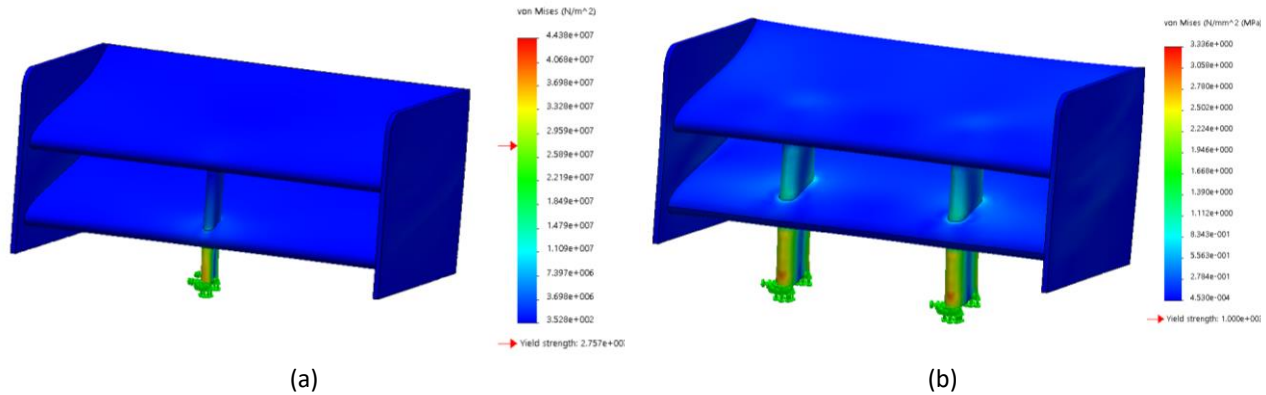


Figure 20 Stress distribution plot for the (a) initial design and (b) the optimized design of the rear wing

Once a second strut was considered, design studies were conducted on the revised rear wing. A constraint was placed that the FOS of the part had to be greater than 1, to prevent yielding, and the goals of the study was to minimize displacement experienced during loading as well as minimize the weight of the wing. A summary of the parameters considered, as well as the optimization results, are shown in Table 6, where HM carbon fiber is a type of carbon fiber material that has previously been used in F1 designs [7] [6].

Table 6 Summary of design study parameters and values optimized, where coloured values are the values chosen as a result of the optimization

Parameters	Values Tested		
Distance of Supports from Front (mm)	125	225	175
Width of Supports (mm)	100	200	-
Thickness of Supports (mm)	20	25	30
Distance Between Supports (mm)	200	400	500
Material of Rear Wing	1060 Alloy	6061 Alloy	HM Carbon Fiber

Figure 18 (b) displays the stress distribution plot of the optimized design for the same loading conditions the initial design was subjected to. The maximum stress of the rear wing is still experienced at the base of the struts; however, the optimized design is not in danger of yielding.

4.4 Final Design Iteration

The final design of the rear wing focused on utilizing the optimization completed from both the structural and aerodynamic sides. The second structural iteration was therefore adjusted in order to accommodate aerodynamic findings. This design was further changed in order to focus on weight reduction of the rear wing by removing material, such as hollowing out the airfoils as shown in Figure 21 (a). The final design is shown in Figure 21 (b).

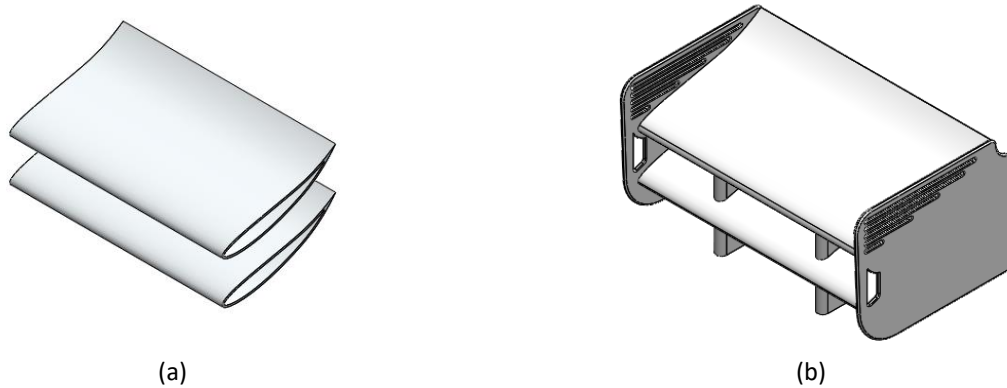


Figure 21 Isometric views of (a) airfoils of the rear wing, and (b) final design of the rear wing in order to display the design changes made from iteration 2 to iteration 3.

This model was given to the aerodynamic team in order to confirm that the redesigned rear wing was still aerodynamically functional. They determined the forces the top and bottom airfoil would be subjected to, which are summarized in Table 5. These values were implemented into a FEA simulation to determine if the final design of the rear wing would be able to succeed under the loading conditions. The relevant results, as well as the results of previous iterations, are listed in Table 7 for comparison. It is evident that the final iteration will not fail during operation based on the given conditions as the FOS is 27.8. Though this is lower than the FOS of the Iteration 2 design, likely due to the material removal, it is still quite high. An FOS of 3 would have been considered sufficient, or even conservative. Additionally, the mass of the rear wing has been cut down by more than half of the mass in the previous iteration, fulfilling the weight reduction goal of this iteration. Due to this, the maximum resultant displacement experienced has increased, but it is still very low at approximately 0.1 mm.

Table 7 Comparison of important parameters for different designs of the rear wing

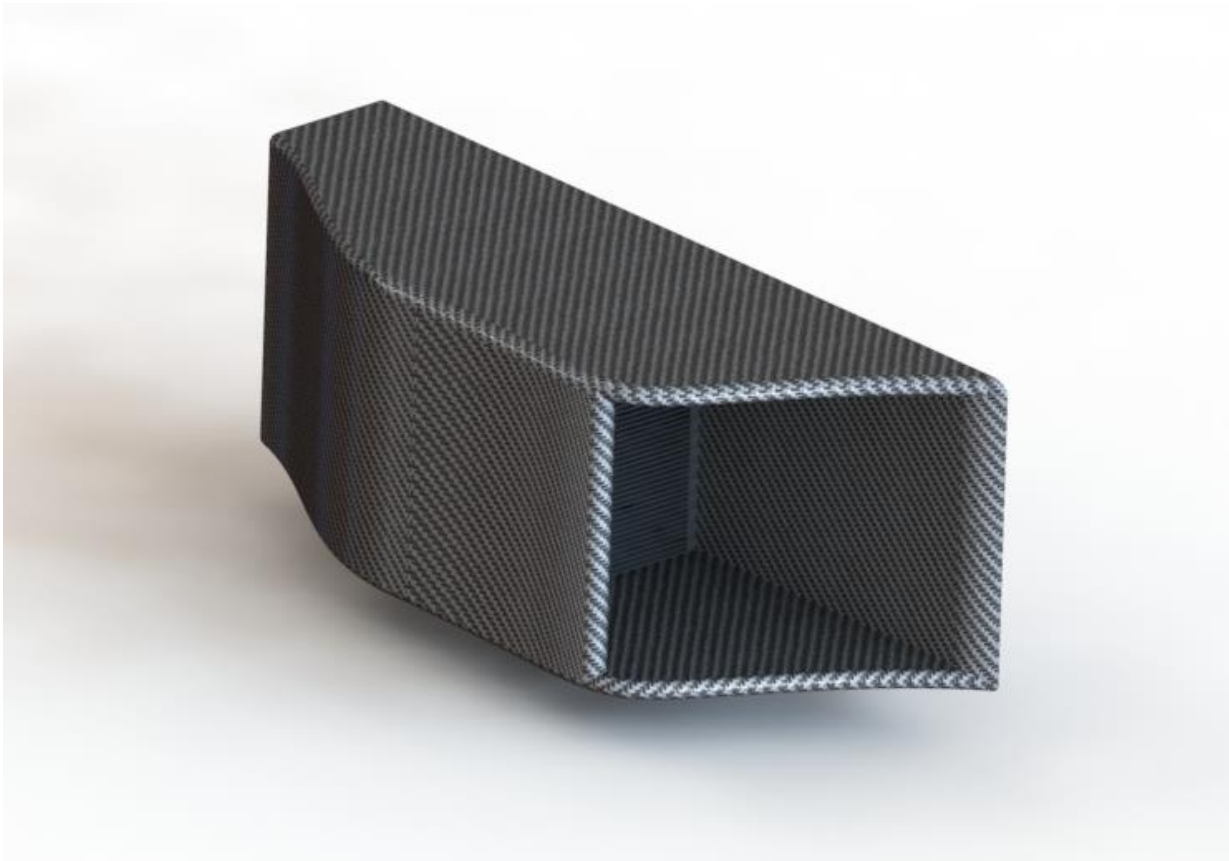
Iteration	Material	Minimum FOS	Mass (kg)	Maximum Displacement (mm)
2 - Initial	1060 Alloy	0.621	53.18	0.624
2 - Optimized	HM Carbon Fiber	368	144.0	0.0185
3 - Final	HM Carbon Fiber	27.8	62.01	0.0993

4.5 Conclusions & Recommendations

In this section the design of a rear wing was considered in regards to its structure. Models were created and used in simulations that would emulate the conditions that a F1 car would be subjected to during racing, such as subjection to an air velocity of 300 km/h. For the initial iteration, an inclined flat plate was loaded in order to determine the best way to conduct the simulations for future iterations. Forces acting on the plate as a point load, line load, and a distributed load were all considered and the results were compared. It was found that the point load had notably different results than the other two simulation styles and as such could be discounted as valid. Additionally the line load and distributed load could not be considered within error of each other; as such a distributed load was determined to be the most accurate method. A hand calculation was completed to determine the maximum deflection of a plate to verify this decision. The second iteration of the rear wing design primarily consisted of design studies meant to optimize the rear wing such that it would have an FOS >1, so that it would not yield, and to minimize the weight and displacement of the rear wing. The loading conditions used in the simulation were obtained from the forces outputted from the aerodynamic simulation. A final design that included the aerodynamic simulation optimization findings was generated. This final design also focused on weight reduction of the rear wing from the previous iteration. The final design ensured that the rear wing would not fail during operation, and had a relatively high FOS of 28. The maximum displacement experienced would be less than 0.1 mm at top speed, and the total mass of the rear wing would be only 62.01 kg. These parameters were accomplished through design optimization studies and utilizing HM carbon fiber as the material for the rear wing.

Further iterations could be done to optimize the design such that it is more aerodynamic, as the main focus was ensure that the design was functional and would not fail. Additionally, a cost analysis is recommended for this design. The overall design is relatively easy to generate in a CAD software program, but machining the part may be difficult. Welding would likely need to be done to create the part, and additional simulations would need to be done on these weldments to determine if these joints would yield under the loading conditions described previously.

5 Aerodynamics and Heat Transfer in the Side Pod



Completed by Daniel Guenter

5.1 Introduction

This section will go over in detail the design process of the aerodynamics and heat transfer in the side pods of the F1 car. Using CFD simulation analysis with along with heat transfer elements of the heat exchanger, the cooling effects were analyzed when air flows through the side pods of the F1 car. The purpose of the radiator heat exchanger is to dissipate the heat from the engine that is lost through the cylinder walls. In the initial design iteration, using real F1 engine specifications and dyno data, estimations on the power output at different car speeds were determined. Considerations of the heat loss through the exhaust as well as other sources were considered when determining the heat required to be removed by the radiator. In the second design iteration, a simple internal flow simulation of the heat exchanger with the given heat generation parameters was modeled. The maximum radiator temperature was determined for different radiator output heat generations at varying car speeds to determine the worst case scenario for the radiator heating. The final design iteration focused reducing the overall drag in the side pod as well as increasing the airflow through it to more effectively cool the radiator. This was done by modelling several iterations of chimneys on the side pods and attempting to streamline the side pod. Throughout all of the analysis, mesh convergence was tested on the finned radiator heat exchange to ensure the values were accurate, as well as the drag force values for the flow over the side pod.

5.2 Initial Design Iteration

Before beginning the initial design of the side pod, the amount of heat dissipation of the coolant in the engine was calculated in order to properly define the problem at hand. This was done by taking a dyno graph of a BMW F1 car engine which gave the engine's rotation speed versus its power output. This data can be found in Appendix E: Section 8.5.1. To calculate the amount of heat that is dissipated through the radiator, it was assumed that the car was 30% efficient with a maximum rated power output of 650 hp (484.7 kW). In order to calculate the amount of heat energy that would need to be cooled by the radiator, calculations were done to estimate the amount of heat that is dissipated out the exhaust, as well as other sources. The calculations were done for the engine running at its maximum speed (15,000 rpm) at a power output of 650hp (484.7 kW), which can be found in Appendix E: Section8.5.1. The maximum amount of heat that is required to be dissipated through the radiators was calculated to be 400 kW (200kW per side). The summarized table of all sources of heat dissipation assumptions considered can be seen in Appendix E: Section 8.5.1. The amount of heat dissipation was assumed to be the directly proportional to the engine input power to simplify the analysis. With this assumption, it was possible to find the radiator heat dissipation versus car speed when the car is in first gear since this is the worst case scenario.

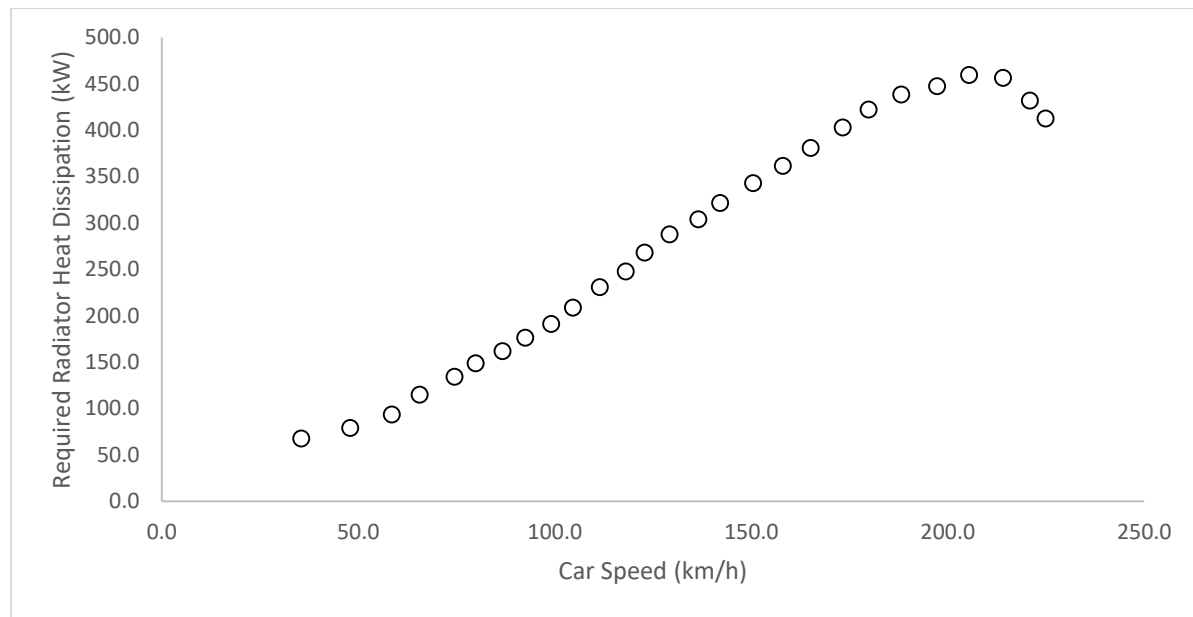


Figure 22 Graph of car speed versus required radiator heat dissipation

Shown above is amount of heat that is expected to be dissipated by the radiator in relation to the car speed. Additional assumptions that were considered for the cooling system are as follows:

- The radiator material was chosen to be copper since it has a very high thermal conductivity allowing heat to pass through it quickly. Other benefits include its corrosion resistance, high melting point, and ease of fabrication
- The maximum running coolant temperature is to be 80 - 90 °C since this is below the boiling temperature of water.
- The side pod material chosen was a Carbon Fiber material (Hexcel AS4C) due to its lightweight and durable properties

5.3 Second Design Iteration

The second iteration of the side pod model consisted of an internal flow CFD simulation of a simple tube box with a finned radiator parallel to the flow. The model of the boundary conditions as well as the heat source added to the radiator can be seen in the figure below.

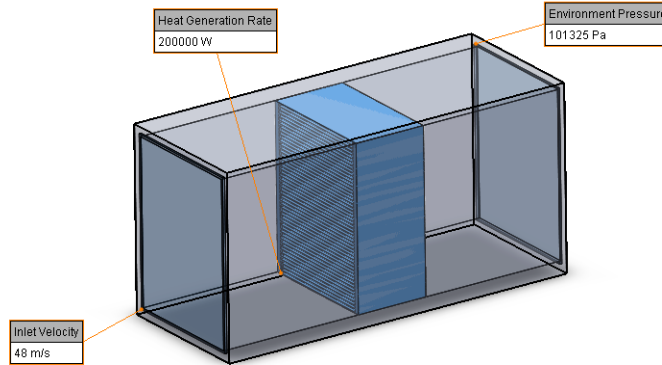


Figure 23 Model of first iteration side pod with boundary conditions

The results of the velocity fields, flow, and pressure plots can all be found in Appendix E: Section 8.5.2. Mesh convergence was done on the finned radiator to ensure the result of the maximum temperature is valid, which can be seen in Appendix E: Section 8.5.2. In order to design for the worst-case scenario, the data found from the first design iteration of the amount of heat dissipated as the speed of the vehicle changed was used. The results of running these simulations showed that the effects of the increasing the power is much greater compared to the increase in the air-cooling from the higher flow speed. This meant that the worst-case scenario would be for when the car runs at its maximum engine speed (15,000 rpm) when the power output is 650hp. The graph of these results can be seen below.

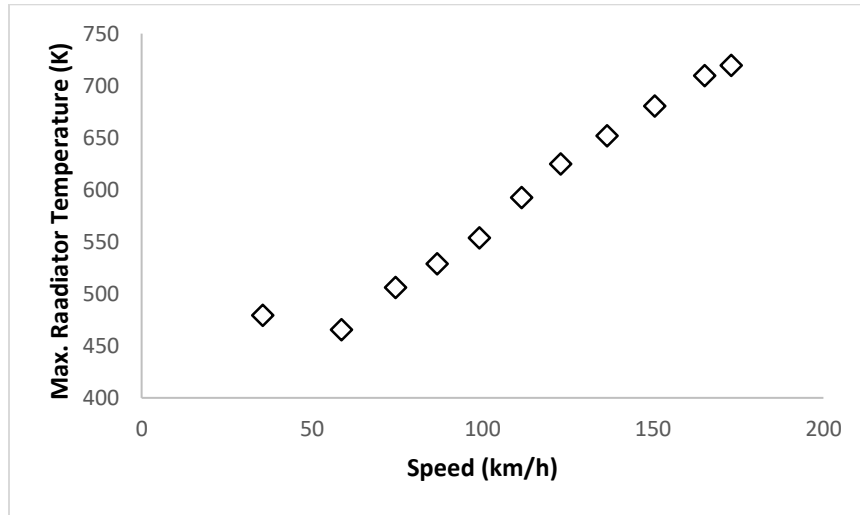


Figure 24 Graph of speed versus maximum radiator temperature

5.4 Final Design Iteration

In the final design iteration, the side pod model was simulated as an external flow CFD to more realistically capture the effects of the flow. Additionally, the external flow simulation was done to create a design study to reduce the

drag and improve airflow through the radiator by streamlining the side pod. The 3-dimensional external flow study was done for several iterations where the chimney effect was also modeled.

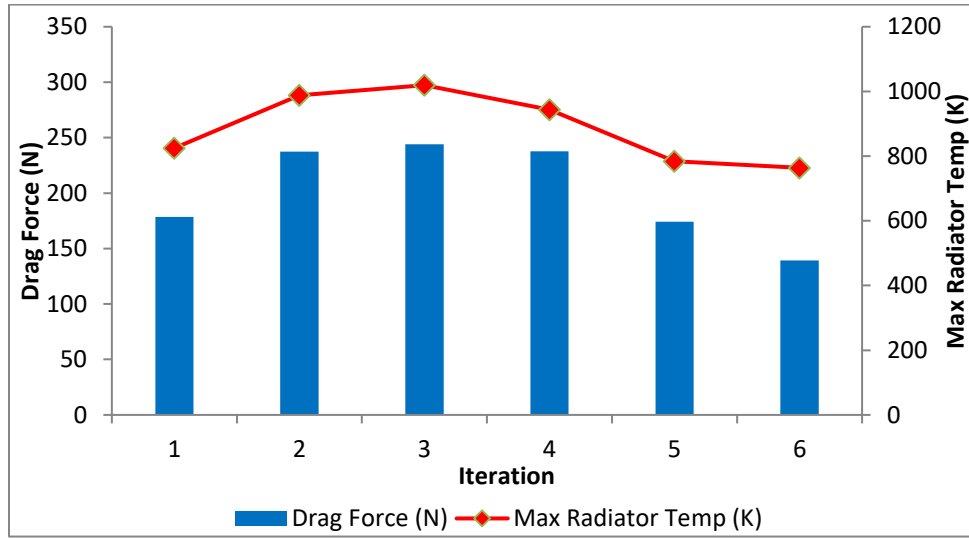


Figure 25 Graph of the drag force and max radiator temperature for each iteration

The above graphs shows the drag force and maximum radiator temperature for each iteration of the side pod. The first iteration in the figure above shows the simple box from the second design iteration. Iterations 2 to 4 show several versions of a chimney that were attempted on the side pods. It can be seen that the chimney effect did not work very successfully. In the last 2 iterations, the chimney was removed and the side pod was instead streamlined which showed significantly better results for both drag force and max radiator temperature. To ensure validity of the results, mesh convergence was done on the more complex models. It was found that the results were able to converge once a finer local mesh was added to the finned radiator and curved section of the side pod. These results can be seen in Appendix F: Section **Error! Reference source not found.**. The final iteration of the side pod that was designed can be seen rendered below. The final results of the flow going through the side pod as well as cut plots of velocity, air temperature, and pressure variation can be all found in Appendix E: Section 0.

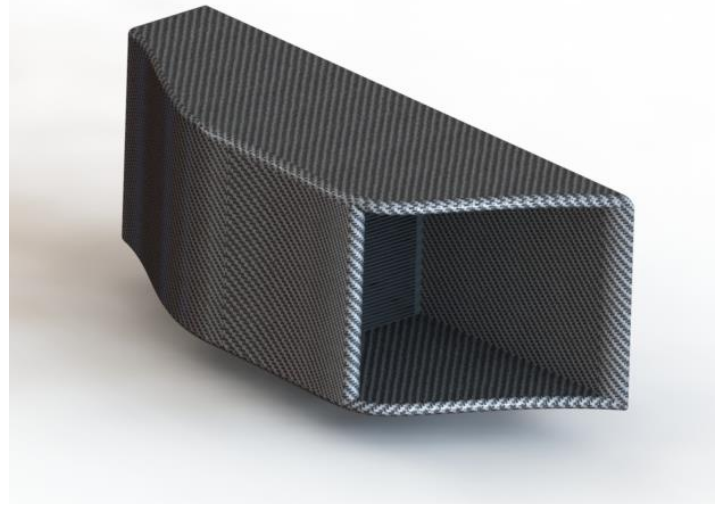
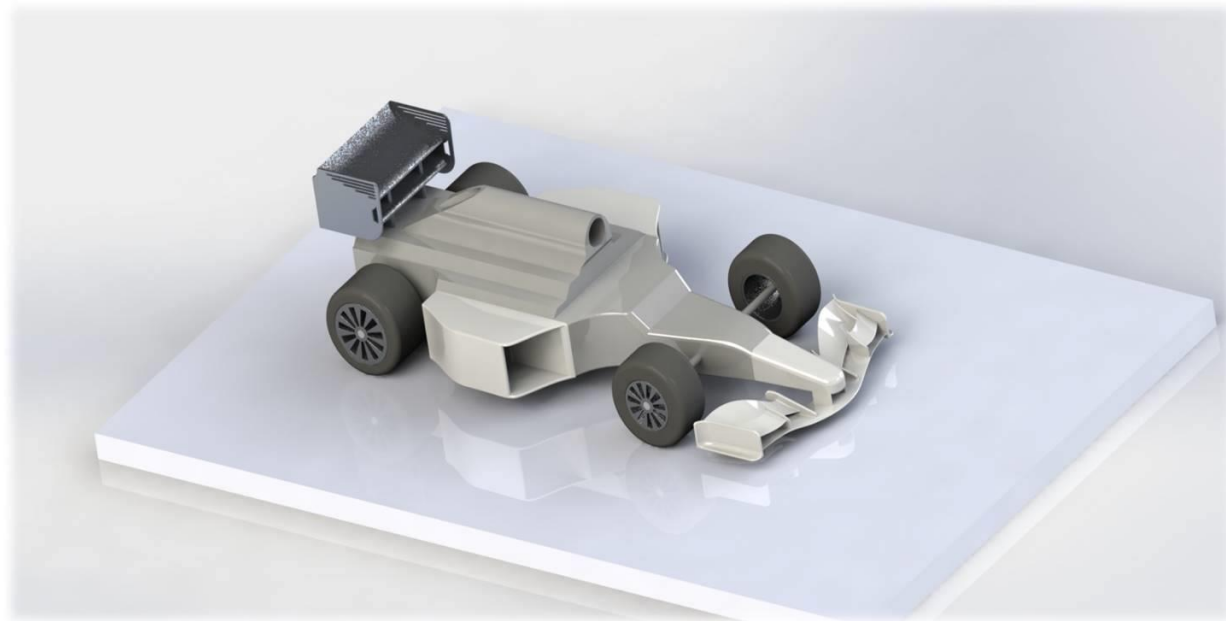


Figure 26 Final rendering of the right side pod model

5.5 Conclusions & Recommendations

A side pod heat exchanger for a F1 car has been designed to meet the requirements set out in this project. The initial design iteration of the side pod design focused on the assumptions and calculations that were required to estimate the amount of heat that will need to be dissipated by the radiator heat exchangers. This was done by gathering dyno data of a BMW F1 engine, which gave the engine speed (RPM) versus the power output data (HP). Using this data, several assumptions were made for the vehicle. It was assumed that the car efficiency was 30% at all engine speeds, the maximum power output capable from the car was 650 hp, and the maximum engine speed is 15,000 rpm. All of these assumptions were gathered from F1 specification guidelines. It was calculated that the maximum amount of heat to be dissipated by the engine through the radiators is 400kW in total (200kW per radiator). It was further assumed that the maximum running temperature of the water coolant would 80 – 90°C, as this is standard to avoid boiling, while the inlet air temperature would be 25°C. The material of the radiator used was copper due to its very high thermal conductivity and the side pod material is a carbon fiber material due to its lightweight. In the second design iteration an internal flow simulation of the side pod was done. This included running simulations for several flow parameters to find the worst case scenario and design for it. This was determined to be at the engines maximum power output and maximum car speed (in its first gear). In the final design iteration, the external flow simulation was done with a design study to minimize the amount of drag force and on the side pod and maximize the cooling effects on the radiator. The final rendition of the side pod was then configured to fit the final car with collaboration of team members. During the design process it was found that there were limitations to the heat exchanger simulation model. A real radiator is made with extremely small fins that have a much larger surface area. Due to limited computational time and power, it was not possible to model a heat exchanger radiator to this level of detail. It is therefore recommended that further analysis be done on the radiator heat exchanger with a much more powerful computer to ensure a higher level of accuracy in the results.

6 Aerodynamics of the Whole Car



Completed by Toya Okeke

6.1 Introduction

The dimensions of the vehicle closely follow the 2018 Formula One Technical Regulations [8]. To develop an initial understanding of the external air flow over the vehicle, the problem was simplified to a symmetric wedge so that only half the wedge could be simulated. For this iteration, wheels and the road were not included. The purpose of this iteration was to conduct a mesh convergence so an understanding of what local mesh refinements were needed to capture the flow around the vehicle. After completing this iteration, the vehicle mesh converged at a speed of 50 km/h. The corresponding drag and lift was ~34 N and ~31 N, respectively. Since the drag and lift converged for this speed, the same mesh was applied for all other speeds.

The second iteration involves cutting a block to match the geometry of a Formula One vehicle. For this iteration, the wheels, front wing, rear wing and side pods were neglected. Again, the vehicle on the road was not simulated. After completing the simulation, the drag and lift force of the vehicle at 50 km/h was 0.040 N and 1.647 N, respectively. The simulations at different vehicle speeds were done using the same local mesh parameters as before.

The third iteration involves new modifications to the geometry of the vehicle and adding wheels to simulate the vehicle on the road. From this iteration, there are two local maximums for the drag to lift ratio. The first is at an optimal speed of ~150 km/h with the drag and lift being 10 and 300 N, respectively. The second is at an optimal speed of ~250 km/h with the drag and lift being 30 and 600 N, respectively.

For the final iteration, the front wing, rear wing and side pods were added to the vehicle. Using the same local mesh parameters, the maximum drag to lift ratio occurs at ~250 km/h with corresponding drag and lift being 6.5 and 1300 N, respectively.

Given the weight of the vehicle is ~2267 kg (22 238 N), the lift force of 1300 N that occurs at 250 km/h will not lift the vehicle off the road. Therefore, the wings of the vehicle generate enough down force to prevent the vehicle from leaving the road. The temperature plots of the side pods show that heat is being conducted effectively in the vehicle. Therefore, the geometry of the design should be optimized to meet the Formula One requirements and that the warm air from the side pods does not flow directly over the wheel.

6.2 Initial Design Iteration

To understand the external flow over the vehicle, the problem was simplified to the 4600 x 1800 x 950 mm wedge. After conducting mesh convergence (see Appendix F), the drag and lift force of the wedge converge to ~34 N and ~31 N, respectively. The mesh of the wedge can be seen in Figure 27.

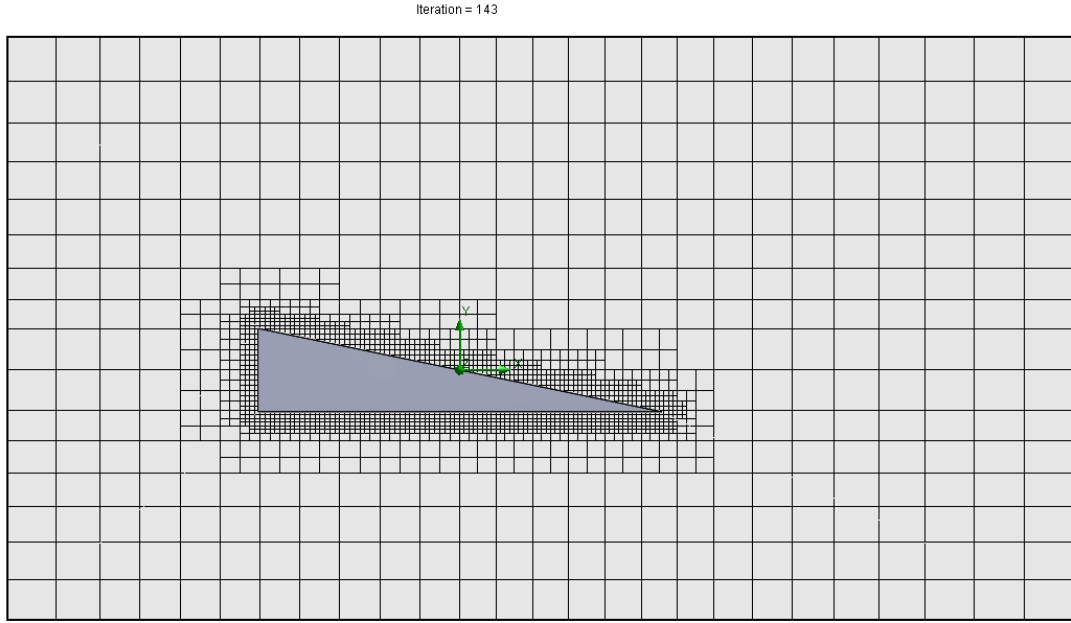


Figure 27 Mesh used for the wedge. 30 047 total/fluid cells were used with 3618 fluid cells contacting the wedge. Since convergence occurred, the same local mesh parameters were applied to the wedge for the other vehicle speeds. The plots in Figure 28 contains the drag, lift and velocity plots of wedge.

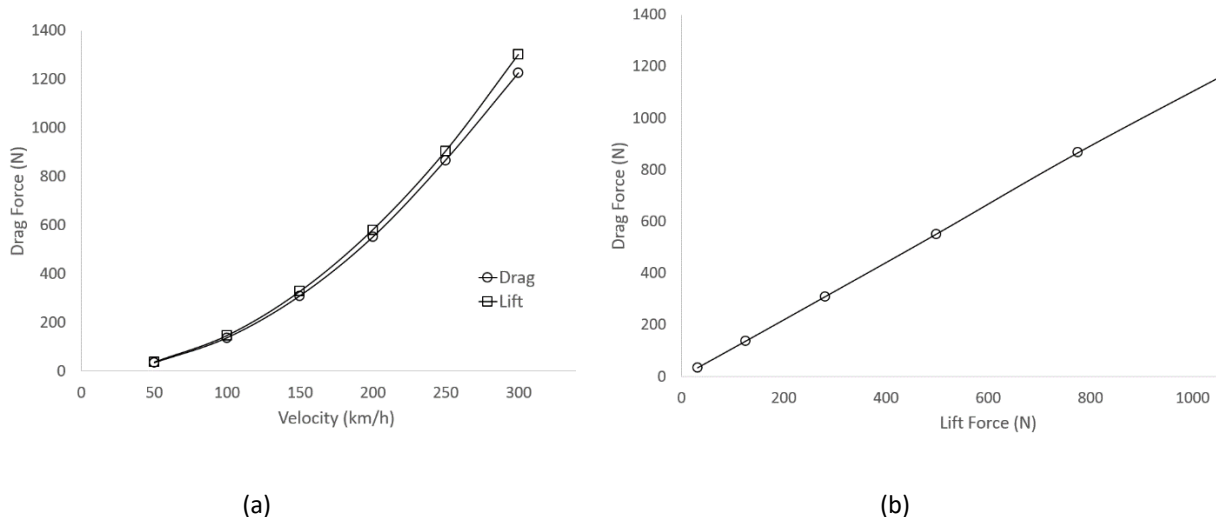


Figure 28 Drag and lift for half the wedge as velocity increases

The drag and lift show an increasing trend as the wedge speed increases. This is likely due to neglecting the wedge moving along the road. Therefore, a conclusion about the optimal drag, lift and velocity cannot be made at this point since there is no maximum force that can be achieved.

6.3 Second Design Iteration

The vehicle was now modified to try and match the Formula One 2018 Technical Regulations. Using the same local mesh parameters in the first iteration, the local mesh plot in Figure 29 was obtained.

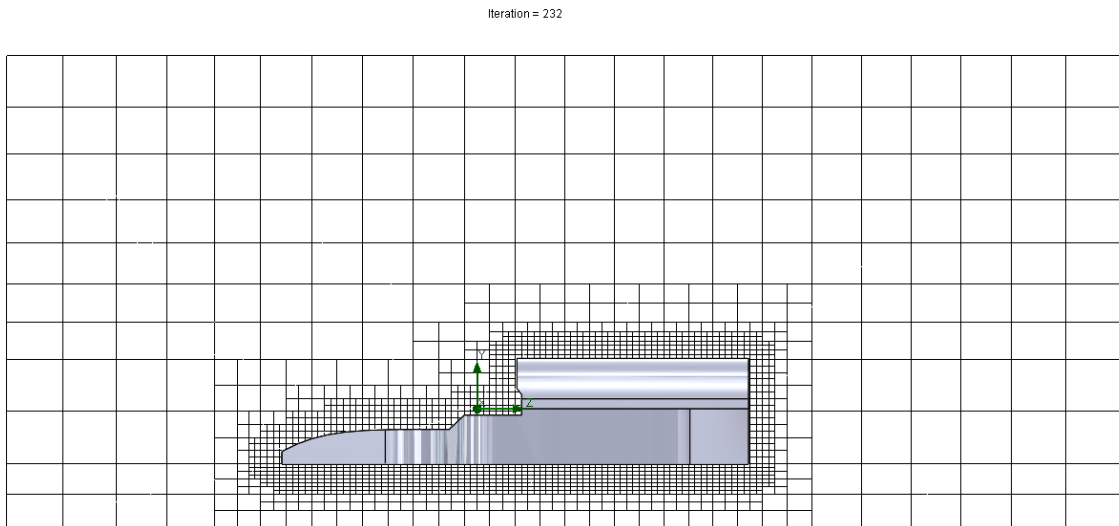


Figure 29 Mesh of the vehicle used for the second iteration. 49021 total/fluid cells were used with 5129 cells contacting the vehicle

The drag and lift plots in Figure 30 suggest drag, lift and velocity do not share a linear relationship shown in the first iteration. Still, no conclusions can be made on how to optimize these parameters since they all have an increasing trend. Again, this is likely due to neglecting the vehicle moving along the road.

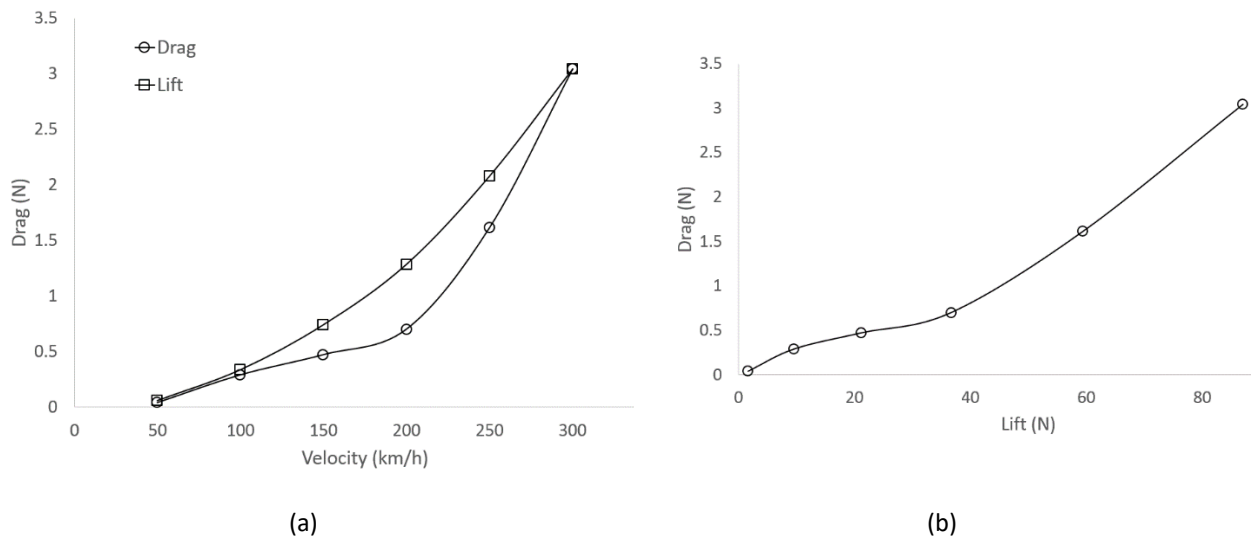


Figure 30 drag and lift of the vehicle as its speed increases.

6.4 Third Design Iteration

For the third iteration, the vehicle was modified to simulate it driving on the road. Using the same local mesh parameters, the plot in Figure 31 was generated.

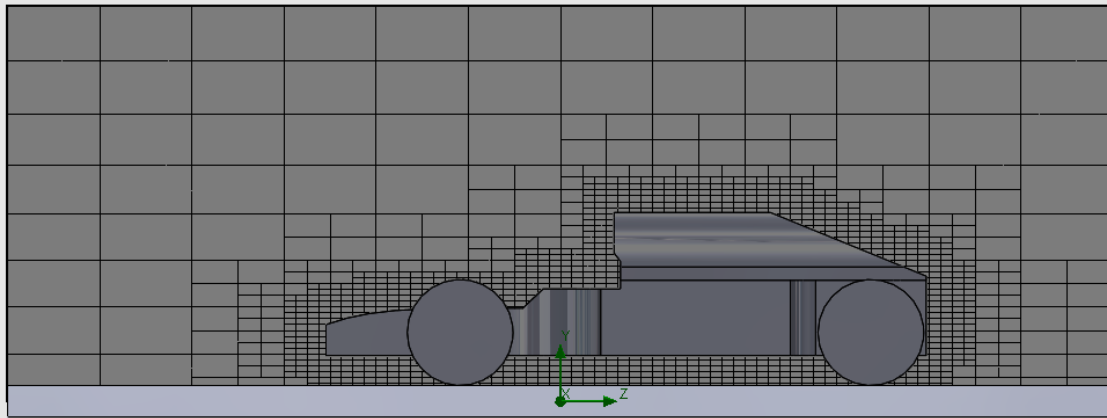


Figure 31 Mesh of the vehicle used for the third iteration. 29612 total/fluid cells were used with 5764 contacting the vehicle

The drag and lift plots in Figure 32 shows an increasing trend in lift, but two local maxima for the drag. Therefore, the drag to lift ratios can be deemed as critical speeds for the vehicle. The maxima occur at 150 and 250 km/h. The drag and lift at these speeds are ~10 and ~300 N, and ~30 and ~600 N, respectively.

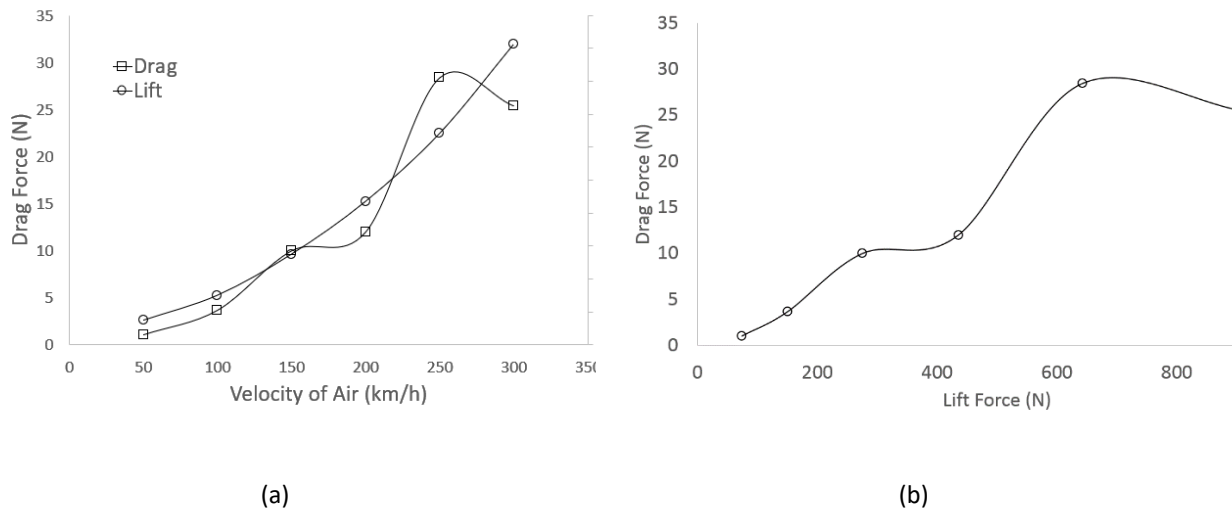


Figure 32 Drag and lift of the vehicle on the road as its speed increases

6.5 Final Design Iteration

The final design iteration simulates the vehicle with the front wing, rear wing and side pods. The drag and lift of the car was determined using the same local mesh parameters. The mesh plot is shown in Figure 33.

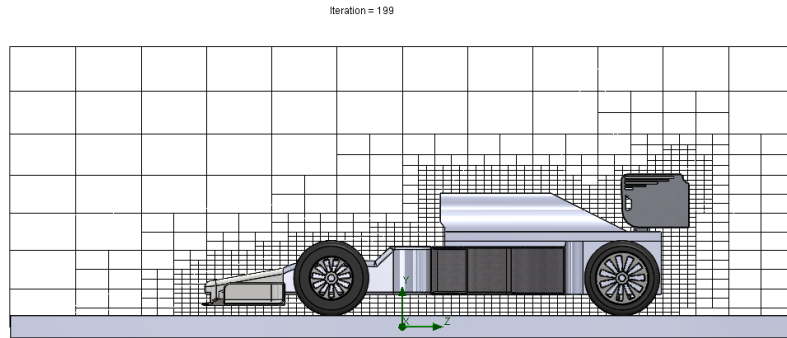


Figure 33 Mesh of the vehicle used for the final design. 59644 total cells and 44349 fluid cells were used with 15295 fluid cells contacting the vehicle

Figure 34 shows relationship between drag, lift and velocity of the vehicle.

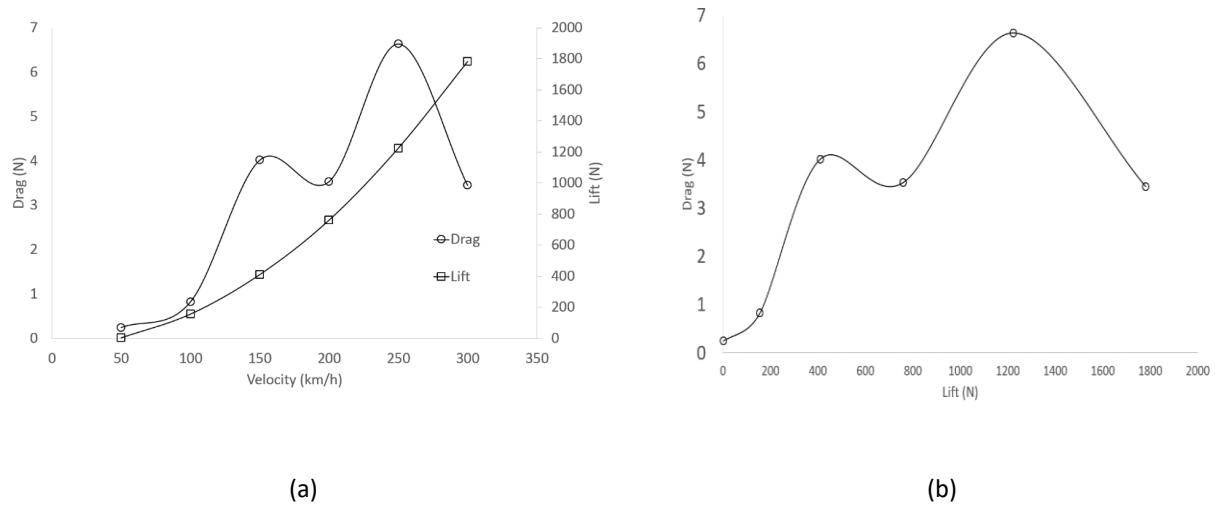


Figure 34 Drag and lift of the vehicle on the road as its speed increases

From this plot, the local maxima of drag were minimized significantly due to the front and rear wings. Although the lift does increase, the ratio between drag and lift reduces significantly at all vehicle speeds. At 150 km/h, the drag and lift are ~4 N and 400 N, respectively; at 250 km/h, the drag and lift are ~6.5 N and ~1300 N, respectively. Given the weight of the vehicle is ~2267 kg (22 238 N), the wings of the vehicle generate enough down force to keep the vehicle on the ground.

Also, the temperature plots in Appendix F show the side pods conduct the air flowing through better as the vehicle speed increases. However, the location of the side pods is transferring the heated air to the rear wheels, meaning the geometry of the design should be optimized in the future to avoid this occurrence.

6.6 Conclusions & Recommendations

To understand the aerodynamics of the whole car, the geometry was simplified to a wedge, and modified further to meet the Formula One Regulations. During the first iteration, the critical pressure regions that would occur on the vehicle were introduced and an initial linear relationship between drag and lift was found. However, the pressure regions reduced in size during the second iteration and a non-linear relationship occurred between drag and lift. Once a simulation of the vehicle on the ground was done, the critical speeds of 150 and 250 km/h were found. The drag to lift ratio at these speeds can be minimized by adding the front and rear wings. In the final iteration, where all main vehicle components were added, the drag to lift ratio was reduced significantly at these speeds. Since the maximum lift force does not exceed the weight of the vehicle, and the drag on the vehicle does not exceed two significant digits, the wings of the vehicle generate enough downforce on the vehicle and enhanced the aerodynamic performance of the vehicle. The temperature plots of the side pod show that they exchange heat efficiently as the speed of the vehicle increases. Therefore, the main design goals for this project were met. Further research would need to be done to optimize the geometry of the vehicle so they are in line with Formula One Regulations, and so the warm air transferred from the side pod is not flowing directly over the rear wheels.

7 References

- [1] "Aerodynamics: Understanding F1 Racing," Formula 1, 15 Mar 2015. [Online]. Available: <https://www.formula1.com/en/championship/inside-f1/understanding-f1-racing/Aerodynamics.html>. [Accessed 30 Nov 2017].
- [2] Y. Çengel and J. Cimbala, Fluid Mechanics Fundamentals and Applications, 3rd ed., McGraw-Hill, 2014, pp. 634-638, 948.
- [3] B. Allen, "NACA Airfoils," NASA, 31 Jan 2017. [Online]. Available: <https://www.nasa.gov/image-feature/langley/100/naca-airfoils>. [Accessed 27 Nov 2017].
- [4] J. Anderson, Fundamentals of Aerodynamics, 6th ed., McGraw-Hill, 2016, pp. 329-331, 389.393, and 395-399.
- [5] Need4Speed, "need4speed.ws - the fastest cars on the web since 1998," [Online]. Available: <http://www.need4speed.ws/videos/top-speed-world-record-with-a-formula-1-bar-honda-413-km-h>. [Accessed 4 December 2017].
- [6] ACP Composites, "Mechanical Properties of Carbon Fiber Composite Materials, Fiber/Epoxy resin (120 C Cure)," ACP Composites, 2014.
- [7] G. Savage, "Composite Materials Technology in Formula 1 Motor Racing," Honda Racing R1 Team, 2008.
- [8] "Regulations- FIA Formula One World Championship," Federation Internationale De l'Automobile, 21 09 2017. [Online]. Available: <https://www.fia.com/regulation/category/110>. [Accessed 25 11 2017].
- [9] "NACA 4 digit airfoil generator," AirfoilTools.com, 06 Nov 2012. [Online]. Available: <http://airfoiltools.com/airfoil/naca4digit>. [Accessed 23 Nov 2017].

8 Appendices

There are seven appendices corresponding to each project discussed in this report and an engineering drawing package.

Appendix A: Project 1- Aerodynamics of Front Wing

Appendix B: Project 2- Structural of Front Wing

Appendix C: Project 3- Aerodynamics of Rear Wing

Appendix D: Project 4- Structural of Rear Wing

Appendix E: Project 5- Aerodynamics and Heat Transfer in the Side Pod

Appendix F: Project 6- Aerodynamics of the Whole Car

Appendix G: Engineering Drawing Package

Appendix A: Aerodynamics of the Front Wing

Completed by Erik Hartikainen

8.1 Appendix A: Aerodynamics of the Front Wing

8.1.1 Simple Airfoil

Prior to beginning design of the front wing, some simple airfoils were considered to establish a basis for comparison of lift and drag characteristics. Using a table of NACA airfoils provided by NASA (2017) [3], it was determined that thinner airfoils generally induce less drag, and greater camber allows higher lift force. Additionally, more camber allows greater reduction of velocity along the concave surface of a cambered airfoil, and therefore a greater increase in pressure to create lift.

8.1.2 2D Convergence Analysis for Simple Airfoil

Convergence analysis was completed to validate the appropriate mesh was used and that results were reasonable prior to continuing to design of the front wing.

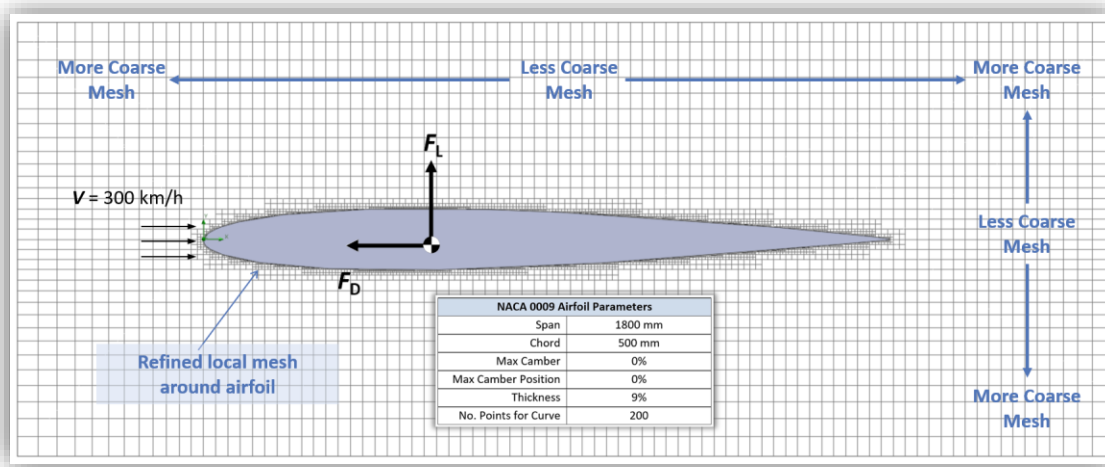


Figure A1 An image of the refined mesh for external flow around the NACA 0009 airfoil.

Shown in Figure A1 is an image of mesh refinement for the NACA 0009 airfoil at an angle of attack of 0° with a velocity of 300 km/h. This was an estimated top speed for a formula one car with front wing span of 1800 mm and chord of 500 mm as obtained from 2018 regulations [8]. Mesh control was applied such that fluid cells were much finer near the airfoil surface and became coarser further away. The mesh was refined to ensure convergence was achieved.

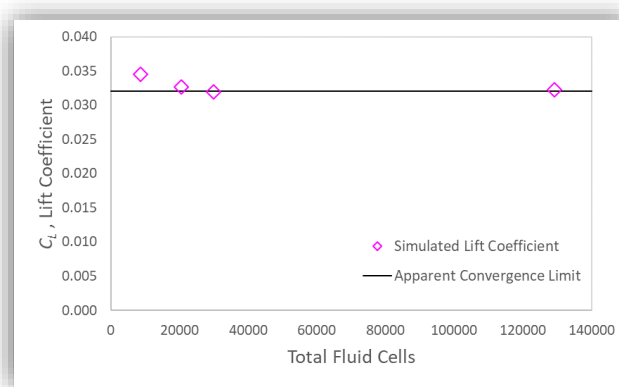


Figure A2 A plot of manual convergence analysis for the lift coefficient on the NACA 0009 airfoil using a 2-D computational domain.

From the plot illustrated in Figure A2, the lift coefficient is shown for four iterations of manual convergence analysis. Since the lift coefficient converged to 1.07% between the last two data points, it was determined that the lift coefficient converged to a value of 0.032 for the NACA 0009 airfoil at an angle of attack of 0° with flow speed of 300 km/h.

8.1.3 Analytical Calculation of Lift for Model Validation

A theoretical estimate of lift coefficient and lift force was completed for an angle of attack of -5° to validate the results obtained through simulation in SOLIDWORKS. First, the Reynold's number was determined to characterize flow over the NACA 0009 airfoil by using

$$R_e = \frac{Vc}{\nu} \quad (A1)$$

with a chord length, c , of 500 mm, flow velocity, V , of 300 km/h (83.33 m/s), and kinematic viscosity, ν , of 1.516×10^{-5} m²/s Reynold's number is solved from equation A1 as

$$R_e = \frac{(83.33 \frac{\text{m}}{\text{s}})(0.500 \text{ m})}{(1.516 \times 10^{-5} \frac{\text{m}^2}{\text{s}})} = 2,748,461$$

From the calculation of Reynold's number, the flow at this velocity is turbulent. Next, the theoretical calculation of lift for a symmetric airfoil given by Anderson (2016) [4] is

$$C_L = 2\pi\alpha \quad (A2)$$

The key assumption for using equation A2 is that this is a thin, symmetric airfoil at a low angle of attack. For an angle of attack of -5° (-0.08727 rad), the theoretical lift coefficient is calculated from equation A2 as

$$C_L = 2\pi(-0.08727 \text{ rad}) = -0.5483$$

Considering this, the theoretical lift force on the airfoil is

$$F_L = \frac{1}{2} C_L \rho V^2 A \quad (A3)$$

With an air density of 1.204 kg/m³, velocity of 300 km/h (83.33 m/s), and planform area, A , given by

$$A = \text{chord} \times \text{span} = 0.5 \frac{\text{m}^2}{\text{unit span}}$$

The area here was considered per unit span to adequately compare with simulation results. The lift force calculated using equation A3 is

$$F_L = \frac{1}{2} (-0.5483) \left(1.204 \frac{\text{kg}}{\text{m}^3}\right) \left(83.33 \frac{\text{m}}{\text{s}}\right)^2 (0.5 \text{ m}^2) = -1146 \text{ N}$$

Next, theoretical and simulated results were compared to validate the flow model established in SOLIDWORKS.

Table A1 Comparison of SOLIDWORKS flow simulation and analytical results for CFD validation.

Parameter	Flow Simulation	Analytical Estimate	% Difference
Lift Force (N)	-833.5	-1146	27.3%
Lift Coefficient	-0.412	-0.548	24.8%

The results of lift parameters for flow simulation in Table A1 are less than the results obtained through analytical estimates based on thin airfoil theory. A possible reason for the discrepancy is that it is difficult to capture the boundary layer in SOLIDWORKS flow simulation as the angle of attack increases. In general, the results obtained were reasonable and the simulation model was determined to be valid.

8.1.4 NACA 0009 Design Plots

Considering the mesh parameters used to obtain convergence, the NACA 0009 airfoil was initialized in SOLIDWORKS for various angles of attack. Since validation was completed, key design plots were developed.

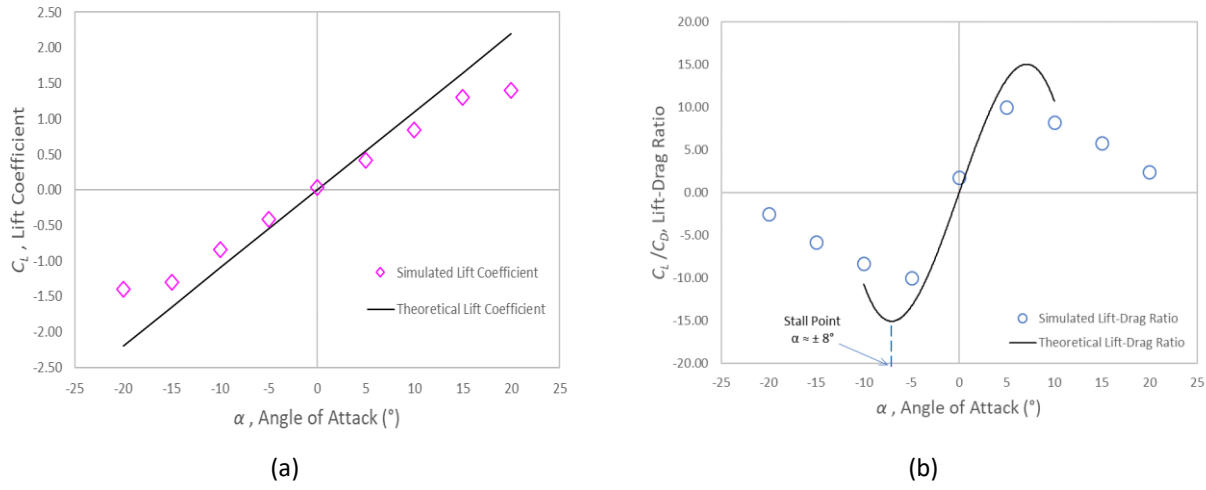


Figure A3 Two plots of (a) lift coefficient and (b) lift-drag ratio for various angles of attack.

From the plots in Figure A3 it is shown that the simulation data generally agrees with theoretical predictions. At higher angles of attack, simulation results become less accurate due to boundary layer separation on the airfoil surface which substantially increases pressure drag as suggested by Anderson (2016) [4]. The maximum simulated lift coefficient occurs at an angle of attack of 20° in (a), but the drag coefficient at this angle is large as can be seen in (b). For the design of the front wing, maximizing downforce was decided to be of greater importance than minimizing drag, since the race car travels at such high speeds and downforce is required to travel around corners faster.

8.1.5 3D Convergence Analysis for Design Iteration 1

Convergence analysis was completed for the 3D case of completed design iteration 1. Since the geometry didn't change substantially for remaining design iterations, the same mesh criteria were applied for iterations 2 and 3.

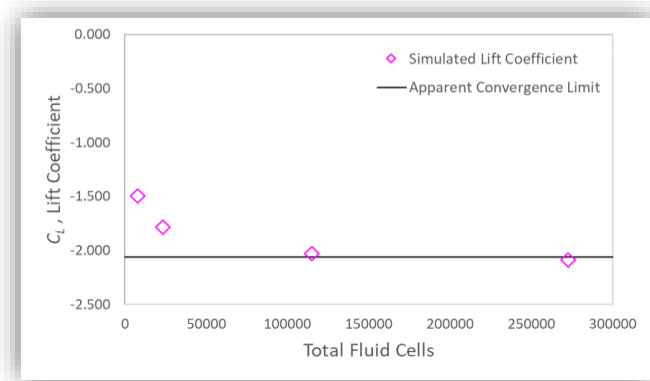


Figure A4 A plot of manual convergence analysis for the lift coefficient of the initial design.

From Figure A4 the lift coefficient was found to converge to -2.06 with a deviation of approximately 2.6% from the previous iteration at convergence. This was determined to be reasonable for continued analysis while considering time constraints.

8.1.6 NACA 6406 Deflector Plate Design Plots

Considering the mesh parameters used to obtain convergence, the NACA 6406 airfoil used for the deflector plate to generate downforce was initialized in SOLIDWORKS for various angles of attack. Design plots were obtained for this airfoil.

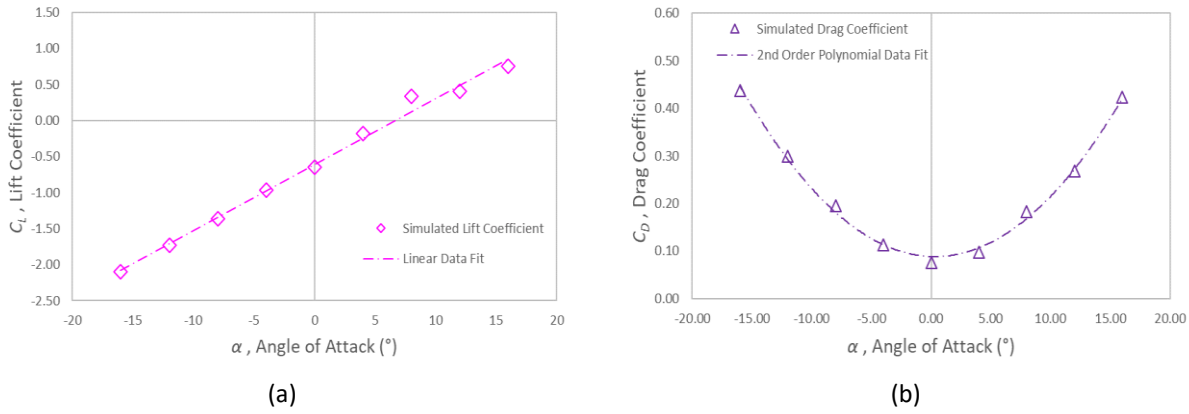


Figure A5 Two plots of (a) lift and (b) drag for the NACA 6406 airfoil deflector plate.

Shown in Figure A5 are lift and drag plots for the NACA 6406 airfoil used for the deflector plate of the front wing. A linear trend is shown between lift and angle of attack which agrees with theory; however, a loss of lift was expected at the stall point. Since this was not captured from the simulation, it can be inferred that SOLIDWORKS insufficiently captures the boundary layer separation at high angles of attack. Further simulation would need to be completed to determine the stall point of the airfoil, but this is computationally expensive and was neglected for the sake of time.

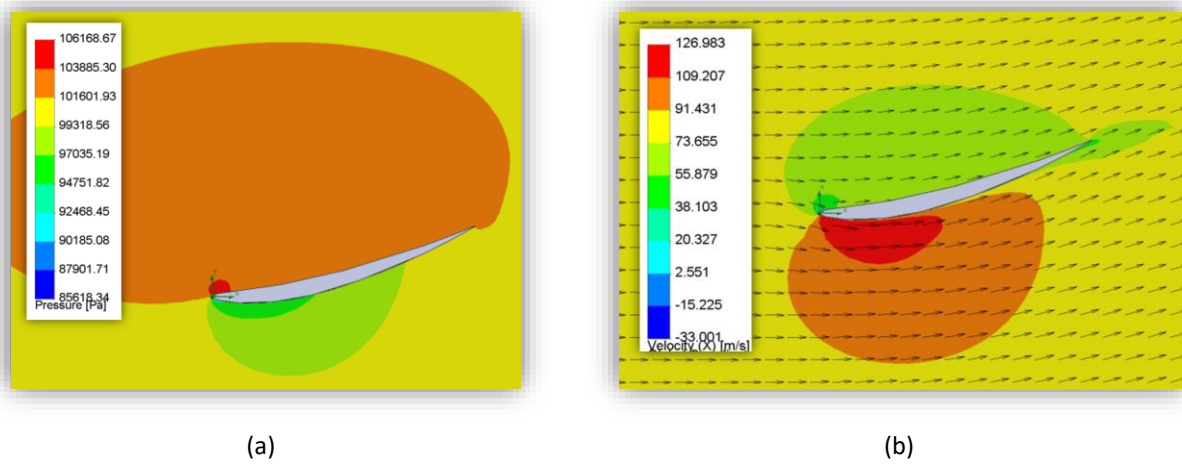


Figure A6 Two cut plots of (a) pressure and (b) velocity for the NACA 6406 airfoil deflector plate.

Shown in Figure A6 are cut plots of pressure and velocity for the NACA 6406 deflector plate. Taken together, the plots agree with Bernoulli since lower velocity on the top concave face of the airfoil causes greater pressure on the top which creates downforce.

8.1.7 Final Design

The aerodynamic goals were achieved in this project. Down force was increased beyond 3.5 times the final weight of the wing and flow was directed around the tires to avoid disturbance of downstream air.

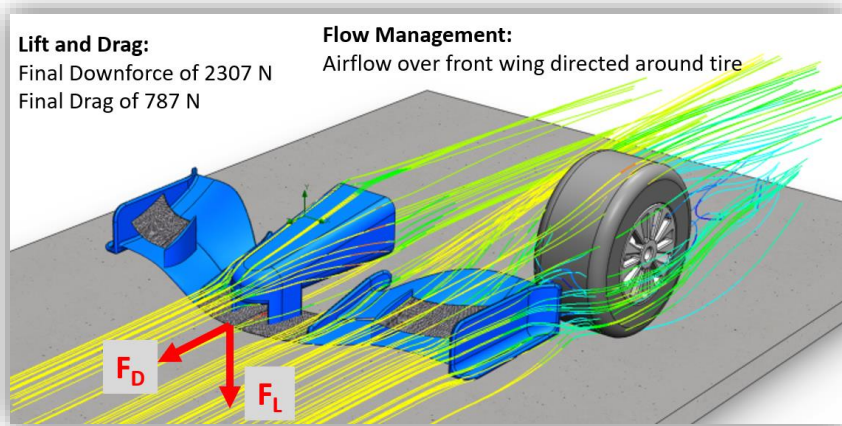


Figure A7 An image of flow trajectory over the final design with summarized goals.

Appendix B: Structural Design of the Front Wing

Completed by Alexander Lin

8.2 Appendix B: Structural of the Front Wing

8.2.1 Initial Design Iteration

8.2.1.1 Lift and Drag Force Calculations

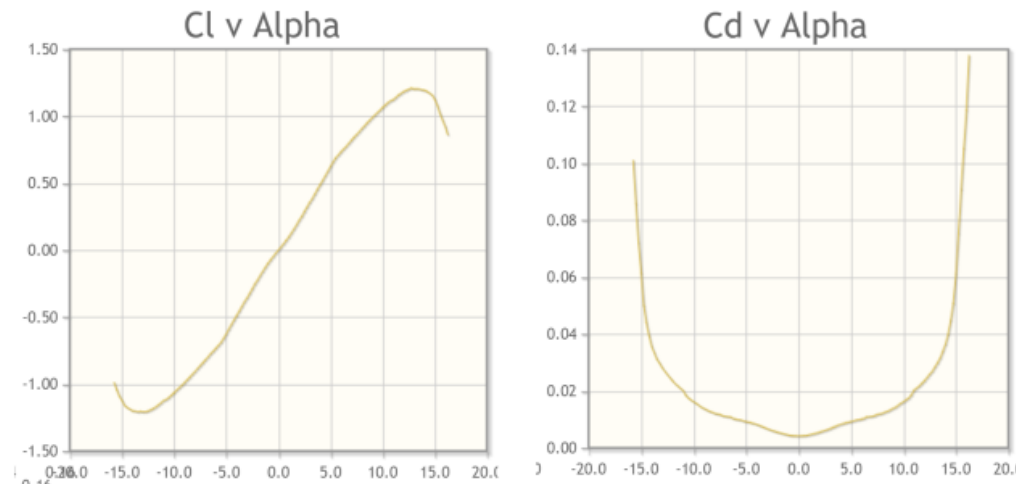
Angle of Attack

$$A := (-15) \text{ deg}$$

Coefficient of Lift and Drag from AirfoilTools.com

$$Cl := -1.25$$

$$Cd := 0.06$$



Figures from: <http://airfoilttools.com/airfoil/details?airfoil=n0009sm-il>

Based on achievable top speed of Formula 1

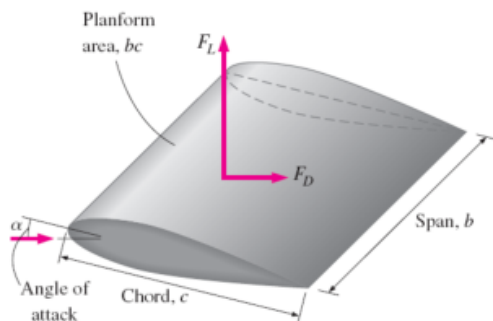
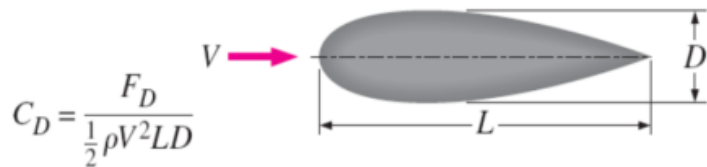
<http://www.need4speed.ws/videos/top-speed-world-record-with-a-formula-1-bar-honda-413-km-h>

Velocity

$$V := 413 \frac{\text{km}}{\text{hr}}$$

Density of Air:

$$\rho := 1.225 \frac{\text{kg}}{\text{m}^3}$$



$$C_L = \frac{F_L}{\frac{1}{2} \rho V^2 A}$$

Y. A. Cengel and J. M. Cimbala,
Fluid Mechanics, Fundamentals and Applications,
New York: McGraw-Hill, 2010.

Total Length of the Base Airfoil:

$$b := 1800 \text{ mm}$$

Chord Length of the Airfoil

$$chord := 500 \text{ mm}$$

Airfoil Width

$$D := chord \cdot 0.09 = 0.045 \text{ m}$$

Lift and Drag Force Across the Full Length of Airfoil

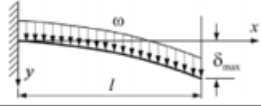
$$F_L := 0.5 \cdot C_L \cdot \rho \cdot V^2 \cdot chord \cdot b = -9068.8813 \text{ N}$$

$$F_D := 0.5 \cdot C_D \cdot \rho \cdot V^2 \cdot D \cdot chord = 10.8827 \text{ N}$$

8.2.1.2 Beam Deflection Calculations

Validation of the SolidWorks simulation deflection output

To validate the model the front wing will be modelled as a cantilever beam to calculate rough deflections to compare to simulation outputs.

3. Cantilever Beam – Uniformly distributed load w (N/m)			
	$\theta = \frac{w l^3}{6 E I}$	$y = \frac{\omega x^2}{24 E I} (x^2 + 6l^2 - 4lx)$	$\delta_{\max} = \frac{\omega l^4}{8 E I}$

Fromm Solidworks Geometry:



The material properties were varied in the simulation. However, for validation aluminum was chosen

$E := 69 \text{ GPa}$

Now plugging in for the max deflection at the tip given the distributed forces calculated from the rough airfoil geometry

$$w := \frac{9.068 \text{ kN}}{L} = 10075.5556 \text{ m Pa}$$

$$\delta := \frac{w \cdot L^4}{8 \cdot E \cdot I_x} = 0.0066 \text{ m}$$

8.2.1.3 Additional Figures

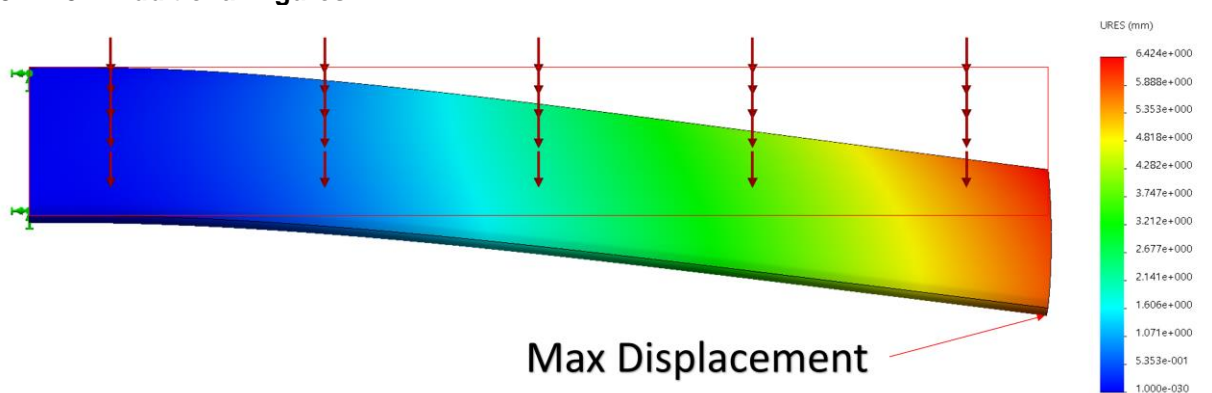


Figure B 1. Displacement distribution of the airfoil. Strong correlation with the calculated deflection indicates that the model is a valid simulation. However, 6 mm, while not large enough to make contact with the track, may be large enough to change the aerodynamic properties of the front wing substantially. This will be taken into consideration in future iterations.

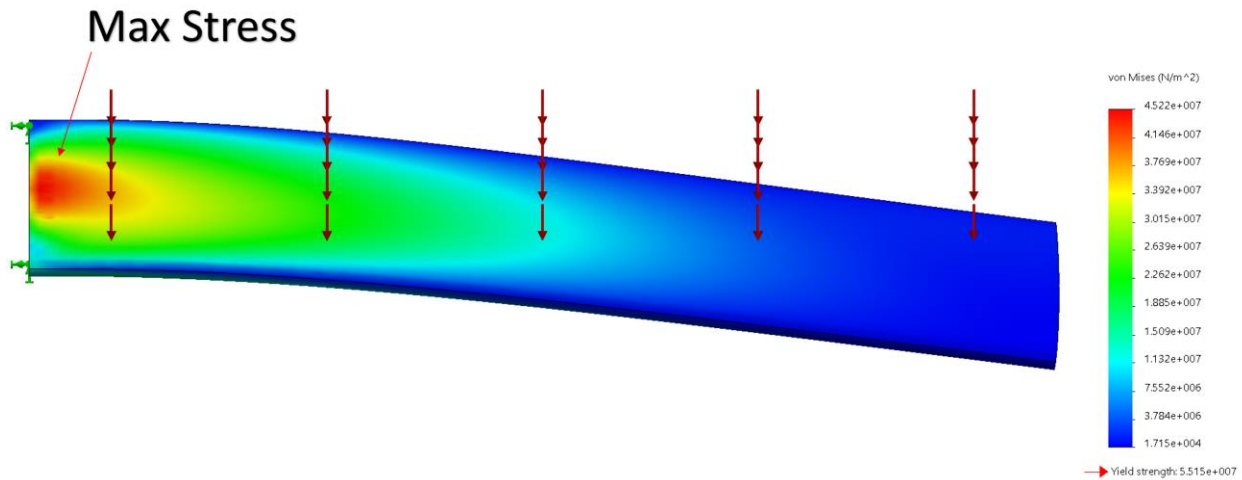


Figure B 2. Stress distribution of the beam, note the change in portrayal angle in order to better illustrate the stress concentration. Mesh analysis showed that this stress concentration is due to having a sharp corner as the result diverged as element sized decreased. However, the model is acceptable as the increase in stress concentration can be identified to be caused by a sharp edge at the boundary.

8.2.2 Second Design Iteration

8.2.2.1 Initial Model from Aerodynamics team

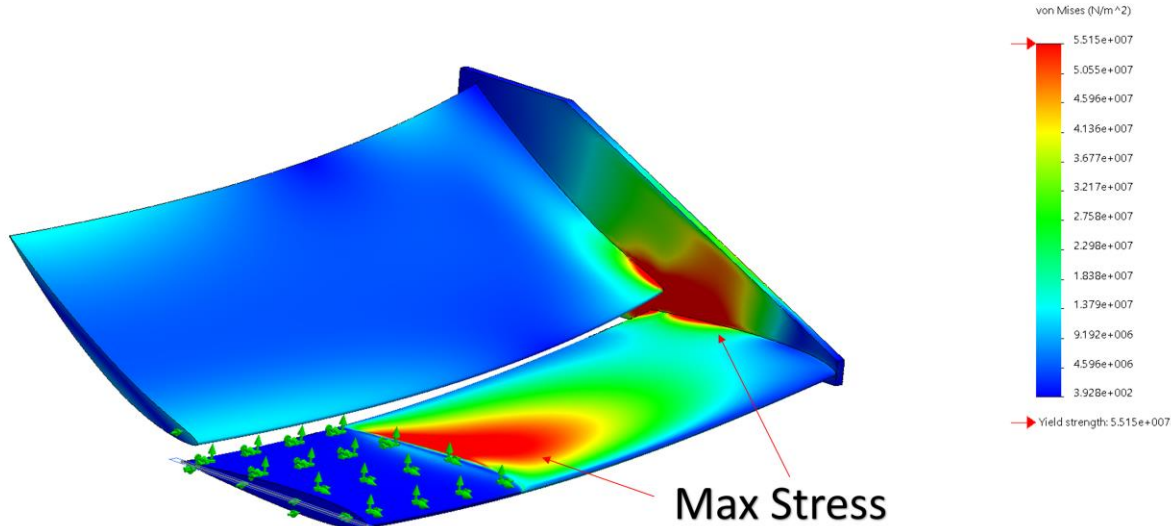


Figure B 3. Depiction of an intermediate iteration that involved the addition of a deflector and end plate. It was noted that the curvature of the deflector plate directed the flow directly into the end plate. This loading caused significant yielding at several points in the plate. Material: aluminum 6061 alloy.

8.2.2.2 Design Studies

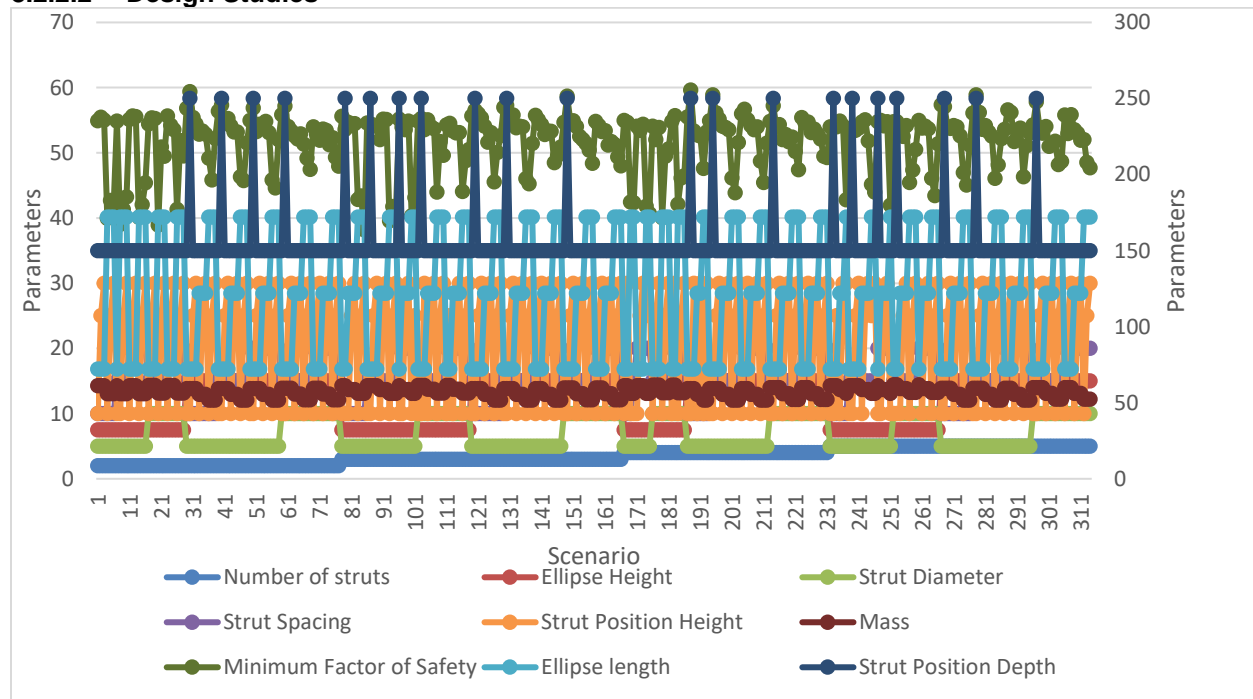


Figure B 4. Initial design study. Over 1200 cases covered. Over 16 hours of simulation time. Overall, illegible. However, FOS remained high throughout the simulations, meaning that the max base airfoil cavity size is acceptable throughout. This allows for the sequential design studies to focus on more specific parameters.

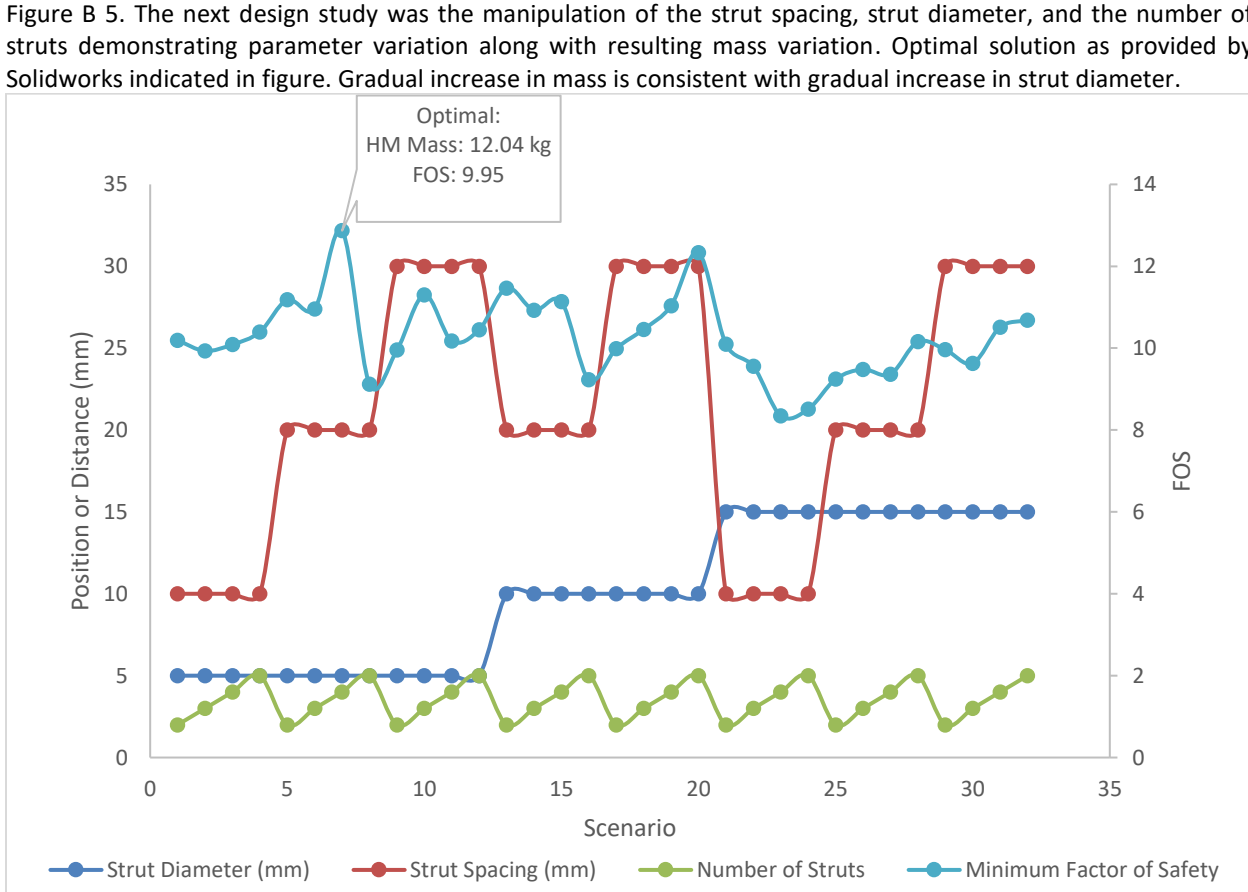
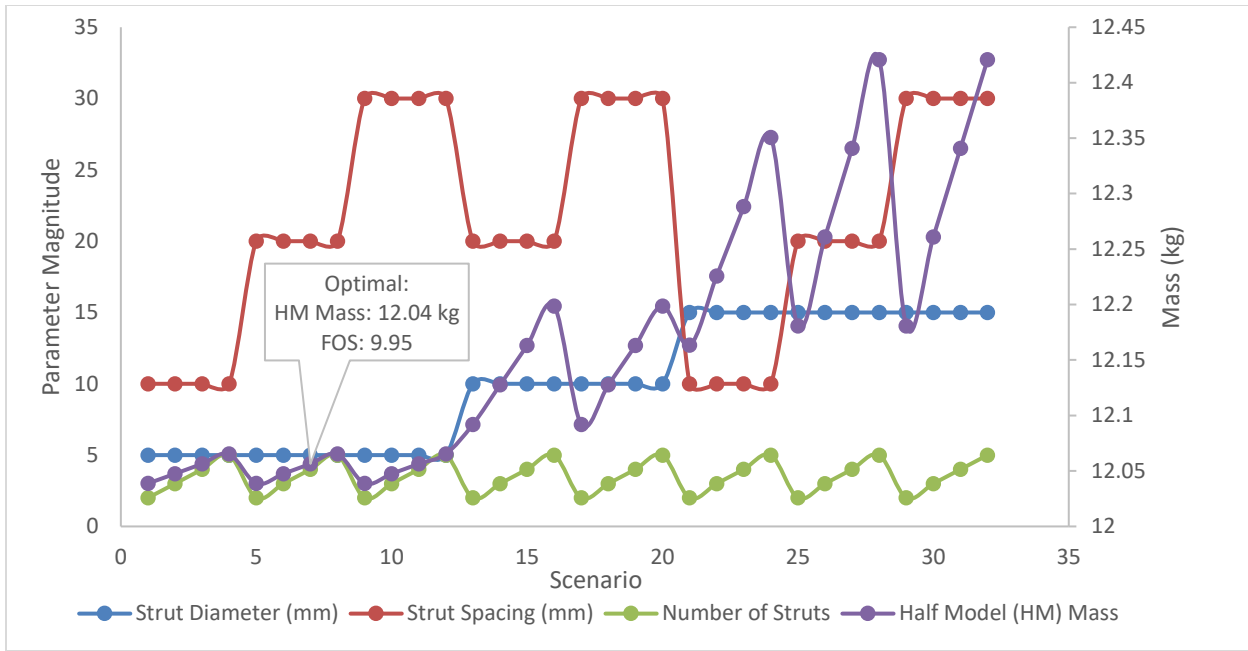


Figure B 6. Design study with the manipulation of the strut spacing, strut diameter, and the number of struts, demonstrating parameter variation along with resulting FOS variation. Optimal solution as provided by Solidworks indicated in figure. Gradual increase in mass is consistent with gradual increase in strut diameter.

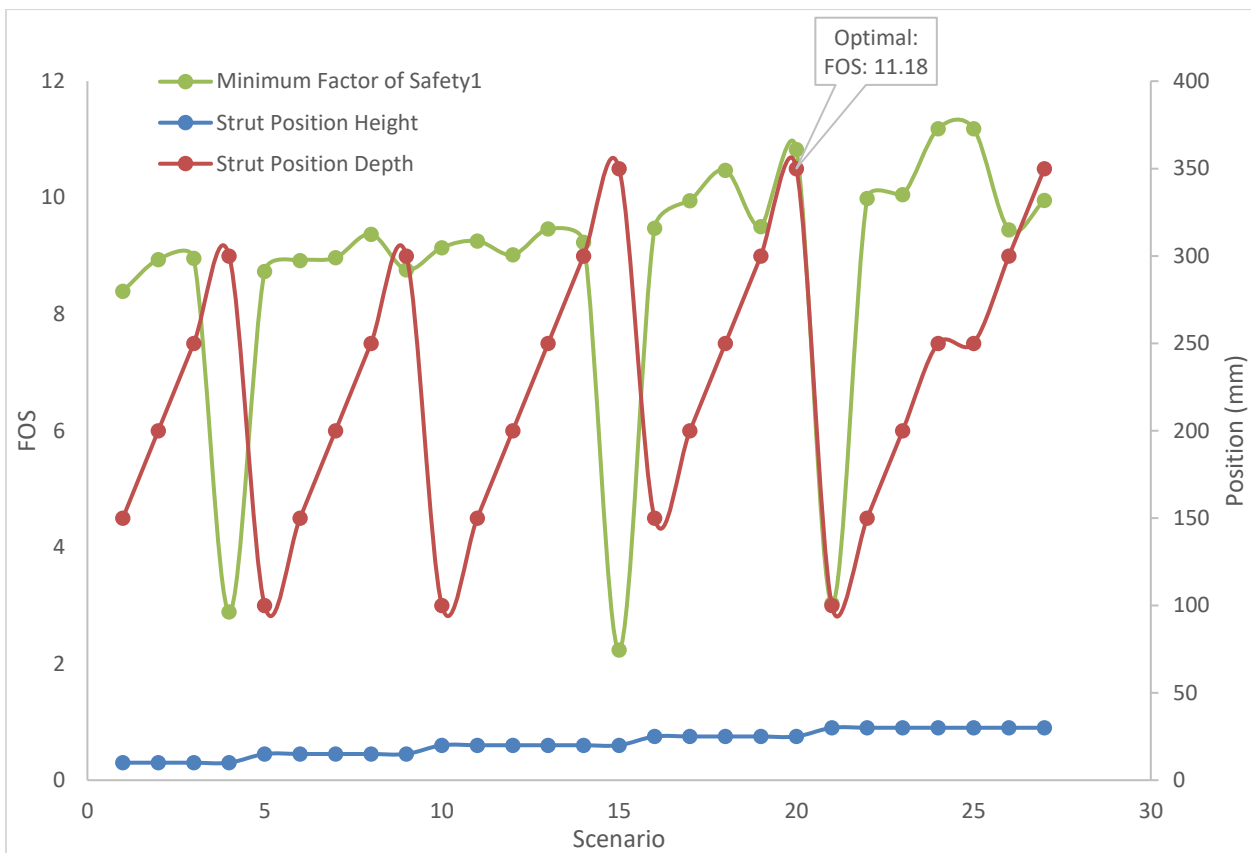


Figure B 7. Design study for placement of the struts. Note that mass is not measured in this design study as it does not vary given that the strut dimensions and number of them are constant. Optimal value for the FOS is thus the largest value observed in the design study as indicated in the figure. Normally the design study shown in Figure B 5 and Figure B 6 would be rerun under the optimal parameters obtained in this design study. Then the strut position study would be run under the newly obtained optimal parameters from the strut dimensions and quantity study and this would repeat until the parameters converged to a single configuration. Alternatively, all five parameters would be run at the same time. However due to the results shown in Figure B 4, this was avoided. There was insufficient time allotted for multiple iterations of design studies to be run, this would be an option for future work.

8.2.2.3 Mesh Dependency

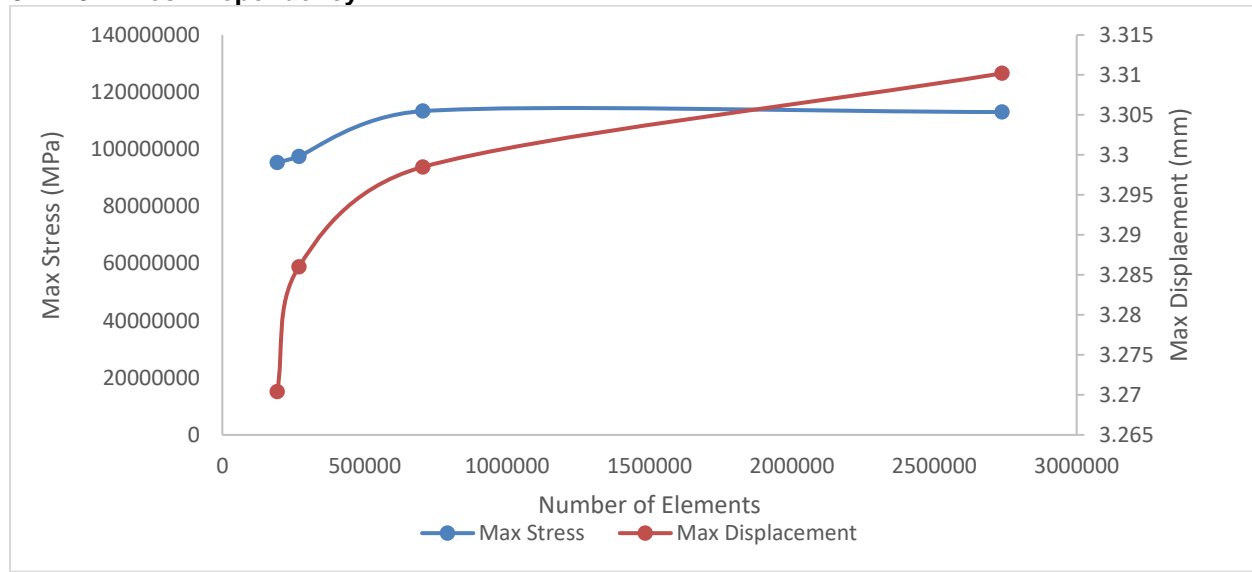


Figure B 8. Mesh dependency for the second iteration of the front wing. Deviations in stress and the displacement of the last two iterations were less than 1 %. Note that the scale distorts the results of the displacement convergence graph.

8.2.3 Final Design Iteration

8.2.3.1 Mesh Dependency

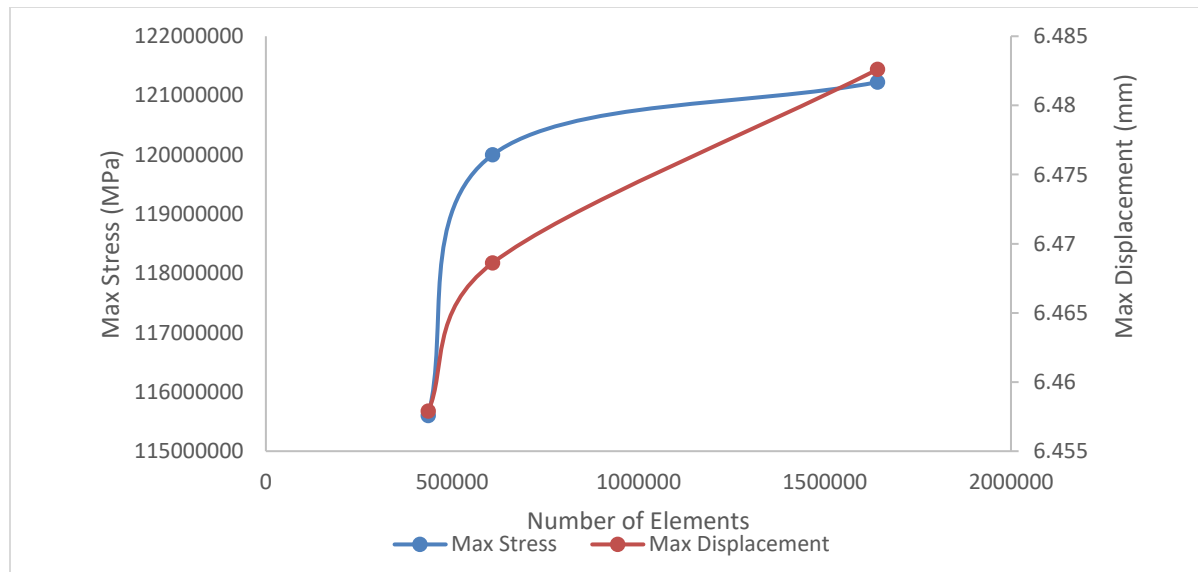


Figure B 9. Mesh dependency for the final iteration of the front wing. Deviations in stress was one percent between the final two tests and the displacement of the last two iterations were less than 1 %. Note that the scale distorts the results of the convergence graph.

Appendix C: Aerodynamics of the Rear Wing

Completed by Anthony Tang

8.3 Appendix C: Aerodynamics of the Rear Wing

8.3.1 Initial Design Iteration

8.3.1.1 Determining Best Airfoil Characteristics

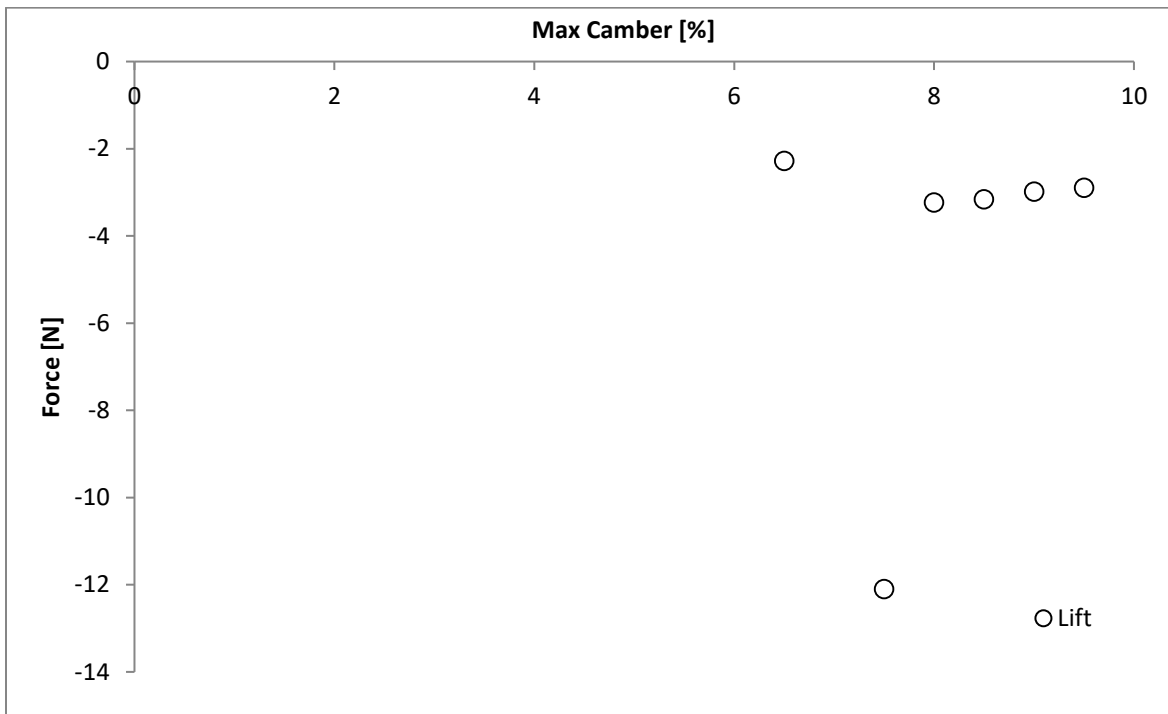


Figure C 1 Lift vs. Max Camber

- The second data point is an outlier

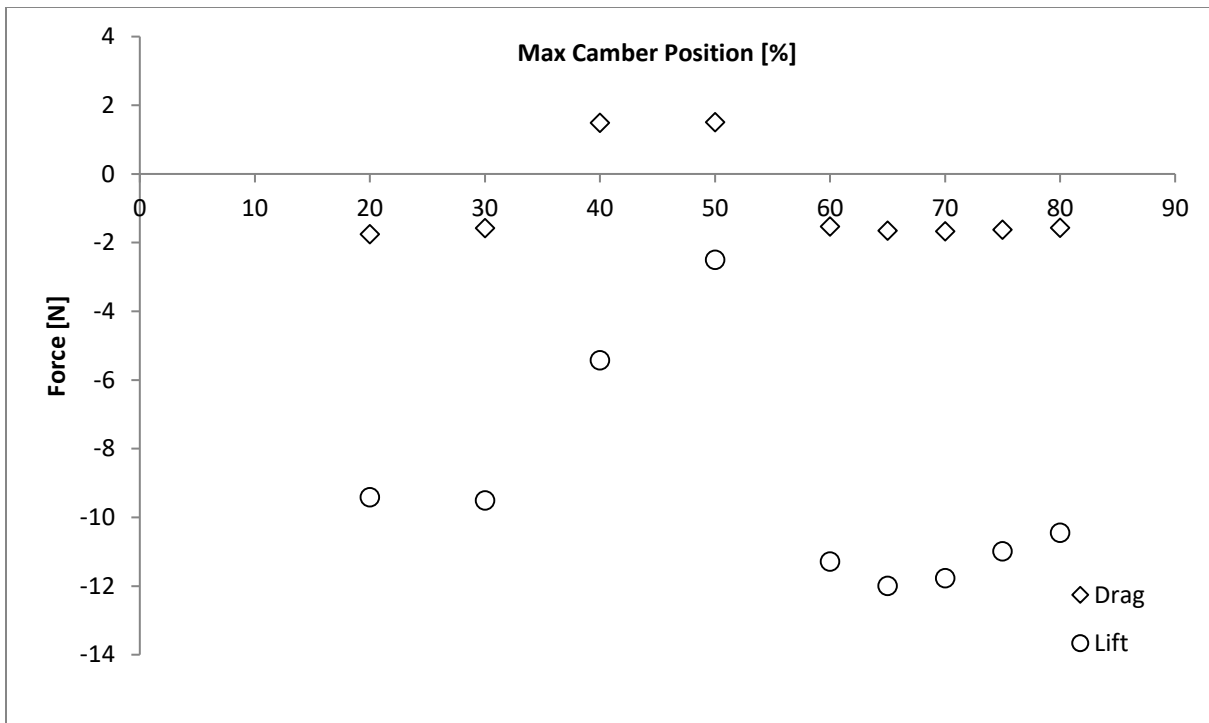


Figure C 2 Lift and Drag vs. Max Camber Position

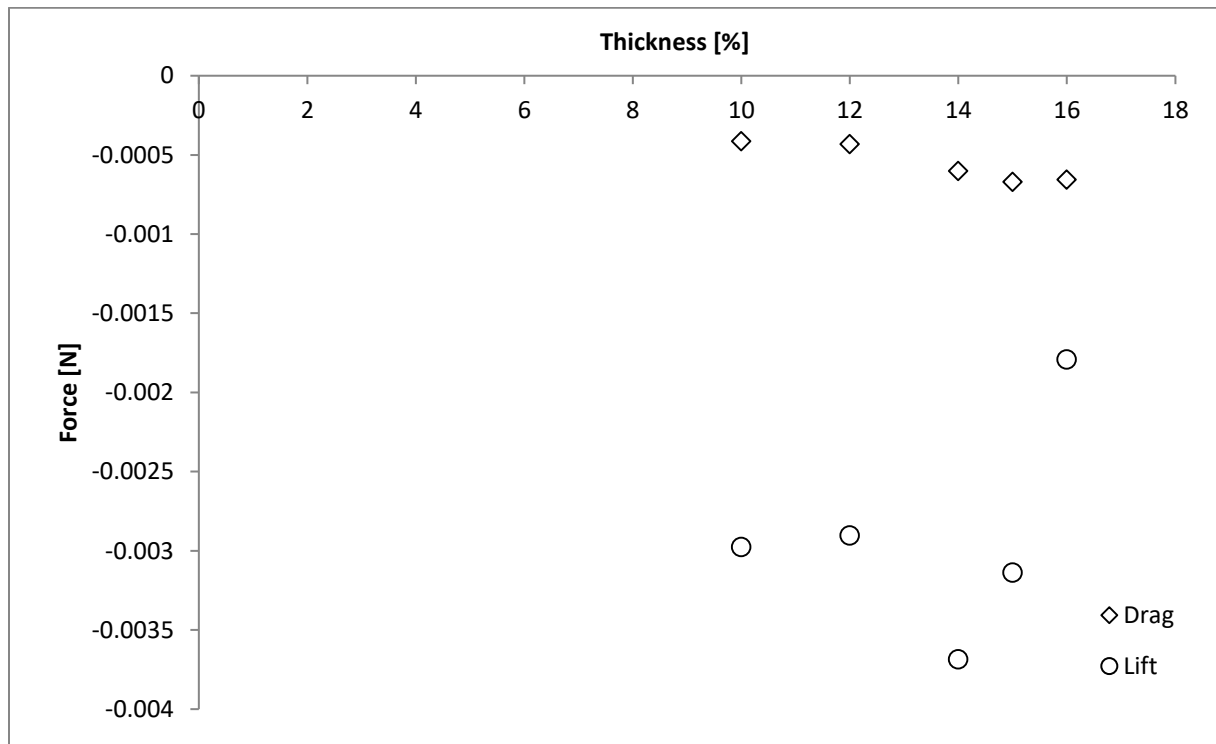


Figure C 3 Lift and Drag vs. Thickness

1.1.1.1 Mesh Convergence Analysis

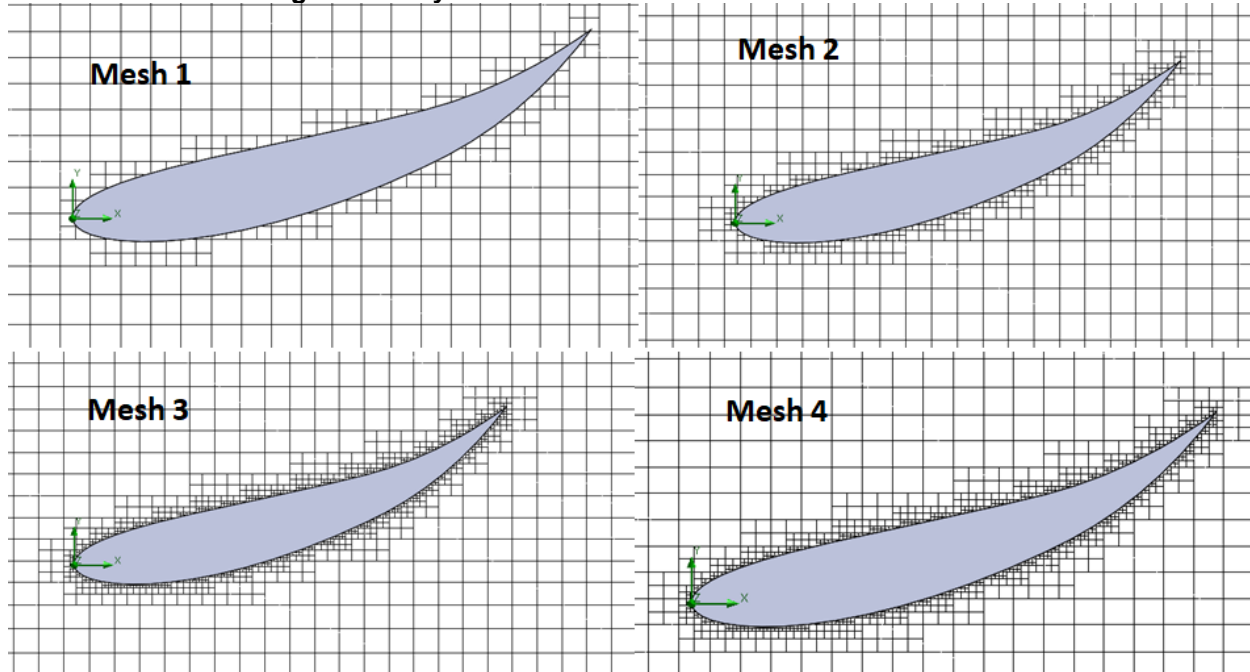


Figure C 4 Visualization of meshes used in initial 2D design iteration

- Lift Coefficient calculation used to observe convergence of solution as mesh was refined
- Equidistant Refinement was used for all Local Meshes, using two shells, and offset distances of 0.2 m and 0.3 m
- Convergent solution (highly agreeable) shown to occur by Mesh No. 3.
-

Table C 1 Summary of results for mesh convergence analysis for initial design iteration

Mesh No.	No. of Fluid Cells	Refining Fluid Cells (level)	Fluid/Solid Boundary (level)	No. of Shells	Initial Mesh (level)	Lift Coefficient	% Difference
1	2736	1	1	2	4	-0.2312	-
2	3949	2	2	2	4	-0.2693	16.50%
3	8626	3	3	2	4	-0.2662	1.16%
4	27042	4	4	2	4	-0.2660	0.08%

- Initial Mesh Level corresponds to the global mesh, which was kept constant throughout the analysis

8.3.2 Second Design Iteration

8.3.2.1 Mesh Convergence Analysis

Table C 2 Summary of results for mesh convergence analysis for second design iteration

Mesh No.	No. of Fluid Cells	Refining Fluid Cells (level)	Fluid/Solid Boundary (level)	No. of Shells	Initial Mesh (level)	Lift (N)	% Difference
1	23799	1	1	2	3	-1108.5234	-
2	56294	1	1	2	4	-1412.1978	27.39%
3	72184	2	2	2	4	-1992.2471	41.07%
4	133842	3	3	2	4	-2065.1380	3.66%
5	377570	4	4	2	4	-2067.3645	0.11%

- Lift was used to observe convergence of solution as mesh was refined
- Equidistant Refinement was used for all Local Meshes, using two shells, and offset distances of 0.2 m and 0.3 m
- Convergent solution (highly agreeable) shown to occur by Mesh No. 4. These settings were used for the final design iteration simulations as well
- Initial Mesh Level corresponds to the global mesh
- The simulation time increase between Mesh No. 4 and 5 was dramatic

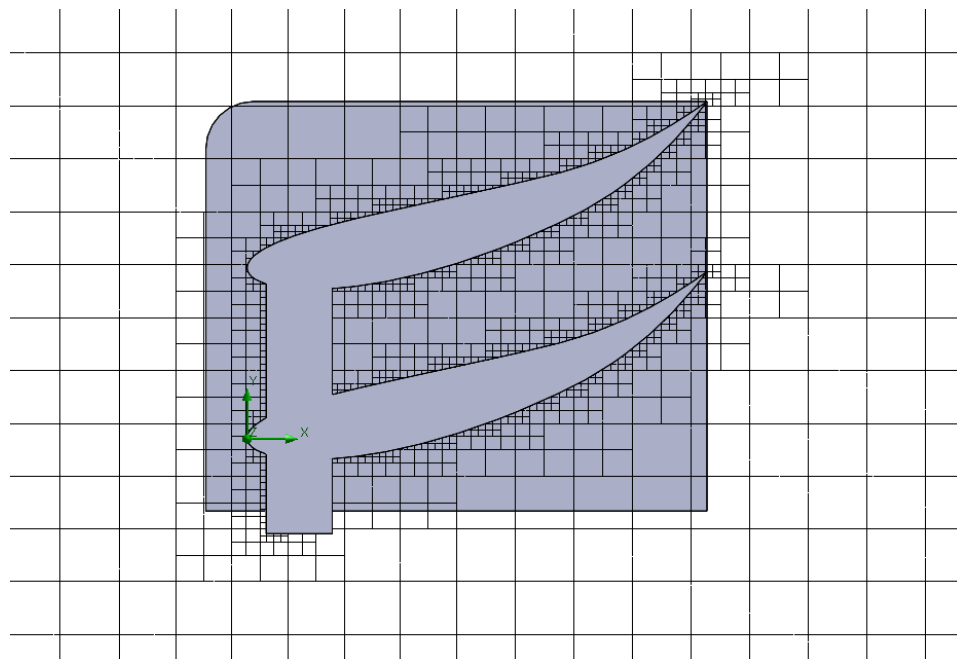
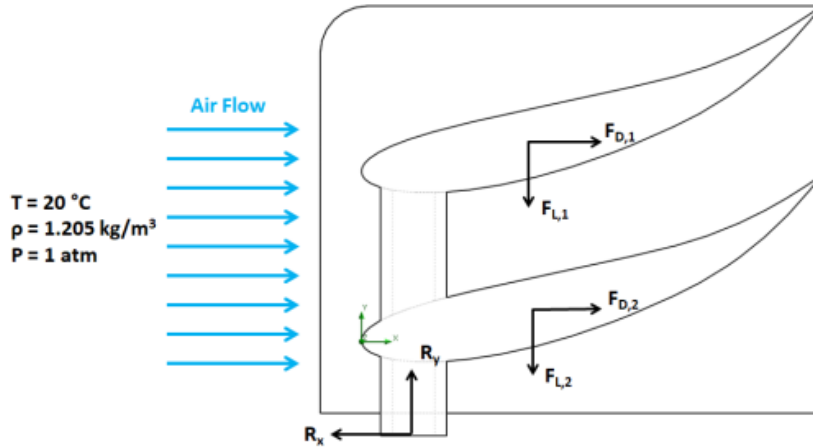


Figure C 5 Visualization of final mesh applied to rear wing

- Mesh Surfaces were filleted front facing surfaces of the single support strut, and the surfaces of each airfoil

8.3.2.2 Validation of Lift and Drag



Assumptions:

- Flow of air before contacting the rear wing is uni-directional
- Lift and drag forces which result from geometry other than the airfoils are ignored in this hand calculation
- The properties of air are shown in the schematic above
- For this iteration of the design, the top and bottom air foils are identical. Therefore, the total forces of lift and drag on the rear wing will be approximated by twice the lift and drag experienced by one airfoil.
- For comparison to the SolidWorks simulation results, the maximum loading scenario will be considered, which occurs when the velocity of air is 300 km/h.
- The lift and drag coefficients were assumed to be 1 and 4 respectively based on values found in textbooks for similar airfoil profiles.

Parameters:

- V is the velocity of air
- L is the chord length of the airfoils
- b is the span of the airfoils
- ρ is the air density
- D is the thickness of the airfoils
- A is the planform area of the airfoils

$$V := 300 \frac{\text{km}}{\text{hr}} = 83.3333 \frac{\text{m}}{\text{s}}$$

$$L := 0.52 \text{ m}$$

$$b := 0.910 \text{ m}$$

$$\rho := 1.205 \frac{\text{kg}}{\left(\text{m}\right)^3}$$

$$D := 0.14 \cdot L = 0.0728 \text{ m}$$

$$A := L \cdot b = 0.4732 \text{ m}^2$$

$$C_D := 4 \quad C_L := 1$$

Calculating Lift and Drag:

$$F_D := C_D \cdot 0.5 \cdot \rho \cdot V^2 \cdot L \cdot D = 633.5622 \text{ N}$$

$$F_L := C_L \cdot 0.5 \cdot \rho \cdot V^2 \cdot A = 1979.8819 \text{ N}$$

- Percent difference compared to simulation results for drag and lift (1200 N and 3880 N respectively) is large, but the values generally exhibit similar ranges of magnitudes.

8.3.3 Final Design Iteration

8.3.3.1 Flow of Final Design

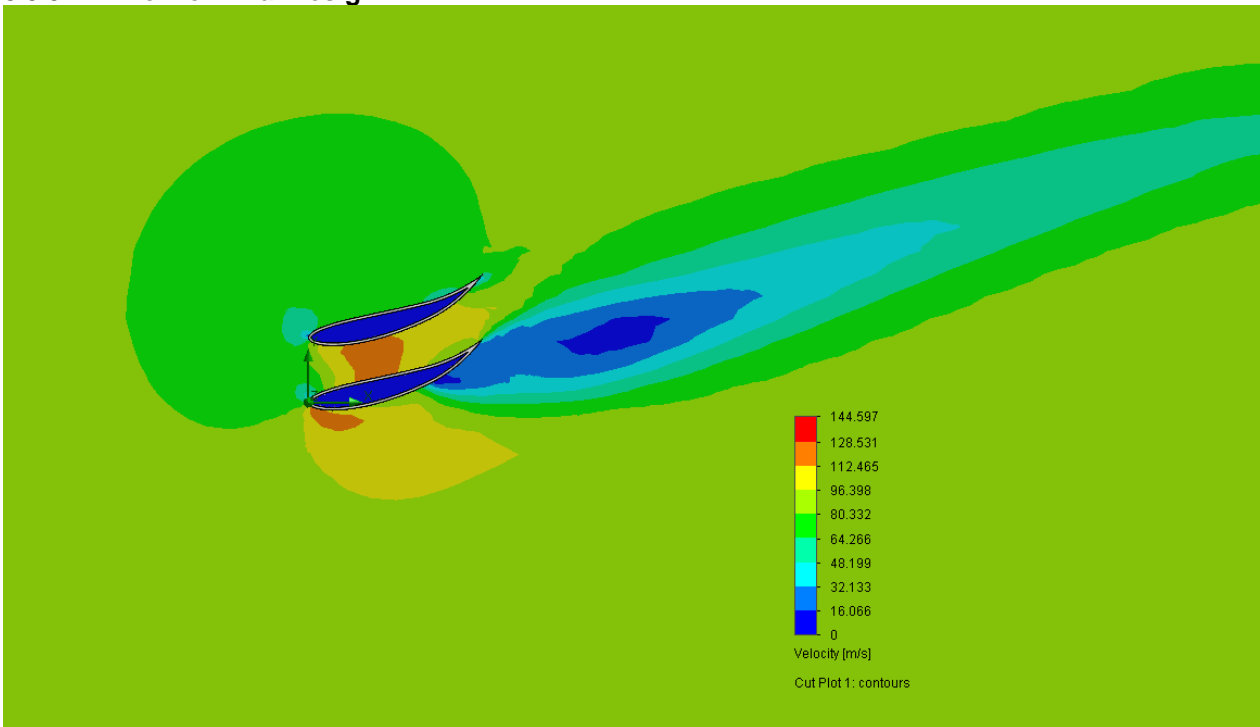


Figure C 6 Velocity cut plot of flow at 300 km/h for final design iteration

- Vortices form primarily beyond the bottom airfoil
- Boundary layer separation does not occur
- High velocity regions between airfoils may reduce negative lift; further iterations may benefit from separating the airfoils even more to reduce interaction, or to reduce the size of the top airfoil

Appendix D: Structural Design of the Rear Wing

Completed by Mellissa Gomez

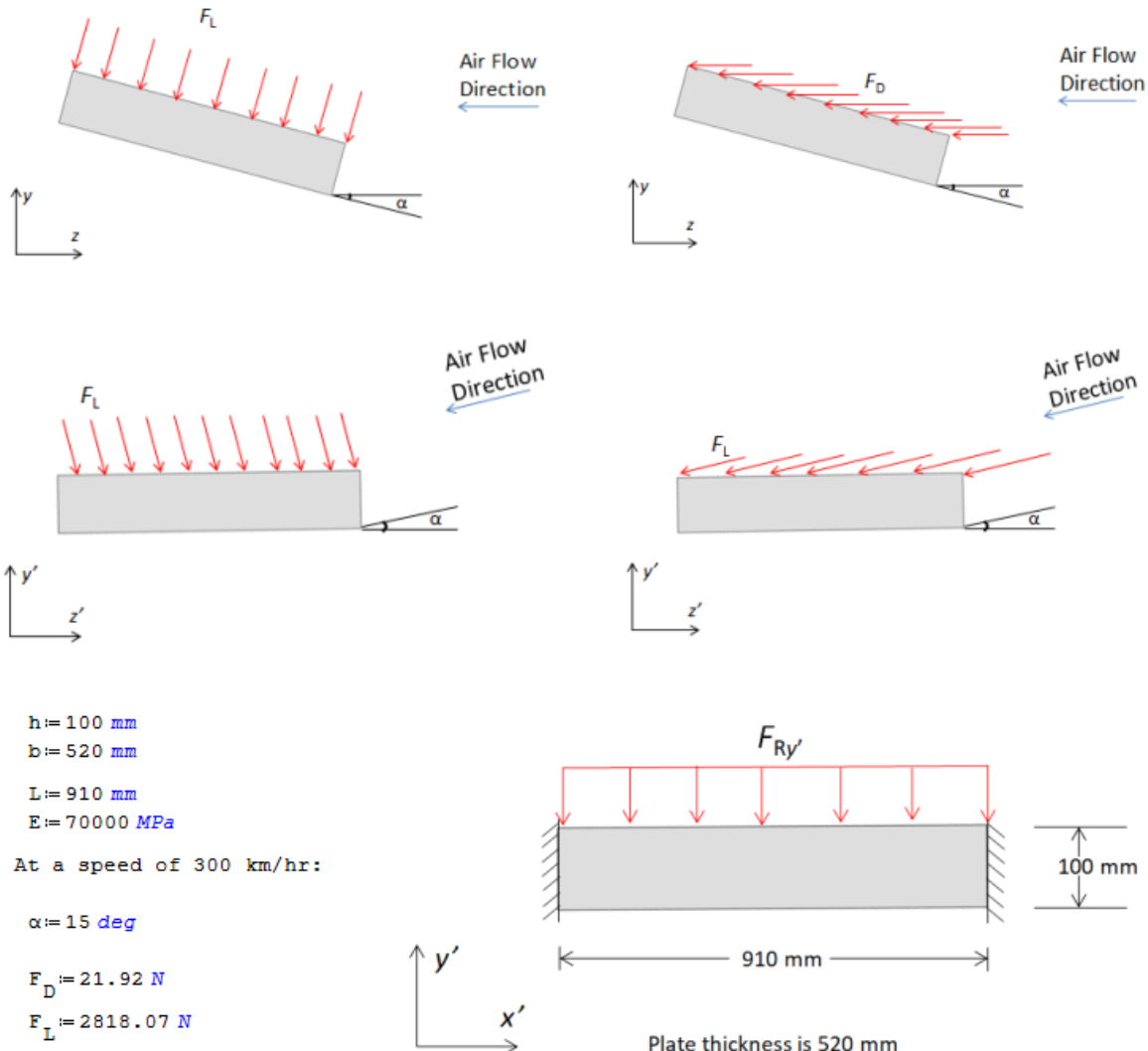
8.4 Appendix D: Structural Analysis of the Rear Wing

8.4.1 Initial Design Iteration

Hand Calculations for Deflection of a Flat Plate in Air Flow

Assumptions:

- Material of the plate is carbon fiber, $E=70000 \text{ MPa}$
- Force exerted by air is constant
- Material properties do not change during loading
- Plate can be approximated beam fixed on both ends that is subjected to a uniform distributed load
- Air is at 15°C



$$I_x := \frac{b \cdot (h^3)}{12} = 4.3333 \cdot 10^{-5} \text{ m}^4$$

$$F_{Ry'} := F_D \cdot (\sin(\alpha)) + F_L \cdot (\cos(\alpha)) = 2727.7199 \text{ N}$$

$$\delta_{\max} := \frac{F_{Ry'} \cdot (L^3)}{384 \cdot E \cdot I_x} = 0.0018 \text{ mm}$$

Table D. 1 Summary of calculated drag and lift forces when air velocity is 300 km/h for an inclined flat plate at various degrees of angle of attack

Angle of Attack α	C_D	C_L	A_D	A_L	Velocity (km/h)	
					300	
					F_D (N)	F_L (N)
3	0.0063	0.30	0.116	0.473	3.10	603.8
6	0.0071	0.60	0.140	0.473	4.24	1207.7
9	0.0096	0.90	0.164	0.473	6.71	1811.5
12	0.0129	1.20	0.187	0.473	10.27	2415.4
15	0.0245	1.40	0.210	0.473	21.92	2818.1
18	0.228	1.25	0.233	0.474	225.47	2517.8

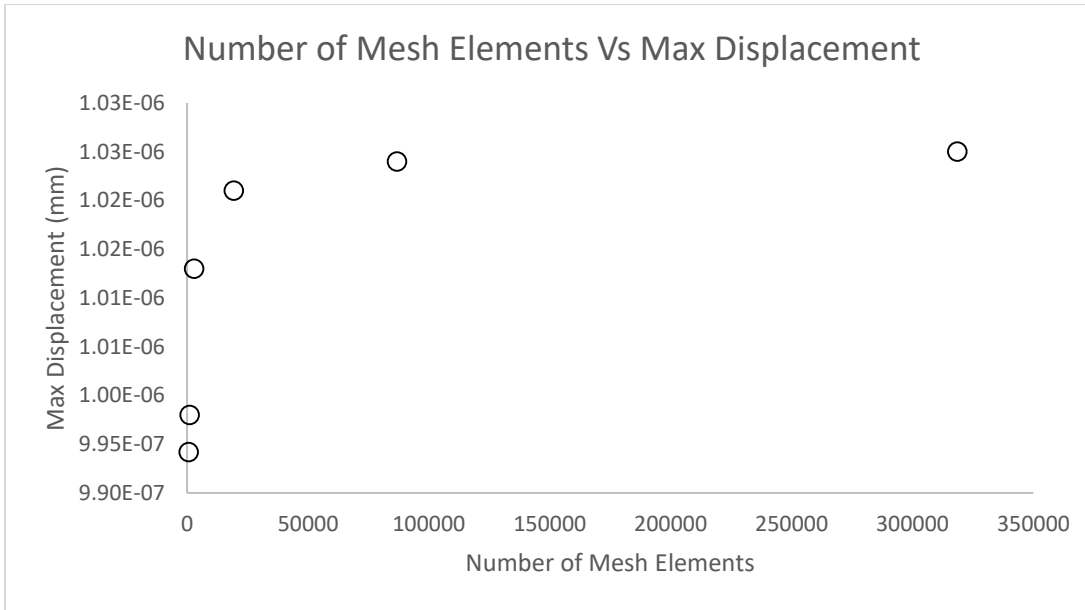


Figure D. 1 Graph displaying manual convergence for the mesh used in simulation of the initial iteration of the rear wing

8.4.2 Second Design Iteration

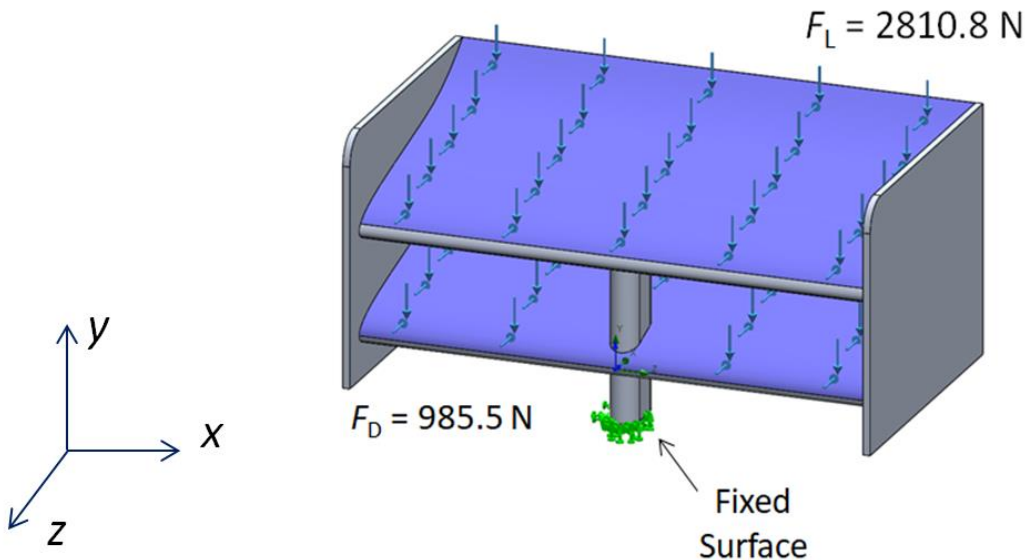


Figure D. 2 Annotated figure of the loading conditions for simulation set up for the second iteration. Forces act as a distributed load over the top surfaces of the airfoils. It should be noted that the negative force lift acts only in the y direction, and the drag force acts only in the z direction

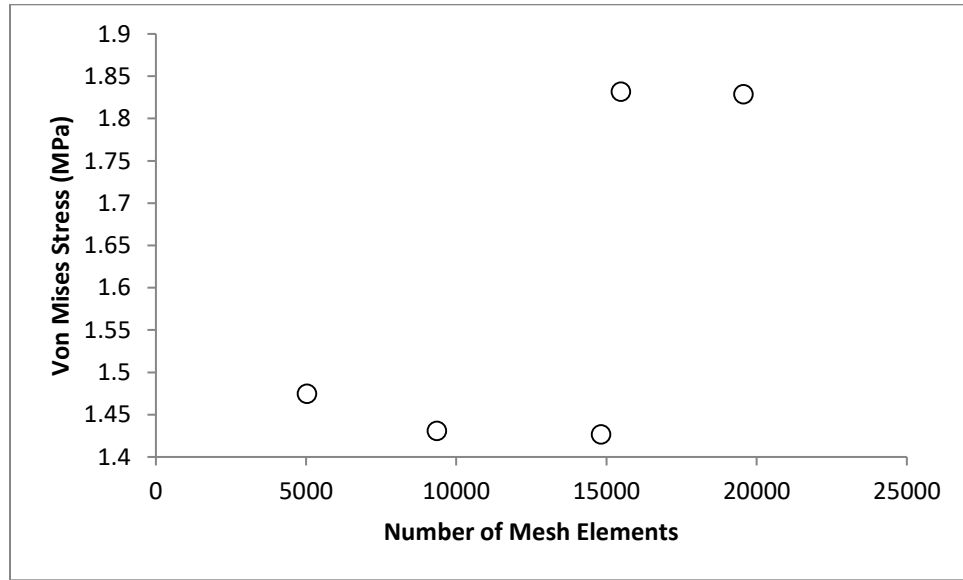


Figure D. 3 Graph displaying manual convergence for the mesh used in simulation of the second iteration of the rear wing

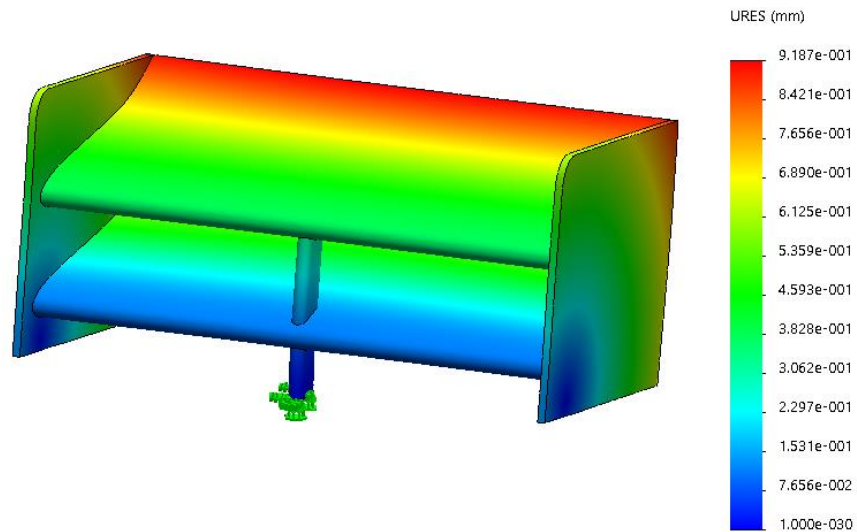


Figure D. 4 SOLIDWORKS FEA simulation results displaying displacement distribution plot for the initial second iteration of the rear wing when subjected to air forces

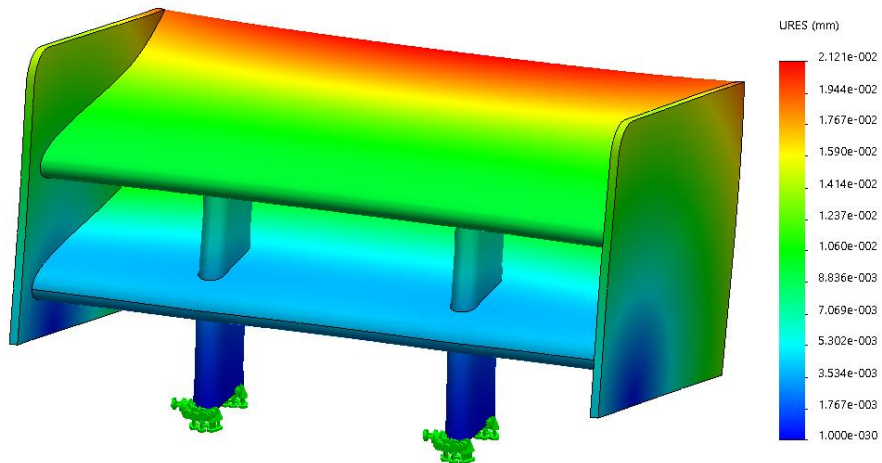


Figure D. 5 SOLIDWORKS FEA simulation results displaying displacement distribution plot for the optimized second iteration of the rear wing when subjected to air forces

8.4.3 Third Design Iteration

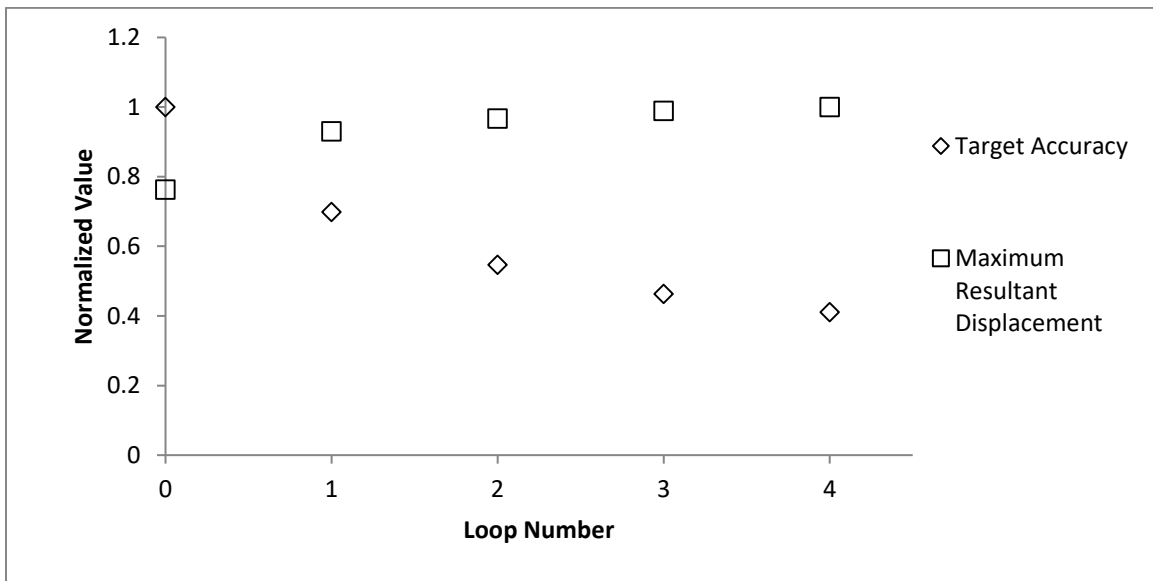


Figure D. 6 H-Adaptive convergence graph for mesh analysis of the third iteration of the rear wing design

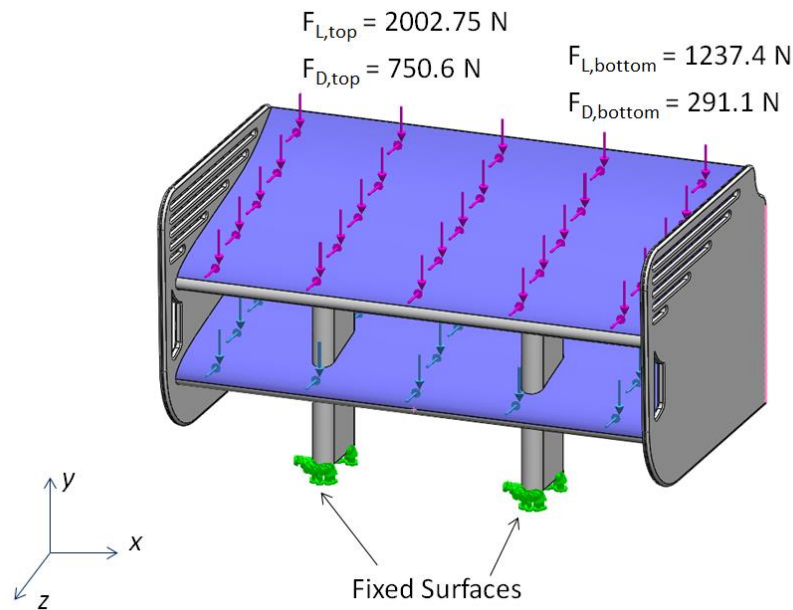


Figure D. 7 Annotated figure of the loading conditions for the simulation set up for the third iteration. Forces act as a distributed load over the top surfaces of the airfoils. It should be noted that the forces acting on the top airfoil are different than the forces acting on the bottom airfoil

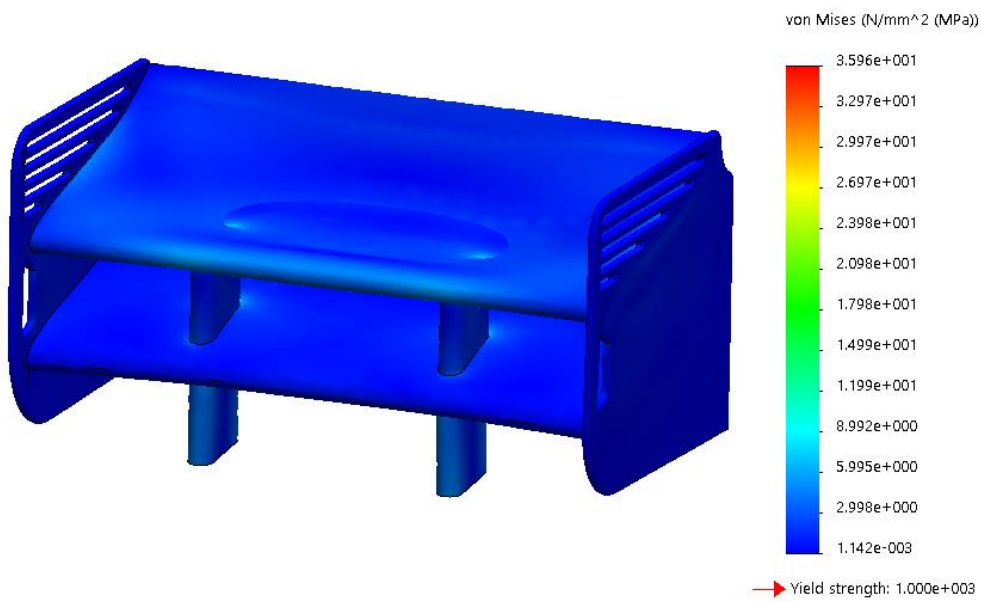


Figure D. 8 SOLIDWORKS FEA simulation results displaying stress distribution plot for the third iteration of the rear wing when subjected to air forces

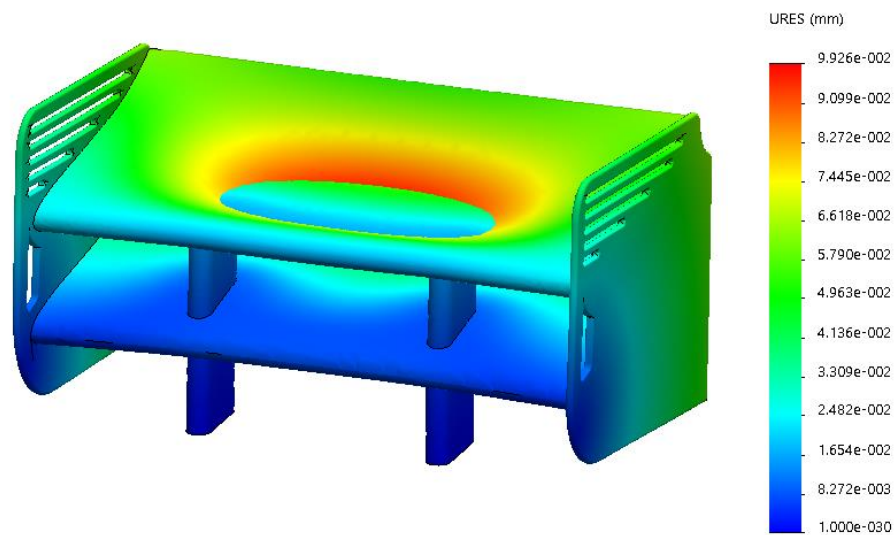


Figure D. 9 SOLIDWORKS FEA simulation results displaying displacement distribution plot for the third iteration of the rear wing when subjected to air forces

Appendix E: Aerodynamics and Heat Transfer of the Side Pod

Completed by Daniel Guenter

8.5 Appendix E: Aerodynamics and Heat Transfer of the Side Pod

8.5.1 Initial Design Iteration

Engine Heat Rejection to Coolant of an F1 Car

Calculation by: Daniel Guenter and Trysten Den Hartog

Known parameters

Engine Parameters

$$P := 650 \text{ hp} \quad \text{Max Power output}$$

$$V_1 := \frac{1.6}{6} L = 0.267 L \quad \text{Displacement of a V6 F1 engine}$$

$$\omega := 15000 \text{ rpm} \quad \text{Engine speed at max power output}$$

$$\Phi := 0.9 \quad \text{Equivalence ratio at max load}$$

$$r_v := 17 \quad \text{Compression ratio of an F1 Engine}$$

Environment conditions

$$P_1 := 1 \text{ bar} \quad \text{Ambient Pressure}$$

$$T_1 := 300 \text{ K} \quad \text{Ambient Temperature}$$

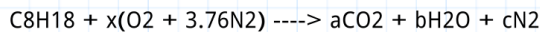
$$R := 8.324 \cdot 10^{-3} \frac{\text{kg} \cdot \text{m}^2}{\text{s}^2 \cdot \text{K}^2 \cdot \text{mol}}$$

Assumptions

- Iso octane (C8H18) used as fuel
- Engine is wide open throttle (WOT, $\eta_v := 1$)
- Cycle is approximated as otto cycle

Calculation

Stoichiometric combustion of Iso-octane:



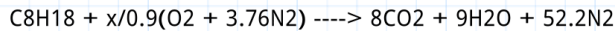
$$\text{C: } a := 8$$

$$\text{H: } b := 9$$

$$\text{O: } x := 12.5$$

$$\text{N: } c := x \cdot 3.76 = 47$$

Actual estimated combustion:



Looking for temperature after compression (T_2). Need to approximate and iterate. Start with
 $\gamma = 1.4$

$$\gamma_1 := 1.4$$

$$T_2 := T_1 \cdot (r_v)^{\gamma_1 - 1} = 931.753 \text{ K}$$

$$H_{P1} := -27.85 \frac{\text{J}}{\text{mol} \cdot \text{K}}$$

$$H_{P2} := -226.489 \frac{\text{J}}{\text{mol} \cdot \text{K}}$$

$$C_{P,P} := \frac{H_{P1} - H_{P2}}{T_2 - T_1} = 0.314 \frac{\text{kg} \cdot \text{m}^2}{\text{s}^2 \cdot \text{K}^2 \cdot \text{mol}}$$

$$H_{air1} := 19.4192 \frac{\text{J}}{\text{mol} \cdot \text{K}}$$

$$H_{air2} := 0 \frac{\text{J}}{\text{mol} \cdot \text{K}}$$

$$C_{P,air} := \frac{H_{air1} - H_{air2}}{T_2 - T_1} = 0.031 \frac{\text{kg} \cdot \text{m}^2}{\text{s}^2 \cdot \text{K}^2 \cdot \text{mol}}$$

$$C_{p,mix} := \left(\frac{1}{1 + \frac{12.5}{.9} (4.76)} \right) C_{P,P} + \frac{66.11}{67.11} (C_{P,air}) = 0.035 \frac{\text{kg} \cdot \text{m}^2}{\text{s}^2 \cdot \text{K}^2 \cdot \text{mol}}$$

$$\gamma_{mix} := \frac{C_{p,mix}}{C_{p,mix} - R} = 1.312$$

$$T_2 := T_1 \cdot r_v^{\gamma_{mix} - 1} = 727.053 \text{ K}$$

Created with PTC Mathcad Express. See www.mathcad.com for more information.

Assuming an ideal perfect gas, pressure at state 1 and 2 can be related

$$P_2 := P_1 \cdot \left(\frac{T_2}{T_1} \right) \cdot r_v = (4.12 \cdot 10^3) \text{ kPa}$$

Assumed constant-volume combustion (adiabatic):
Internal energy of reactants must equal internal energy of products

$$U_{R1} := -107.6 \cdot 10^6 \text{ J}$$

$$U_{R2} := 66.11 \cdot 6.78 \cdot 10^6 \text{ J} = (4.482 \cdot 10^8) \text{ J}$$

$$U_{R,sum} := U_{R1} + U_{R2} = (3.406 \cdot 10^8) \text{ J}$$

Temperature of products needs to be guessed first:

$$T_p := 3000 \text{ K}$$

$$U_{P1} := 8 \cdot (-265.564) \cdot 10^6 \text{ J} = -2.125 \cdot 10^9 \text{ J}$$

$$U_{P2} := 9 \cdot (-140.410) \cdot 10^6 \text{ J} = -1.264 \cdot 10^9 \text{ J}$$

$$U_{P3} := 1.39 \cdot (73.172) \cdot 10^6 \text{ J} = (1.017 \cdot 10^8) \text{ J}$$

$$U_{P4} := 52.2 \cdot (67.811) \cdot 10^6 \text{ J} = (3.54 \cdot 10^9) \text{ J}$$

$$U_{P,sum1} := U_{P1} + U_{P2} + U_{P3} + U_{P4} = (2.532 \cdot 10^8) \text{ J}$$

Products internal energy does not equal reactants. New guess for temperature is made:

$$T_p := 3100 \text{ K}$$

$$U_{P1} := 8 \cdot (-260.160) \cdot 10^6 \text{ J} = -2.081 \cdot 10^9 \text{ J}$$

$$U_{P2} := 9 \cdot (-135.656) \cdot 10^6 \text{ J} = -1.221 \cdot 10^9 \text{ J}$$

$$U_{P3} := 1.39 \cdot (76.345) \cdot 10^6 \text{ J} = (1.061 \cdot 10^8) \text{ J}$$

$$U_{P4} := 52.2 \cdot (70.689) \cdot 10^6 \text{ J} = (3.69 \cdot 10^9) \text{ J}$$

Created with PTC Mathcad Express. See www.mathcad.com for more information.

$$U_{P,sum2} := U_{P1} + U_{P2} + U_{P3} + U_{P4} = (4.939 \cdot 10^8) \text{ J}$$

To equal the internal energies, interpolation of the two temperature guesses must be done.

$$T_P := \frac{(3100 - 3000)}{(U_{P,sum2} - U_{P,sum1})} \cdot (U_{R,sum} - U_{P,sum1}) + 3000 = 3.036 \cdot 10^3$$

$$T_3 := 3036 \text{ K}$$

Assuming an ideal perfect gas, pressure at state 2 and 3 can be related since there is no change in volume.

$$P_3 := P_2 \cdot \left(\frac{T_3}{T_2} \right) \cdot \left(\frac{8 + 9 + 1.39 + 52.2}{66.11 + 1} \right) = (1.81 \cdot 10^7) \text{ Pa}$$

Initial guess of $\gamma := 1.4$ is made to estimate the exhaust temperature

$$T_4 := T_3 \cdot \left(\frac{1}{r_v} \right)^{\gamma-1} = 977.512 \text{ K}$$

$$c_{p,CO2} := \frac{((-361.318) - (-238.342)) \cdot 10^3}{T_4 - T_3} \frac{\text{J}}{\text{mol}} = 59.741 \frac{\text{J}}{\text{mol} \cdot \text{K}}$$

$$c_{p,H2O} := \frac{((-216.318) - (-112.757)) \cdot 10^3}{T_4 - T_3} \frac{\text{J}}{\text{mol}} = 50.309 \frac{\text{J}}{\text{mol} \cdot \text{K}}$$

$$c_{p,O2} := \frac{((21.929) - (99.583)) \cdot 10^3}{T_4 - T_3} \frac{\text{J}}{\text{mol}} = 37.724 \frac{\text{J}}{\text{mol} \cdot \text{K}}$$

$$c_{p,N2} := \frac{(20.730) - (93.974)) \cdot 10^3}{T_4 - T_3} \frac{\text{J}}{\text{mol}} = 35.581 \frac{\text{J}}{\text{mol} \cdot \text{K}}$$

$$c_{p,exhaust} := \left(\frac{1}{8 + 9 + 1.39 + 52.2} \right) \cdot (8 \cdot c_{p,CO2} + 9 \cdot c_{p,H2O} + 1.39 \cdot c_{p,O2} + 52.2 \cdot c_{p,N2})$$

Created with PTC Mathcad Express. See www.mathcad.com for more information.

$$c_{p,exhaust} = 40.239 \frac{J}{mol \cdot K}$$

$$R := 8.314 \frac{J}{mol \cdot K}$$

$$\gamma_{exhaust} := \frac{c_{p,exhaust}}{(c_{p,exhaust} - R)} = 1.26$$

The exhaust temperature is therefore:

$$T_4 := T_3 \cdot \left(\frac{1}{r_v} \right)^{\gamma_{exhaust} - 1} = (1.452 \cdot 10^3) K$$

$$T_4 := 1452 K$$

Assume an isobaric (constant-pressure) combustion reaction to determine heat loss through exhaust:

$$H_{R,fuel} := -223.66 \cdot 10^6 J$$

$$H_{R,air} := 0 J$$

$$H_{P,CO2} := 8 \cdot (-334.65) \cdot 10^6 J = -2.677 \cdot 10^9 J$$

$$H_{P,H2O} := 9 \cdot (-195.942) \cdot 10^6 J = -1.763 \cdot 10^9 J$$

$$H_{P,O2} := 1.39 \cdot (38.825) \cdot 10^6 J = (5.397 \cdot 10^7) J$$

$$H_{P,N2} := 52.2 \cdot (36.718) \cdot 10^6 J = (1.917 \cdot 10^9) J$$

$$H_{P,sum} := H_{P,CO2} + H_{P,H2O} + H_{P,O2} + H_{P,N2} = -2.47 \cdot 10^9 J$$

Created with PTC Mathcad Express. See www.mathcad.com for more information.

The amount of heat lost through the exhaust is (per kmol of fuel):

$$Q_{exhaust} := -(H_{P,sum} - H_{R,fuel}) = (2.246 \cdot 10^9) \text{ J}$$

$$Q_{exhaust} := 2.246 \cdot 10^6 \frac{\text{J}}{\text{mol}}$$

$$V_s := \frac{\pi}{4} \cdot (98 \text{ mm})^2 \cdot 64.9 \text{ mm} = 0.49 \text{ L}$$

$$V_1 := \frac{V_s}{1 - \frac{1}{r_v}} = 0.52 \text{ L}$$

$$N_{mix} := \frac{P_1 \cdot V_1}{R \cdot T_1} = 0.021 \text{ mol}$$

$$N_{fuel} := N_{mix} \cdot \left(\frac{1}{14.89} \right) = 0.001 \text{ mol}$$

$$Q_{net} := Q_{exhaust} \cdot N_{fuel} = (3.146 \cdot 10^3) \text{ J}$$

$$Q_{rate,exhaust} := Q_{net} \cdot 15000 \cdot \frac{1}{60 \text{ s}} \cdot \frac{1}{2} = (3.932 \cdot 10^5) \frac{\text{J}}{\text{s}}$$

$$Q_{rate,exhaust} = 527.285 \text{ hp}$$

Created with PTC Mathcad Express. See www.mathcad.com for more information.

This is the amount of energy being lost through the exhaust. To determine the amount of heat that is dissipated to the cylinder walls of the engine (amount of heat that needs to be cooled), the following was assumed:

$$Q_{rate.mechanical} := 650 \text{ hp} \quad \eta_{overall} := 30\%$$

$$Q_{rate.energylost} := \frac{Q_{rate.mechanical}}{(\eta_{overall})} - Q_{rate.mechanical} = (1.517 \cdot 10^3) \text{ hp}$$

The heat rate loss due to incomplete combustion (IC) is approximately 15%.

$$Q_{rate.IC} := 0.15 \cdot Q_{rate.energylost} = 169.647 \text{ kW}$$

The heat rate loss due to miscellaneous losses (oil, gearbox inefficiency, hydraulics, etc.) is approximately 15%.

$$Q_{rate.misc} := 0.15 \cdot Q_{rate.energylost} = 169.647 \text{ kW}$$

$$Q_{rate.cooling} := Q_{rate.energylost} - (Q_{rate.exhaust} + Q_{rate.IC} + Q_{rate.misc})$$

$$Q_{rate.cooling} = 534.382 \text{ hp}$$

$$Q_{rate.cooling} = 398.488 \text{ kW}$$

The maximum amount of heat required to be cooled by the heat exchanger is given by the above value when the engine power output is 650hp.

Created with PTC Mathcad Express. See www.mathcad.com for more information.

Table E. 1 Table of car Dyno data and heat dissipation to radiator

Power (kW)	Car Speed (km/h)	Speed (m/s)	Heat Dissipated Tailpipe (kW)	Heat Dissipated Radiator (kW)	Heat Dissipated per Radiator (W)
82	35.5	9.9	66.9	67.8	33899
96	47.9	13.3	78.1	79.2	39578
114	58.6	16.3	92.5	93.8	46879
140	65.6	18.2	113.3	114.9	57426
163	74.5	20.7	132.5	134.3	67161
181	79.8	22.2	146.9	148.9	74462
197	86.7	24.1	159.8	161.9	80952
215	92.5	25.7	174.2	176.5	88253
232	99.1	27.5	188.6	191.1	95555
254	104.6	29.1	206.2	209.0	104479
281	111.5	31.0	227.8	230.9	115431
302	118.1	32.8	244.6	247.9	123949
326	122.9	34.1	264.6	268.2	134090
350	129.2	35.9	283.8	287.6	143825
370	136.5	37.9	299.8	303.9	151937
391	142.1	39.5	317.4	321.7	160861
417	150.5	41.8	338.3	342.8	171407
440	158.1	43.9	356.7	361.5	180737
463	165.2	45.9	375.9	380.9	190472
490	173.3	48.1	397.5	402.8	201424

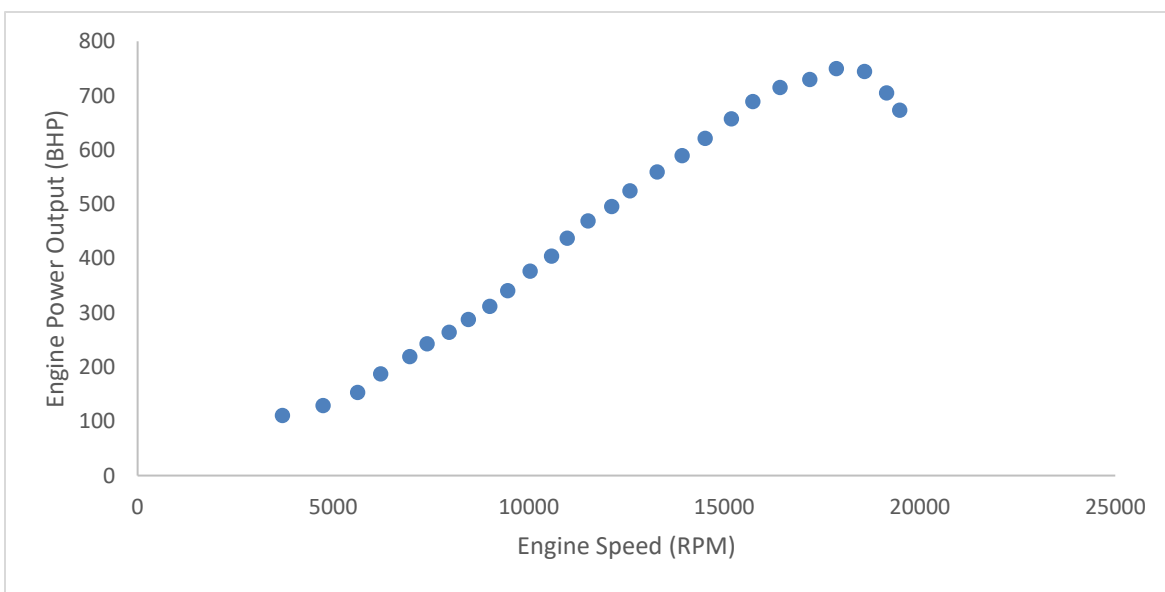


Figure E. 1 Engine Dyno data of engine speed versus power output of a BMW F1 engine

Table E. 2 Table of assumptions made from the hand calculations

Constant Fraction Tailpipe Heat Dissipation	24%	Engine Input HP 2177	Max Brake HP 650
Constant Fraction Radiator Heat Dissipation	25%		
BHP Efficiency	30%		
Miscellaneous Losses	21%		

8.5.2 Second Design Iteration

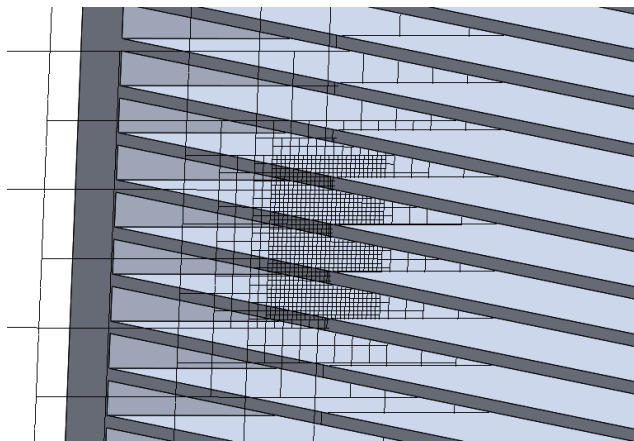


Figure E. 2 Model of the local mesh on the finned heat exchanger radiator

- The mesh refinement is small enough to capture the smallest gap in between the fins
- It was assumed that this small area of mesh refinement can be applied to the entire model due to computational restrictions
- Mesh convergence was not considered on the initial side pod design since it was too simplistic to require it. Instead, a full mesh convergence was done on the final design.

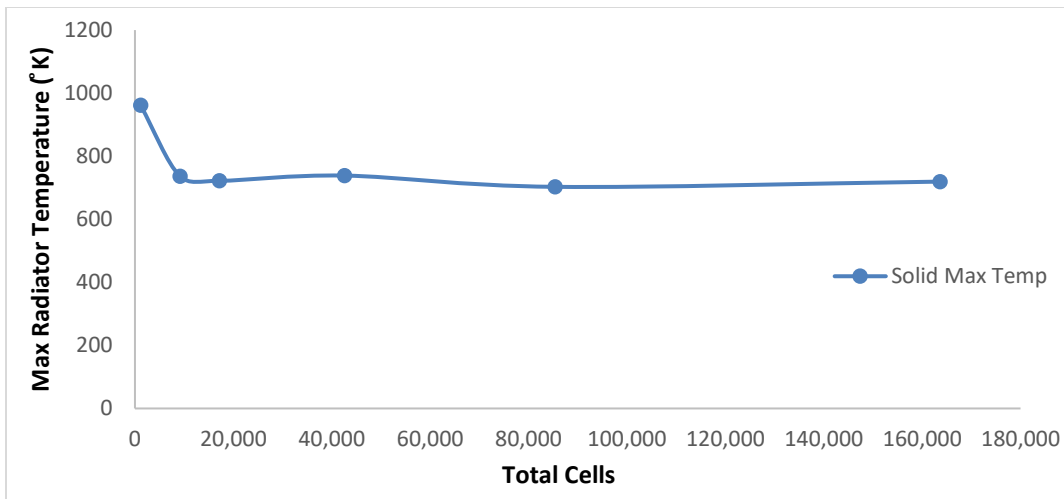


Figure E. 3 Graph showing the mesh convergence of max radiator temperature and drag over the model as the total number of cells increases

- The percent difference in values is less than 1% for both drag and temperature meaning that the mesh convergence is valid

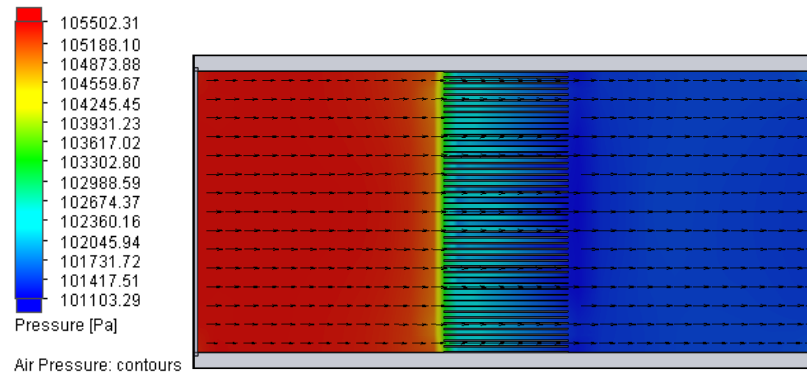


Figure E. 4 Cut plot of pressure gradient across the initial side pod design at 173km/h (top view)

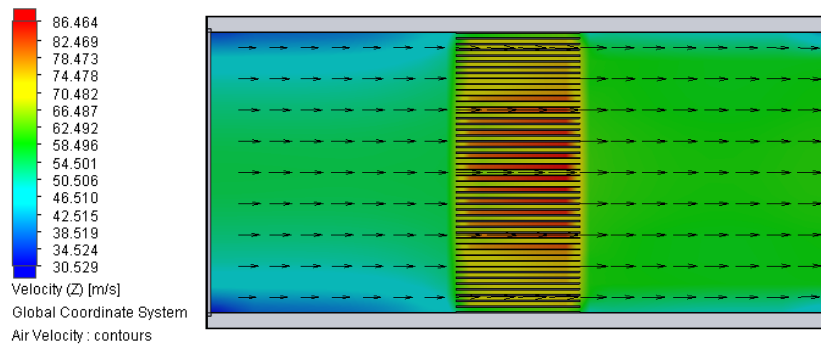


Figure E. 5 Cut plot of velocity across the initial side pod design at 173km/h (top view)

8.5.3 Final Design Iteration

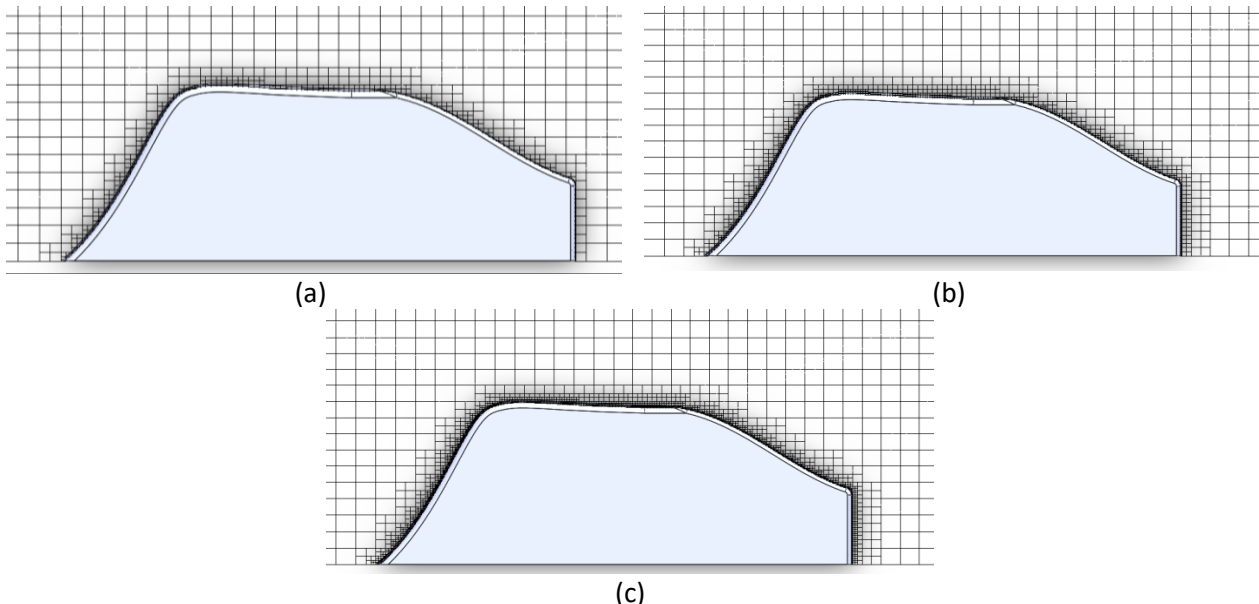


Figure E. 6 Models of final design iteration of the side pod mesh convergence of a local mesh of level 4 (a), level 5 (b), and level 6 (c) (top view)

- The local mesh analysis of level 6 was used for the final design iteration for the side pod

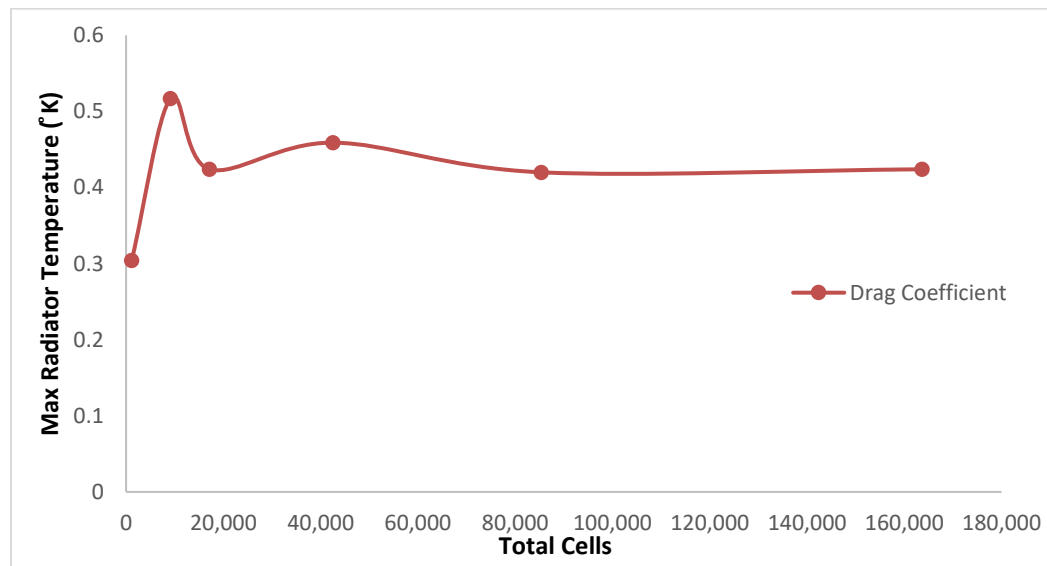


Figure E. 7 Graph showing the mesh convergence of max radiator temperature and drag over the model as the total number of cells increases

Table E. 3 Table of summarized results of the final side pod design

Speed (km/h)	Heat Dissipation (kwh)	Max Temperature Radiator (K)	Max Fluid Temperature (K)	Drag Force (N)	Life Force (N)
173	200	719.5	385.2	143.4	35.63

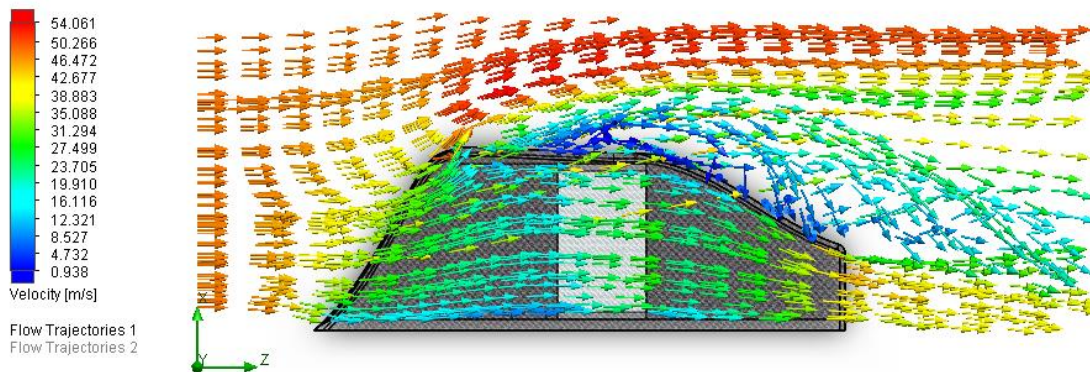


Figure E. 8 Velocity flow trajectory of final design iteration at 173km/h (top view)

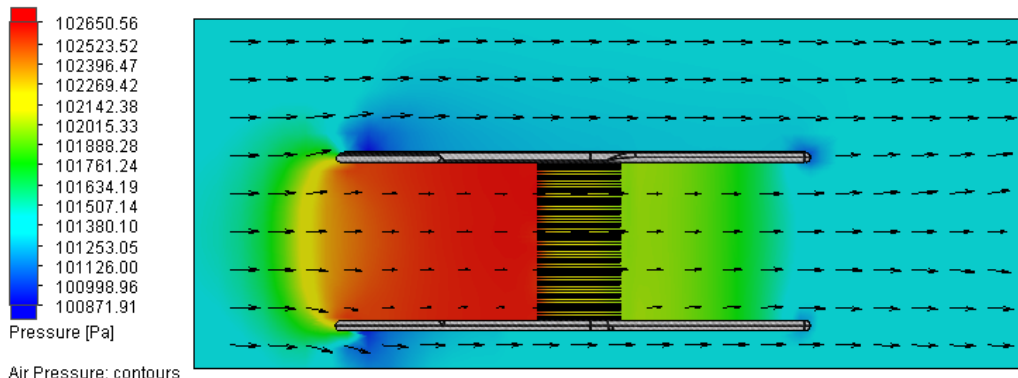


Figure E. 9 A cut plot of pressure gradient across the final side pod design at 173km/h (side view)

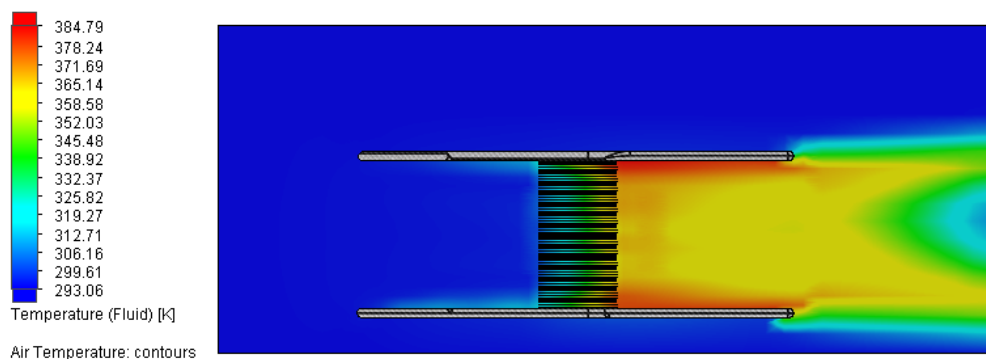


Figure E. 10 A cut plot of the air temperature across the final side pod design at 173km/h (side view)

Appendix F: Aerodynamics of the Whole Car

Completed by Toya Okeke

8.6 Appendix F: Aerodynamics of the Whole Car

8.6.1 Initial Design Iteration

To understand the external flow of the vehicle, the problem was simplified to the 4600 x 1800 x 950 mm wedge geometry shown in Figure F 1.

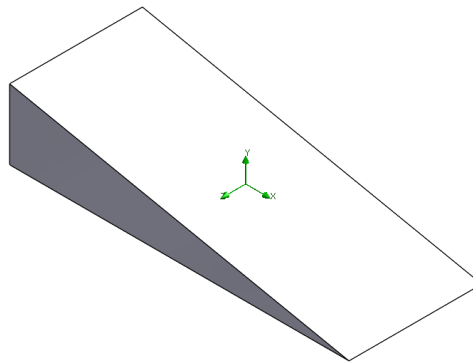


Figure F 1 Isometric view of the wedge used for the first design iteration

To reduce the computational time, only half of the wedge was simulated. Table F 1 contains the mesh convergence analysis for half of the wedge moving at 50 km/h.

Table F 1 Mesh Convergence for Half of the Wedge

Total Cells	Fluid Cells	Fluid Cells Contacting Solids	Drag Force (N)	Lift Force (N)	Percent Difference in Drag	Percent Difference in Lift
13380	13380	3618	42.359	31.153		
20674	20674	3618	34.854	32.540	19.44%	4.36%
23299	23299	3618	35.140	31.309	0.82%	3.86%
30047	30047	3618	34.401	31.639	2.13%	1.05%

Based on this and convergence plot in Figure F 2, the drag and lift force of the wedge converge to ~34 N and ~31 N, respectively.

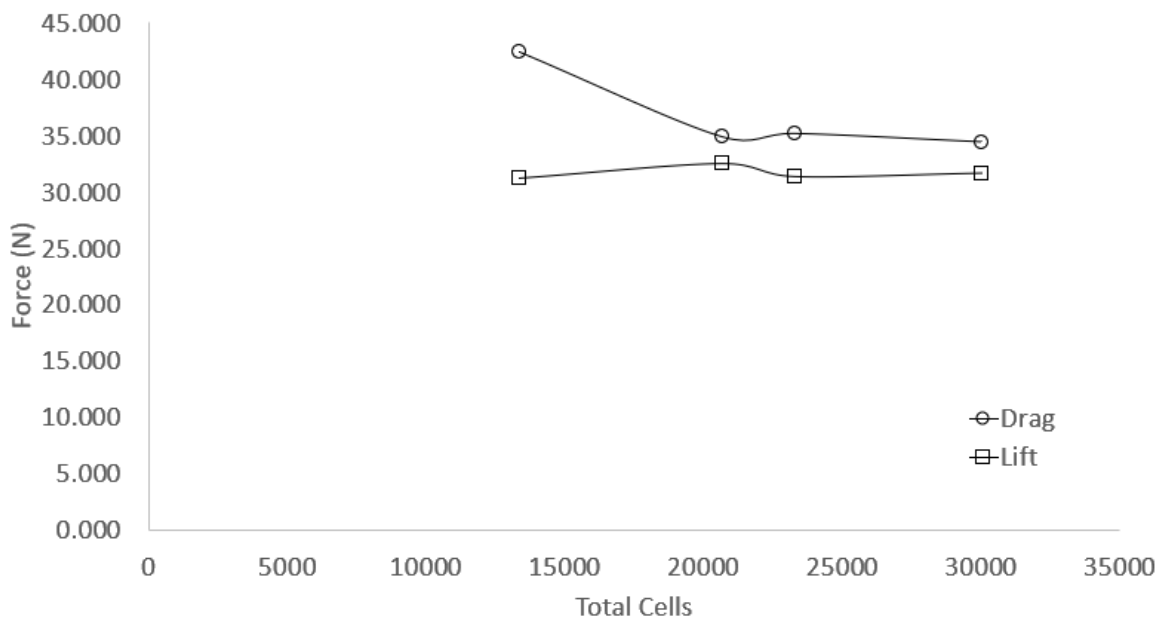


Figure F 2 Mesh convergence plot for half of the wedge

The mesh of the wedge can be seen in Figure F 3.

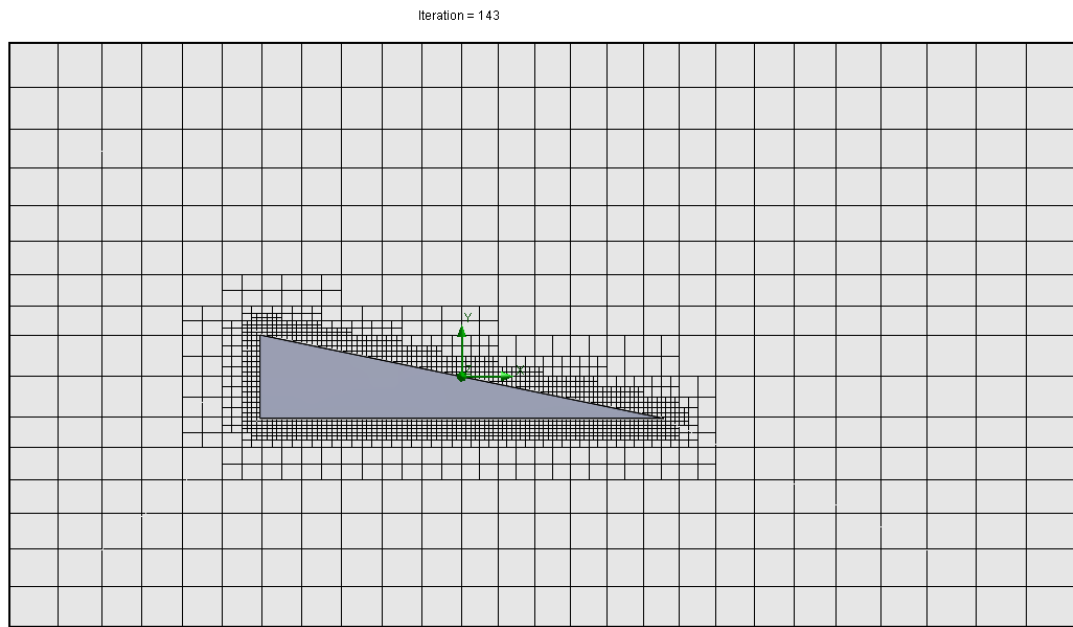
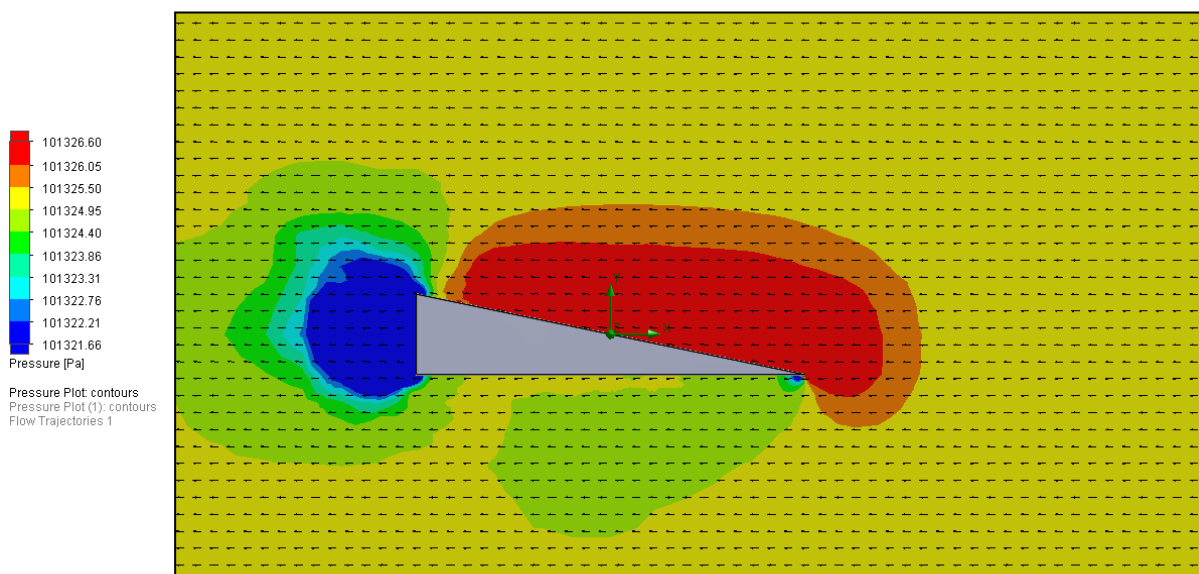


Figure F 3 Mesh used for the wedge. 30 047 total/fluid cells were used with 3 618 fluid cells contacting the wedge.

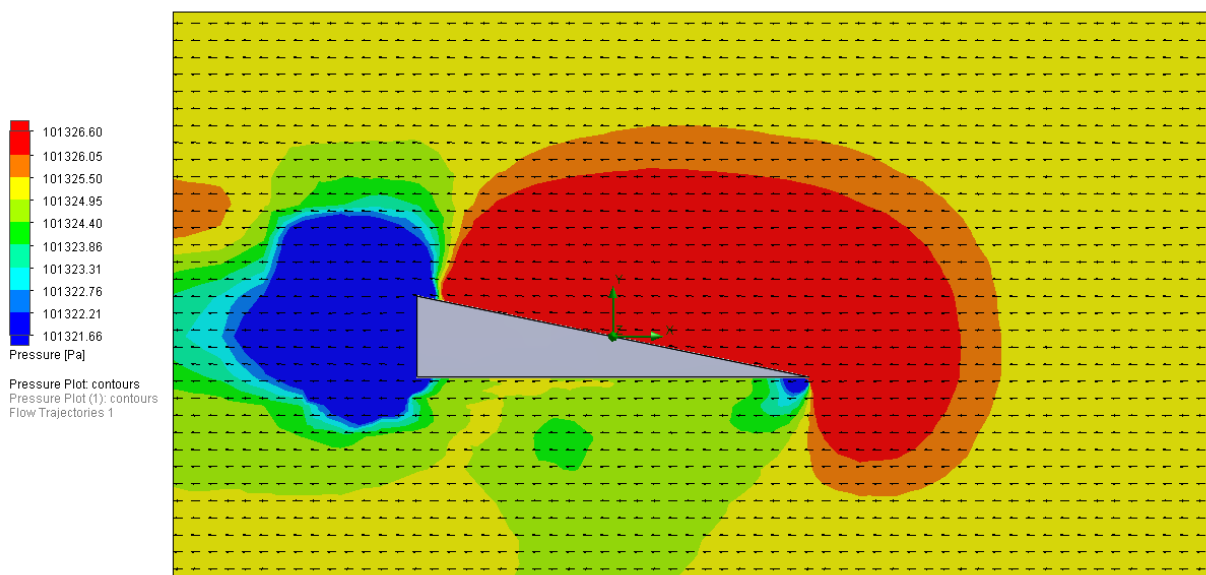
Using this mesh, the pressure plots in Figure F 4 were generated for each speed. Note the velocity of the air is flowing from the tip of the wedge to the back face.

Iteration = 143



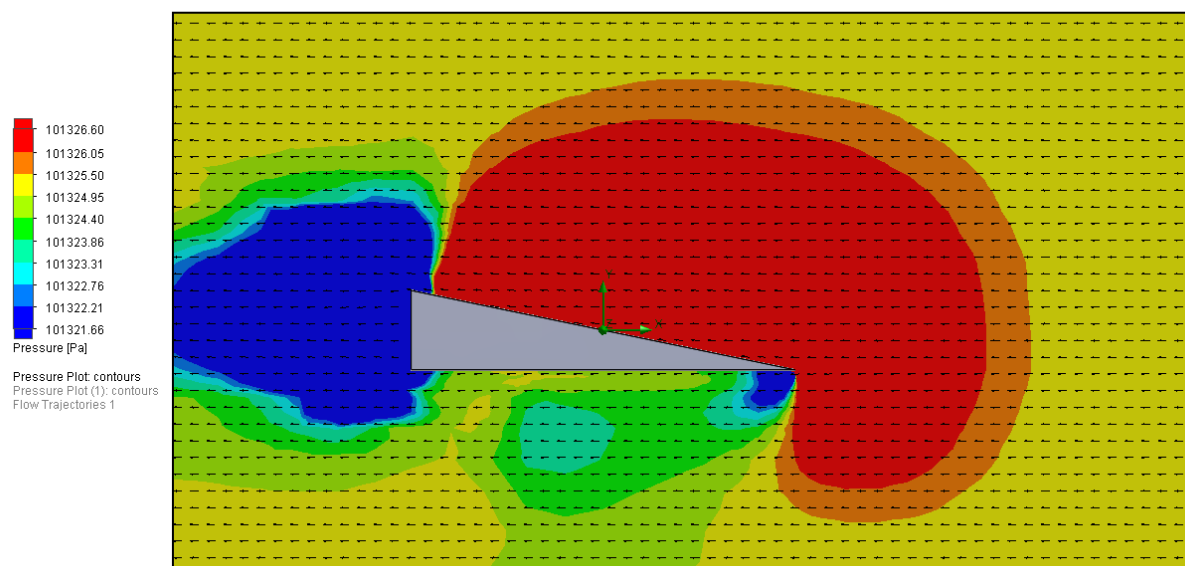
(a)

Iteration = 167



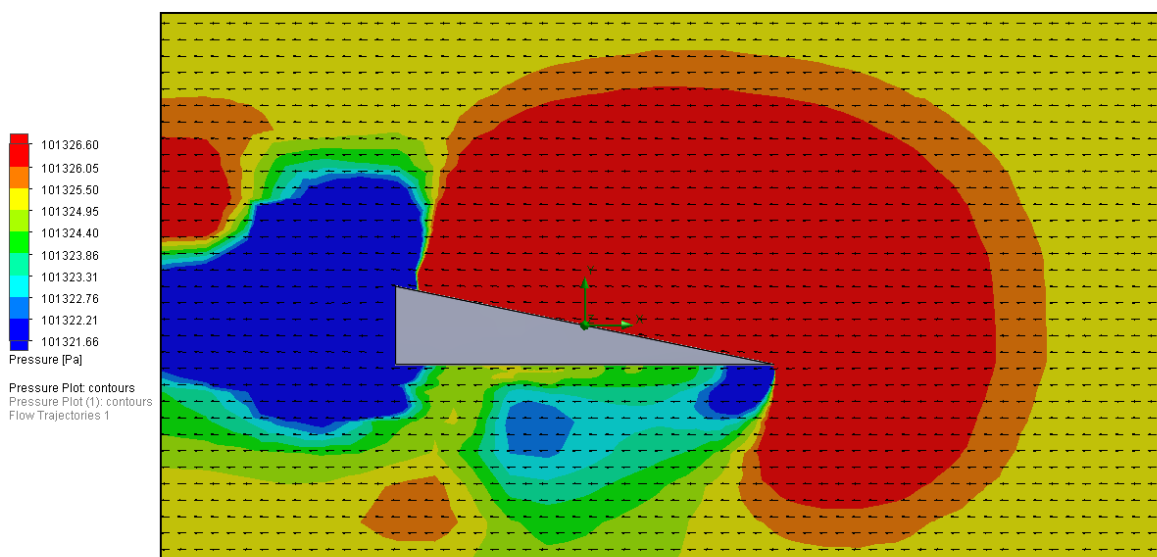
(b)

Iteration = 132



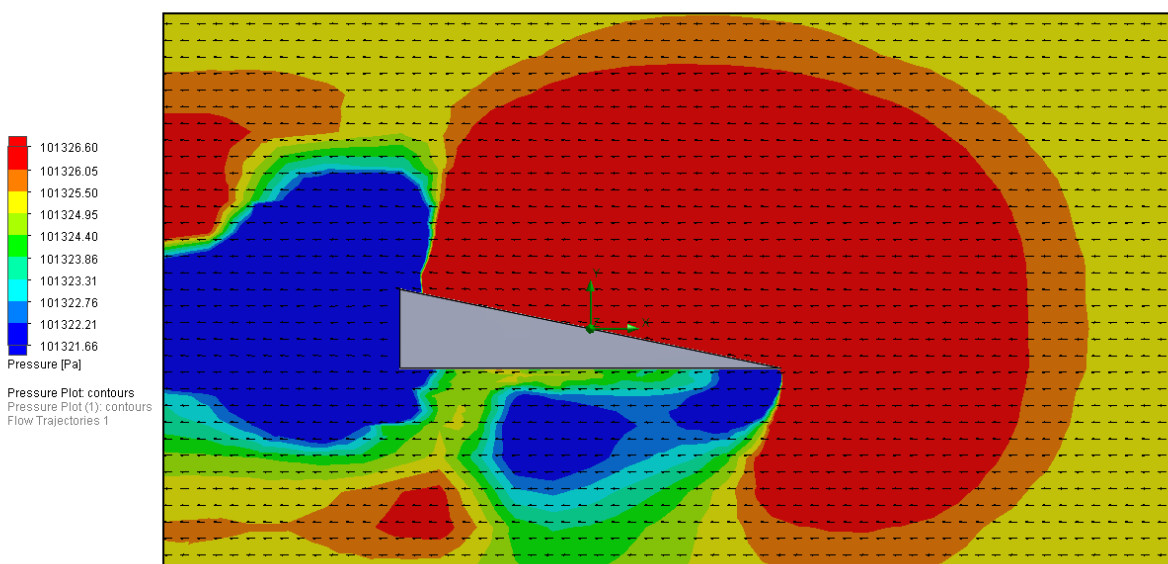
(c)

Iteration = 162



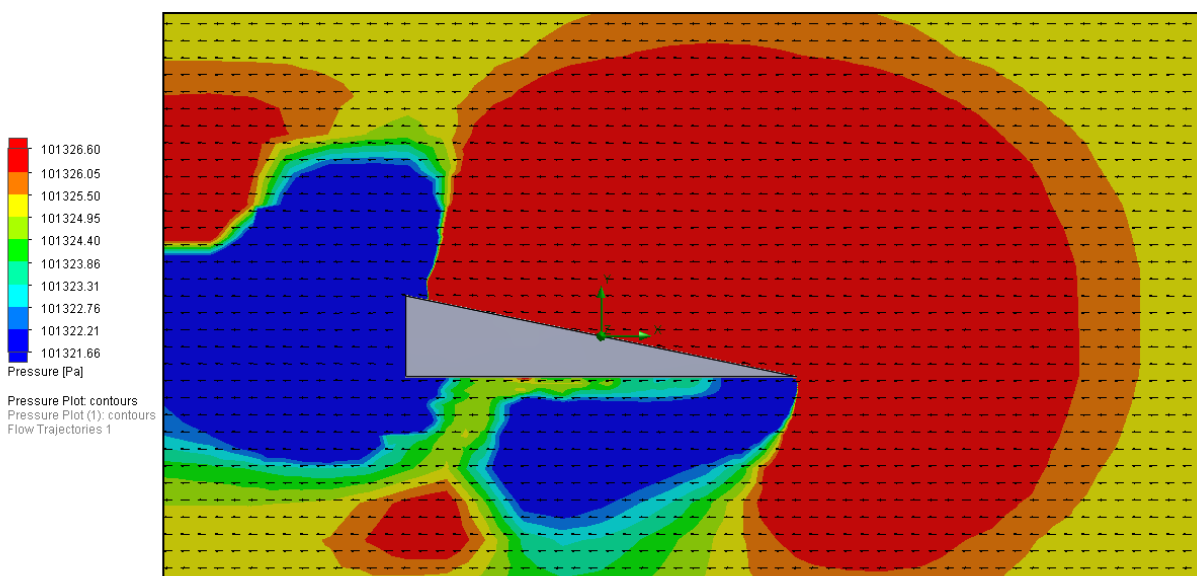
(d)

Iteration = 142



(e)

Iteration = 163



(f)

Figure F 4 Pressure plots for half the wedge moving at (a) 50 km/h, (b) 100 km/h, (c) 150 km/h, (d) 200 km/h, (e) 250 km/h and (f) 300 km/h

From these, high pressures at the front of the vehicle and low pressures at the back should be expected for the final vehicle design. These pressure regions should also increase as the vehicle speed increases. However, low pressure regions start to form at the bottom of the bottom of the wedge. This is likely due to neglecting the use of wheels on the wedge and simulating it moving along the road.

8.6.2 Second Design Iteration

The vehicle design for this iteration can be seen in Figure F 5 and its key dimensions are shown in Figure F 6.

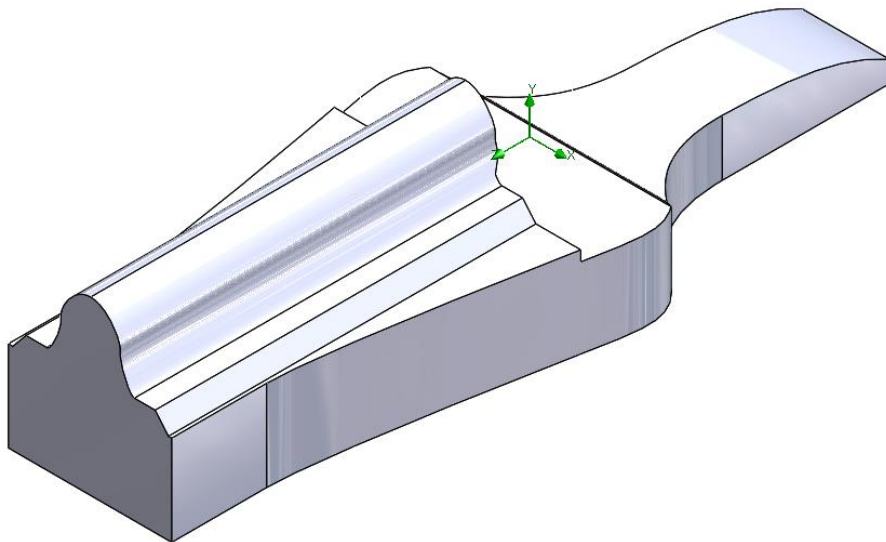


Figure F 5 Isometric view of the vehicle used for the second iteration

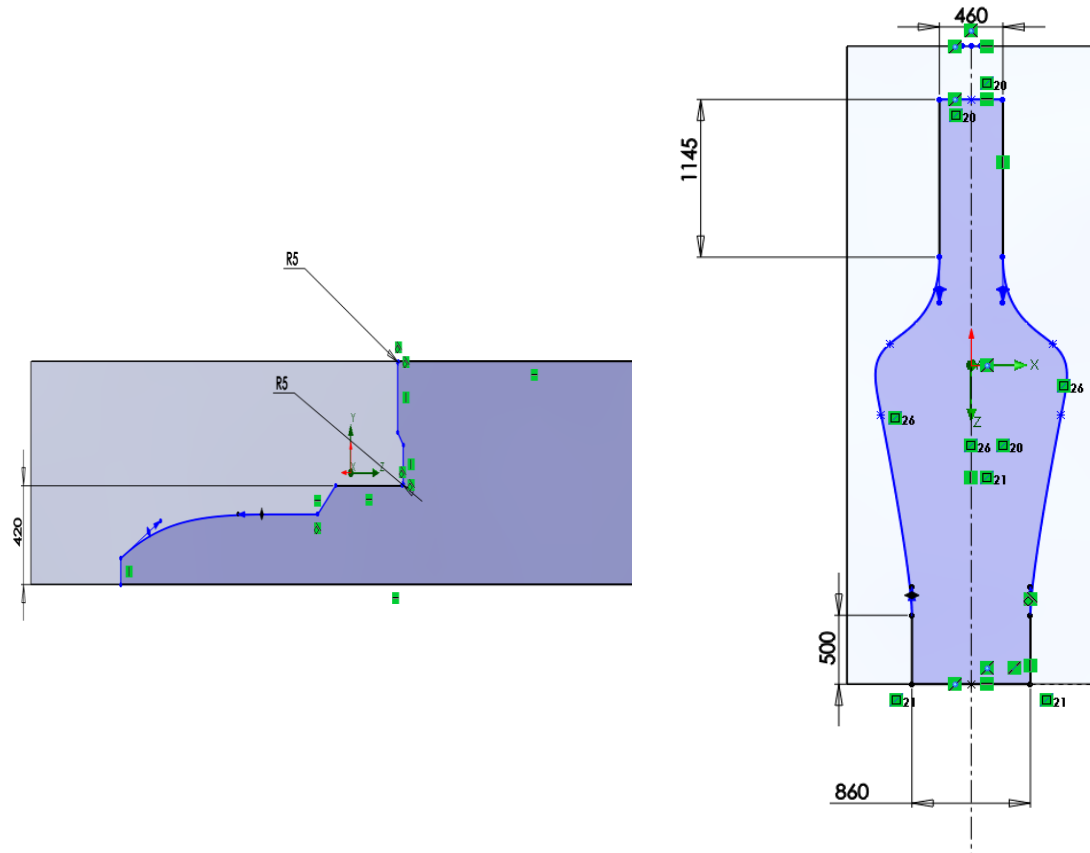


Figure F 6 Key dimensions of the vehicle used for the second iteration. Note the vehicle is 950 mm high, 3980 mm long and 1390 mm wide

Using the same local mesh parameters, Figure F 7 was generated.

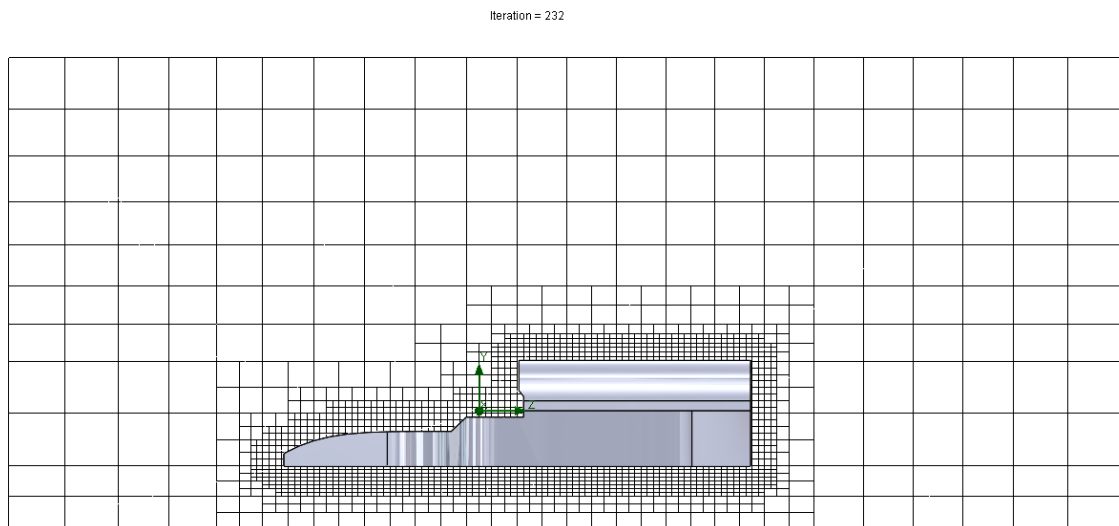
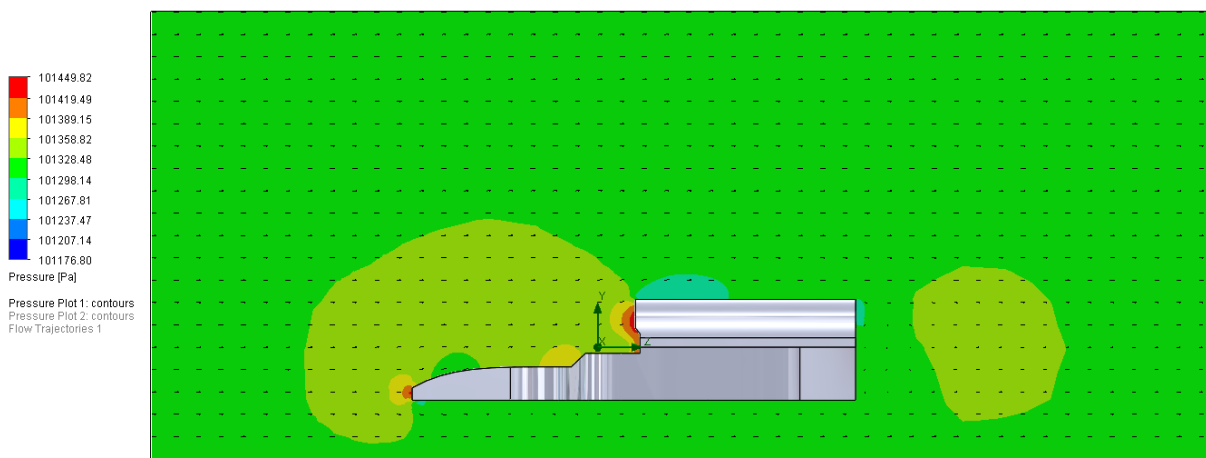


Figure F 7 Mesh of the vehicle used for the second iteration. 49021 total/fluid cells were used with 5129 cells contacting the vehicle

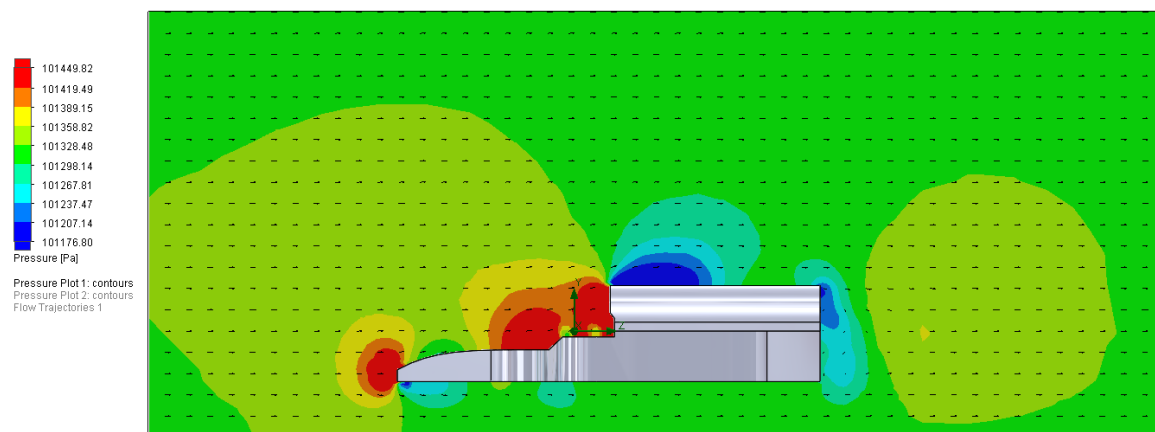
The pressure plots from this mesh can be seen in Figure F 8.

Iteration = 232



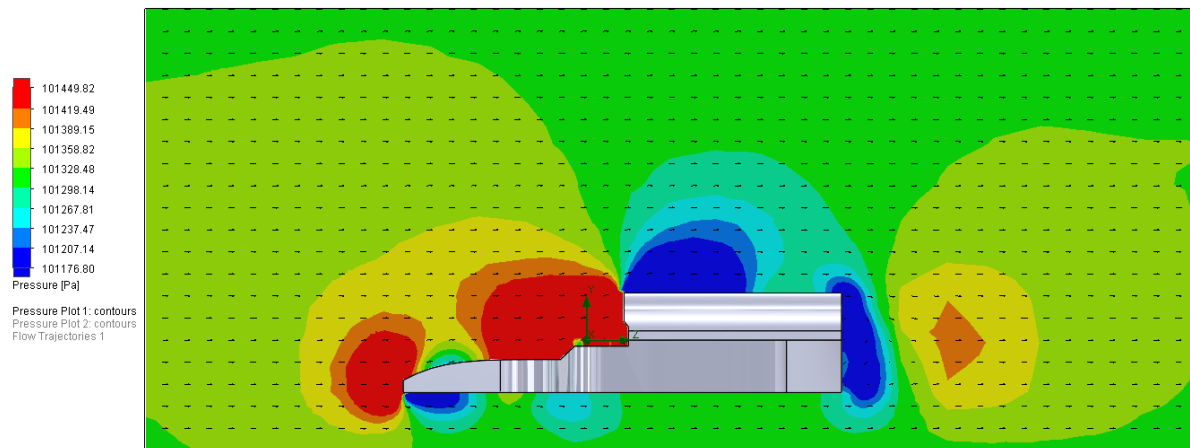
(a)

Iteration = 111



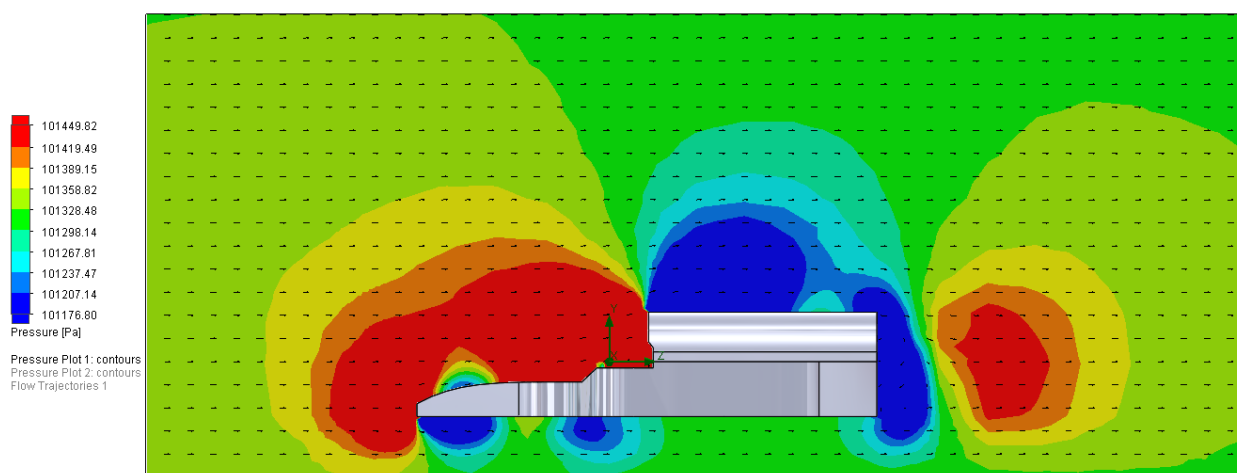
(b)

Iteration = 139



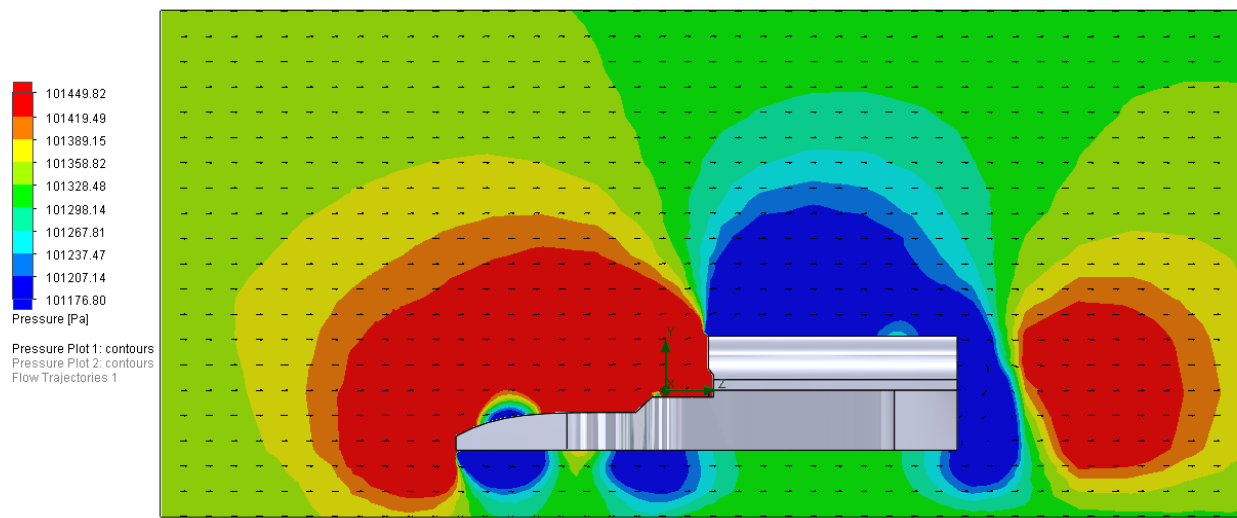
(c)

Iteration = 152



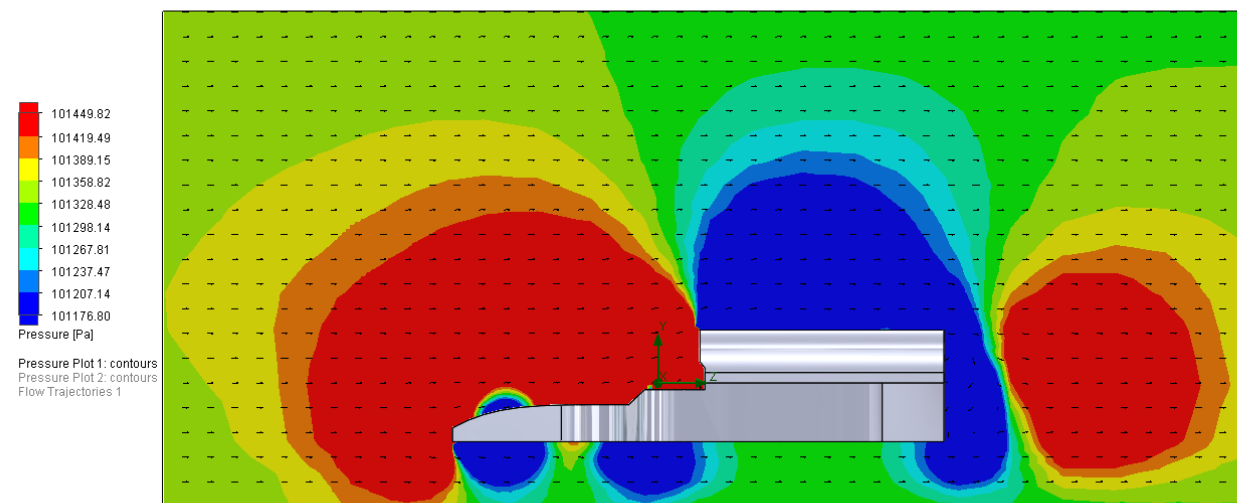
(d)

Iteration = 142



(e)

Iteration = 144



(f)

Figure F 8 Pressure plots for the vehicle moving at (a) 50 km/h, (b) 100 km/h, (c) 150 km/h, (d) 200 km/h, (e) 250 km/h and (f) 300 km/h

High pressure regions occur at the front of the vehicle and low pressure regions at the back, similar to the first iteration. However, the regions are significantly smaller, but the pressures are larger in magnitude. Low pressure regions still occur at the bottom of the vehicle. Again, this likely due to neglecting the vehicle moving along the road.

8.6.3 Third Design Iteration

The third design iteration involves simulating the vehicle driving along the road, as shown in Figure F 9. The dimensions of the vehicle were modified again so the front wing, rear wing and side pods could be easily installed for the final design iteration, as shown in Figure F 10.

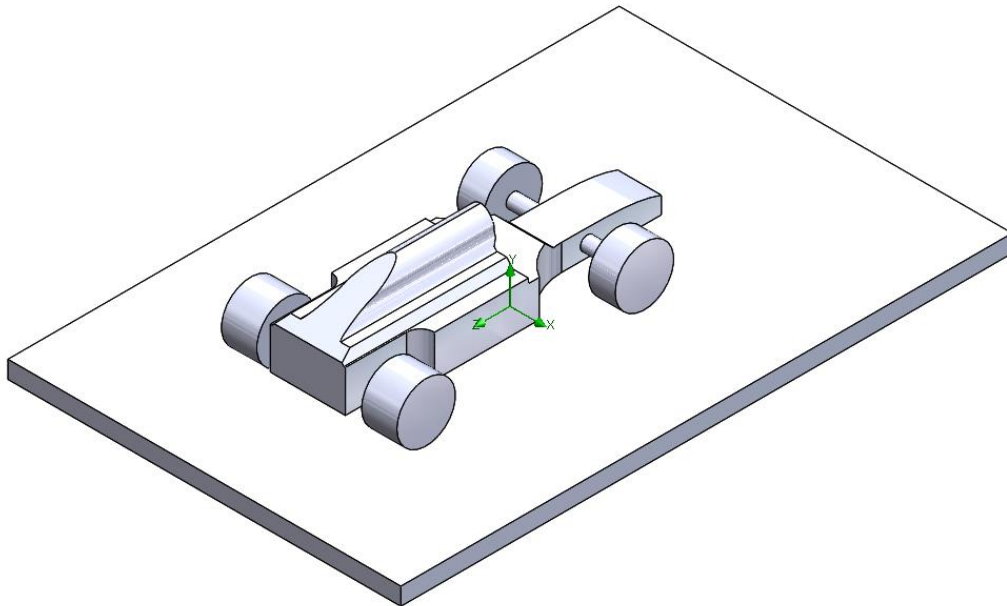


Figure F 9 Isometric view of the vehicle on the road

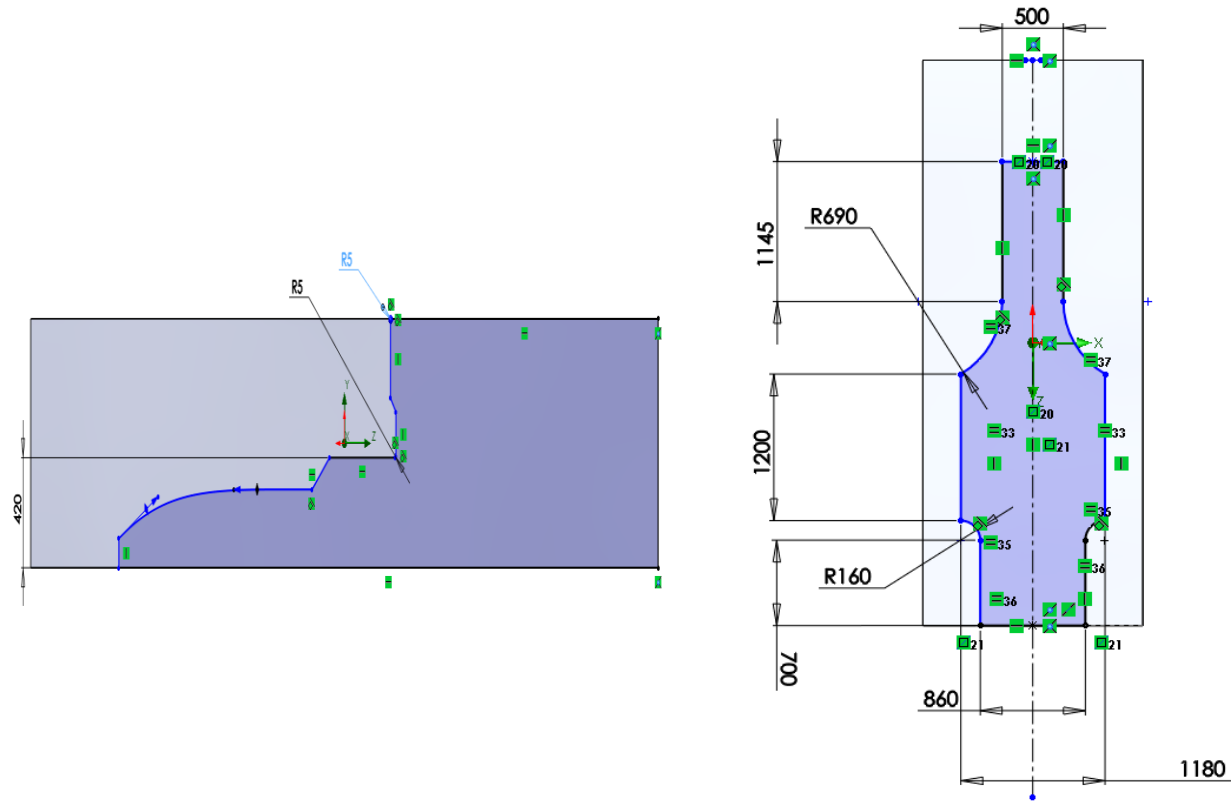


Figure F 10 Key dimensions of the vehicle used for the third design iteration. Note the vehicle is 3 800 mm long, 1 180 mm wide and 950 mm high.

Wheels were added to the vehicle so simulation along the road could be done. The dimensions of the wheel can be seen in Figure F 11.

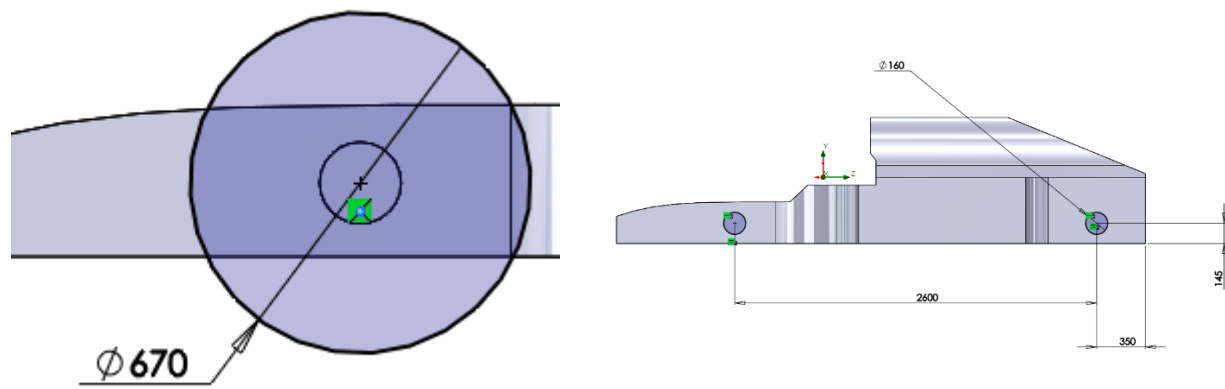


Figure F 11 Dimensions of the wheels and their locations. Note the front and rear wheels are 305 and 405 mm thick, respectively.

Using the same local mesh parameters, the mesh and pressure plots in Figure F 12 and Figure F 13 were generated.

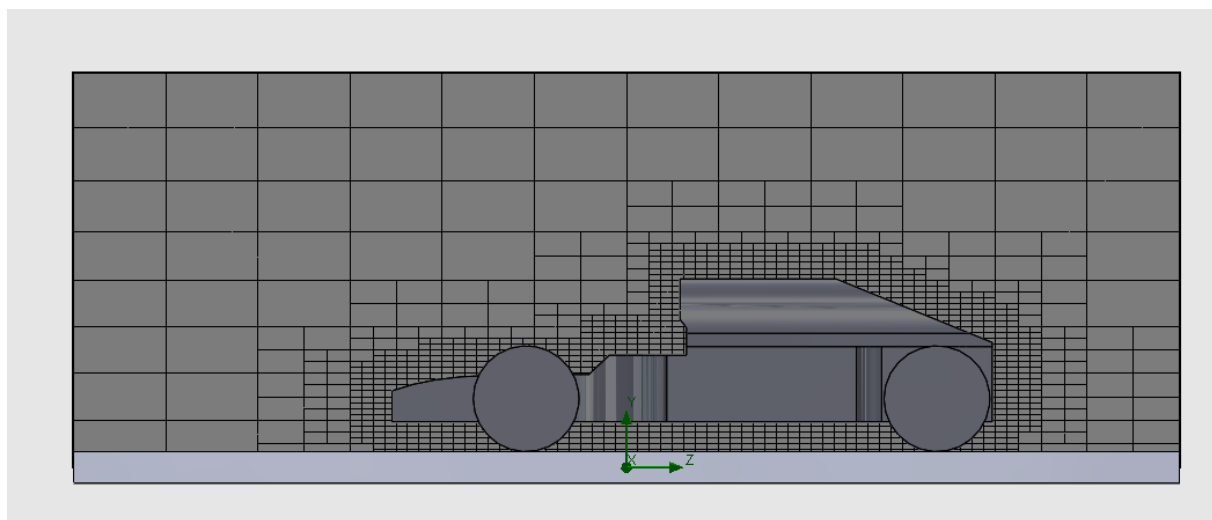
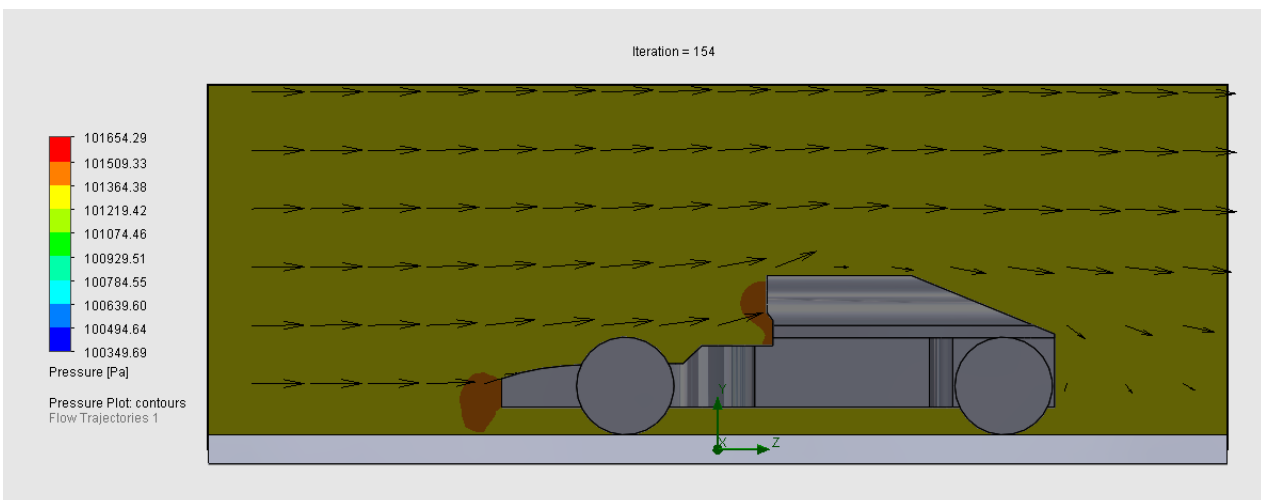
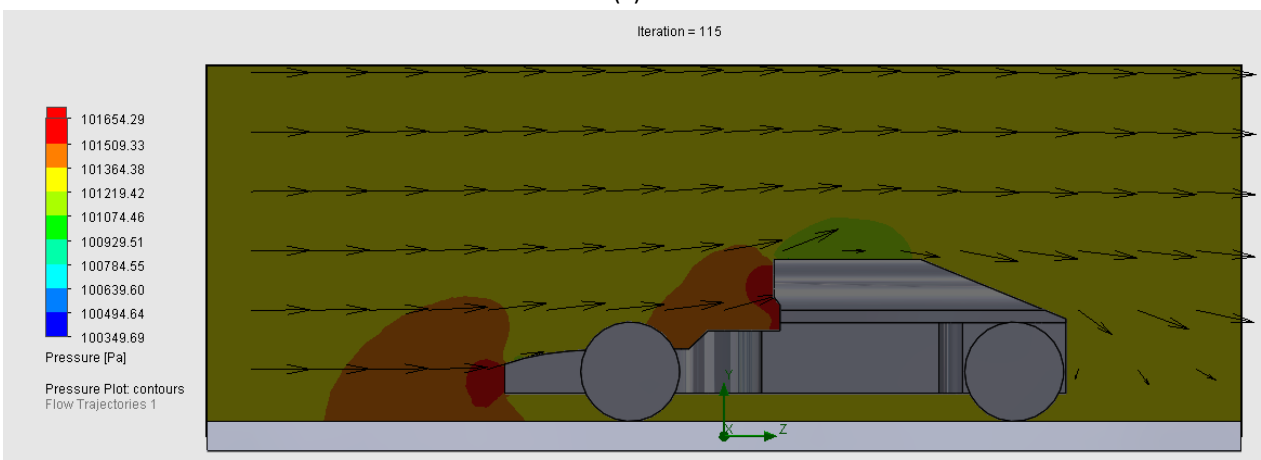


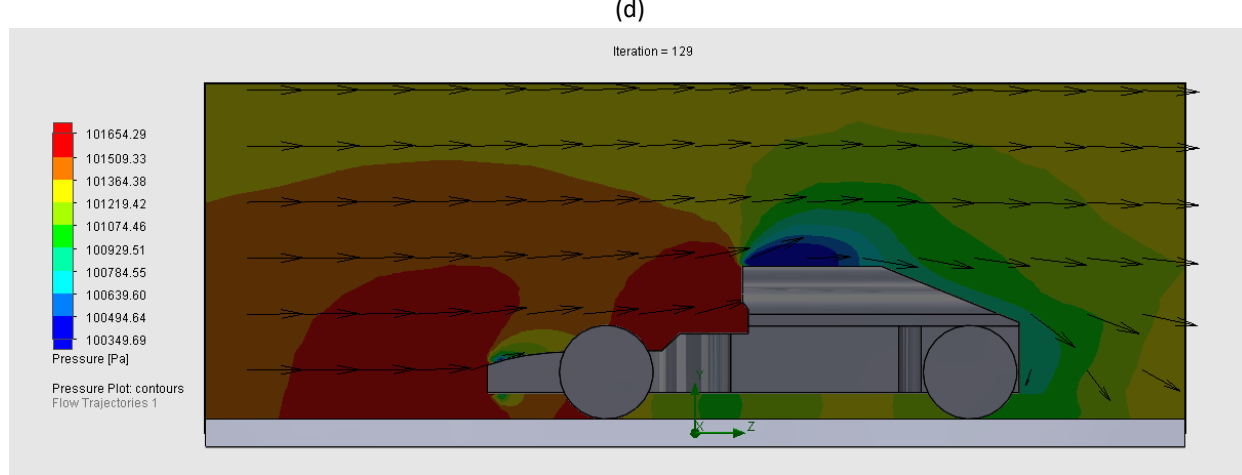
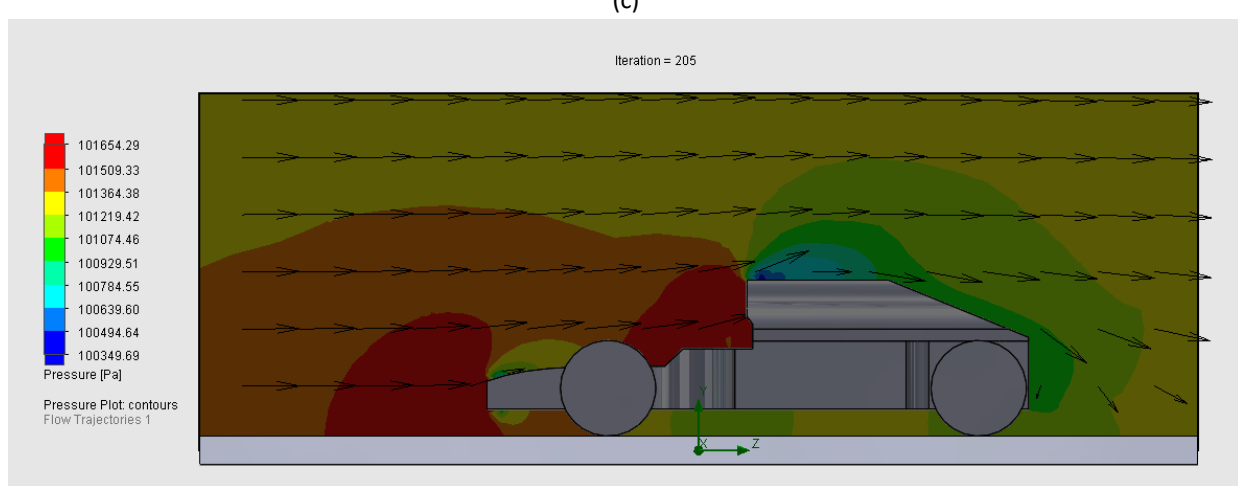
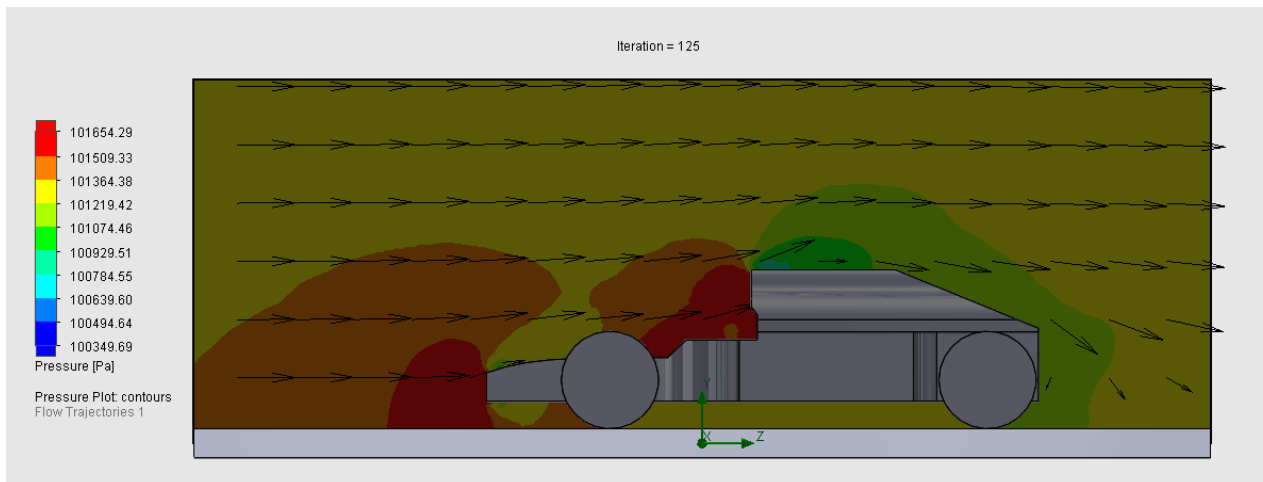
Figure F 12 Mesh of the vehicle used for the third iteration. 29612 total/fluid cells were used with 5764 contacting the vehicle

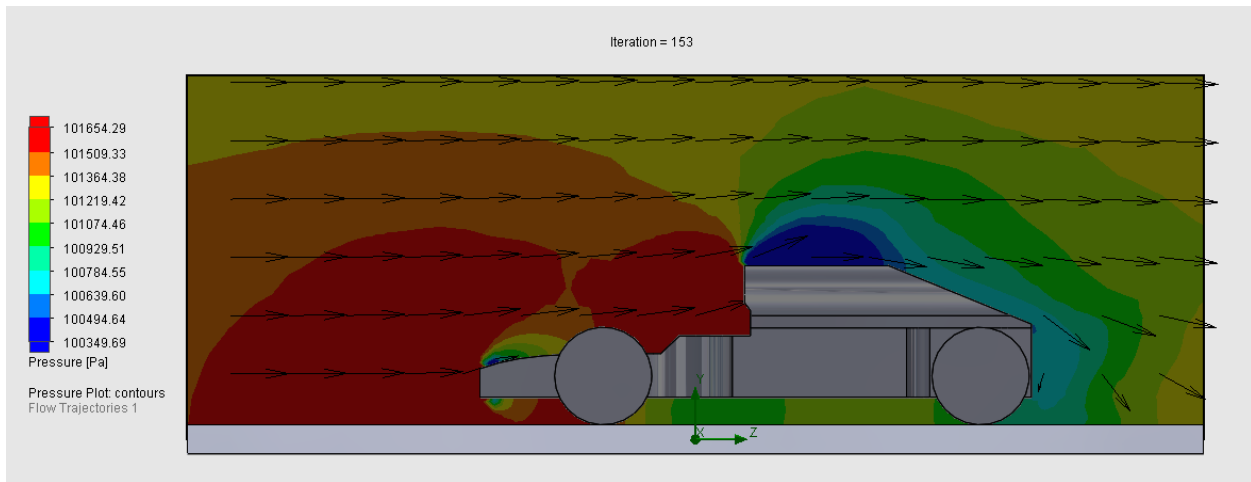


(a)



(b)





(f)

Figure F 13 Pressure plots for the vehicle moving on the road at (a) 50 km/h, (b) 100 km/h, (c) 150 km/h, (d) 200 km/h, (e) 250 km/h and (f) 300 km/h

Notice that the top of the vehicle is meant to have an air intake. For this simulation, it left as a solid, causing the air to flow around that portion of the vehicle. For the final design, a hole will be added in that area so the air can flow through to the rear wing.

8.6.4 Final Design Iteration

The front wing, rear wing and side pods were all added to the vehicle for the final design iteration, as shown in Figure F 14. The main body of the car was modified so each component could be attached. Additionally, a circular hole was added to the top of the vehicle to simulate an air intake leading to the rear wing. These can be seen in Figure F 15 and Figure F 16.

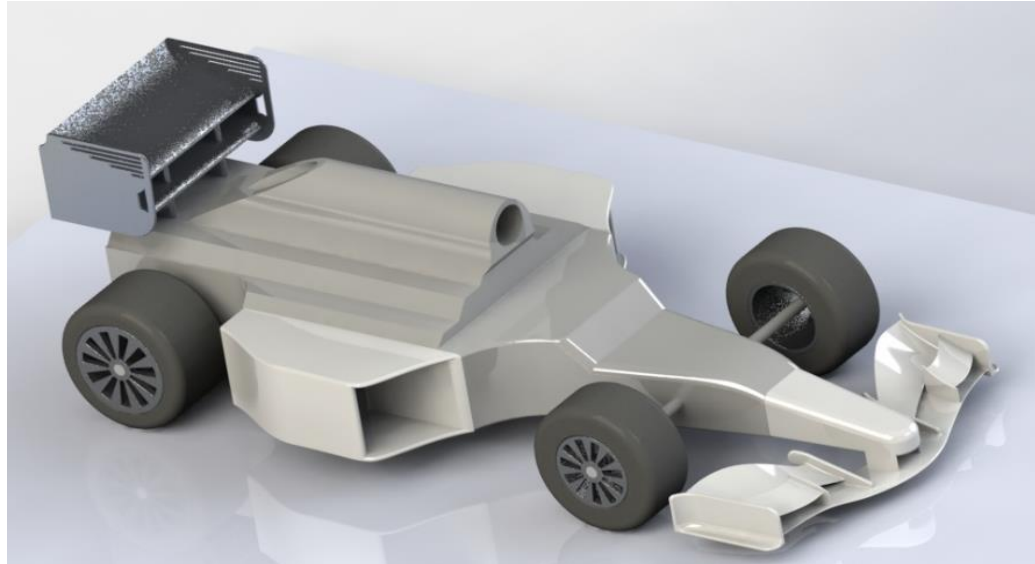


Figure F 14 Isometric view of the final vehicle design

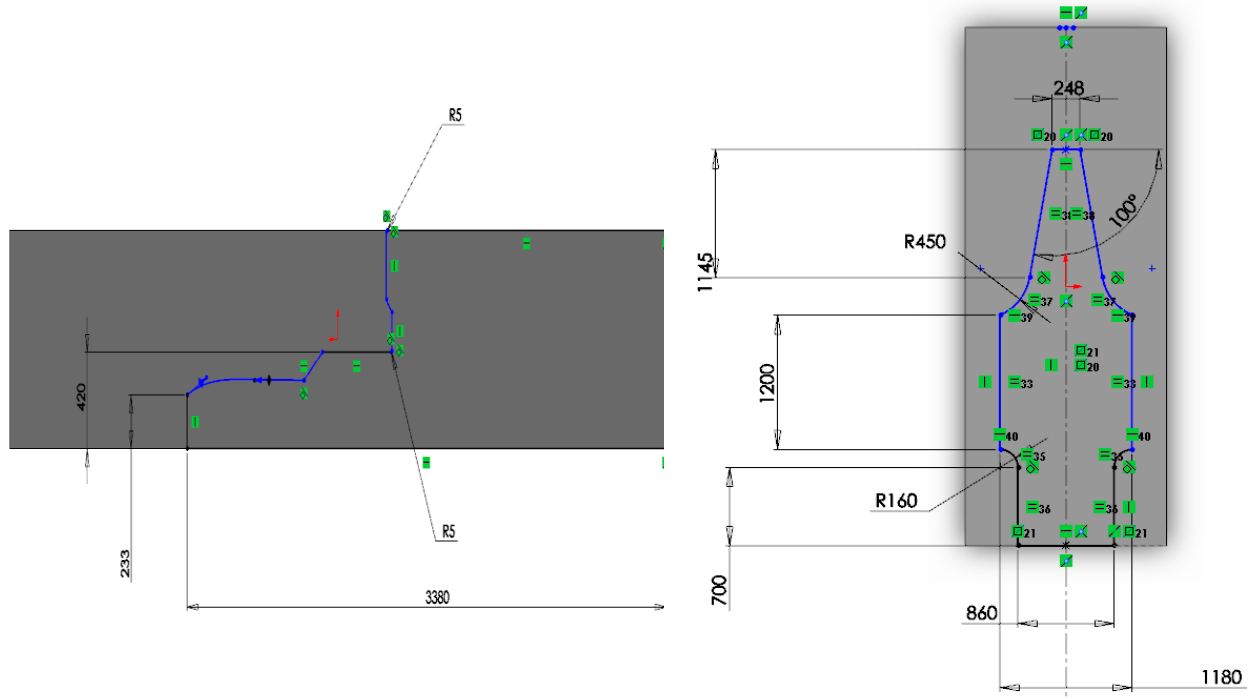


Figure F 15 Key dimensions of the vehicle used for the final design iteration. Note the vehicle is 3800 mm long, 1180 mm wide and 950 mm high.

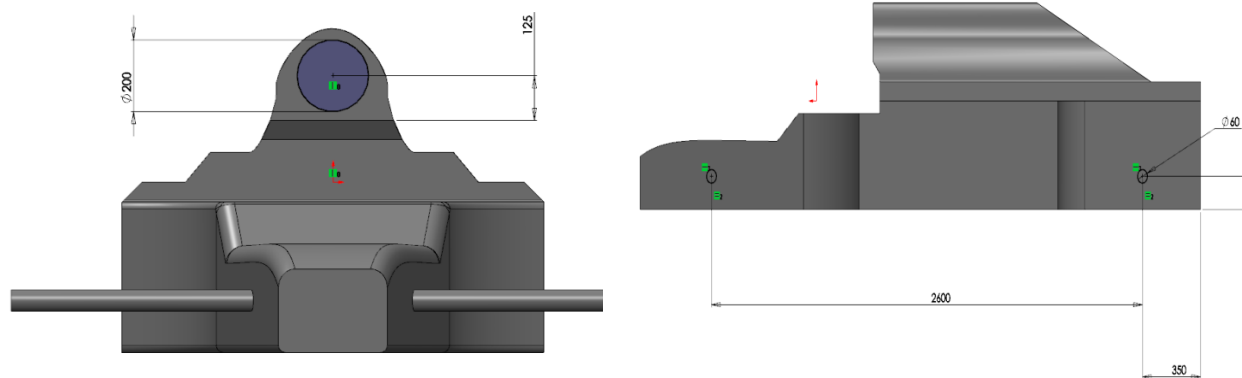


Figure F 16 Dimensions of the wheel locations and the circular hole at the top of the vehicle.

Using the same local mesh parameters, the mesh and pressure plots in Figure F 17 and Figure F 18 were generated.

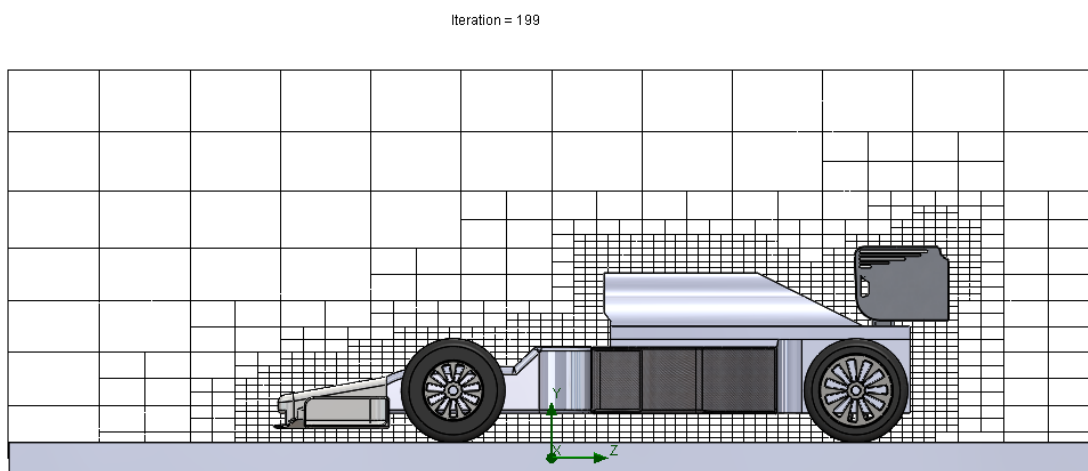
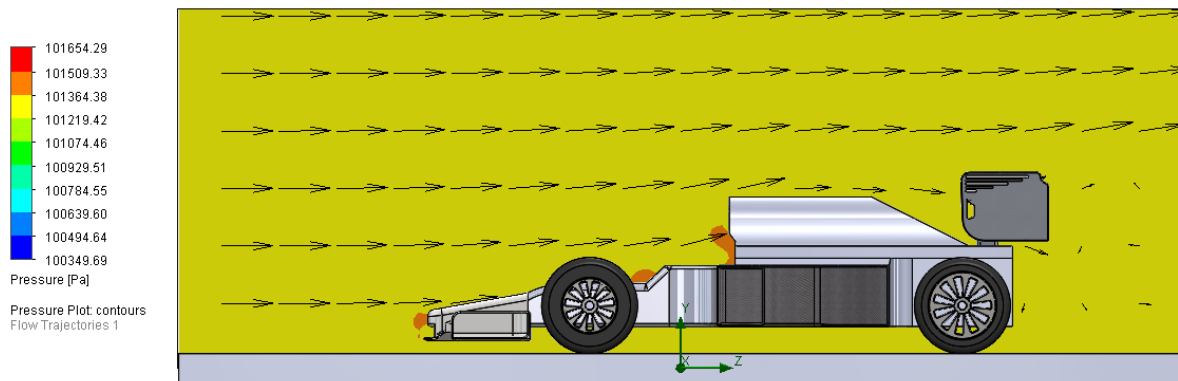
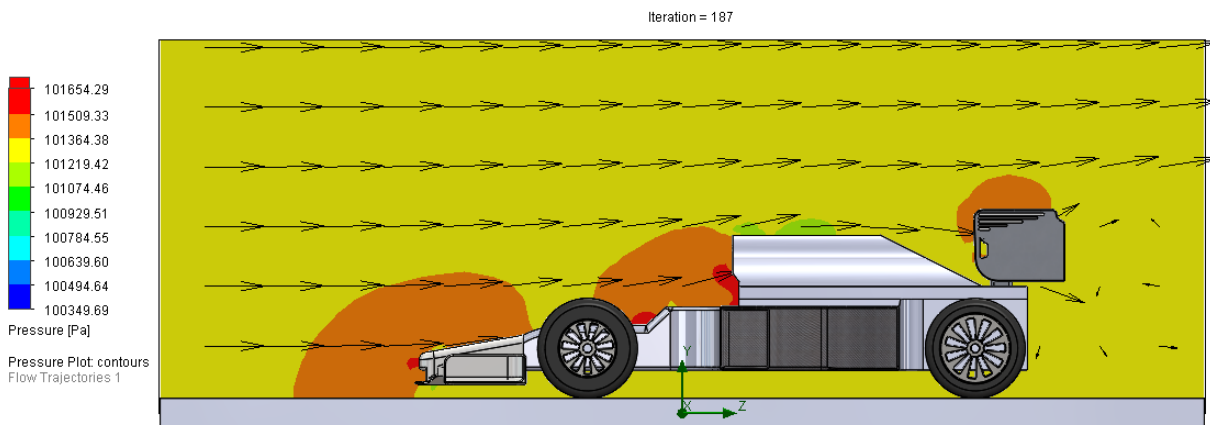


Figure F 17 Mesh of the vehicle used for the final design. 59644 total cells and 44349 fluid cells were used with 15295 fluid cells contacting the vehicle

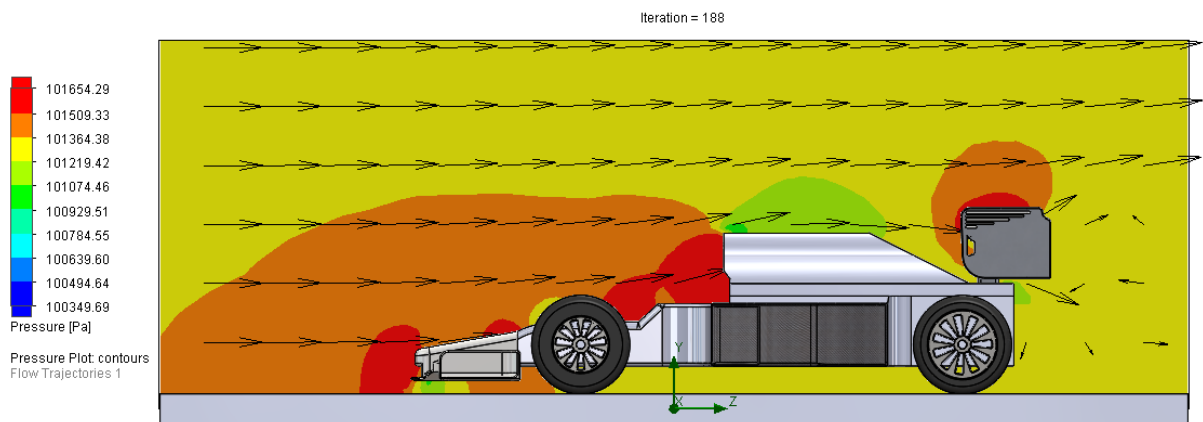
Iteration = 199



(a)

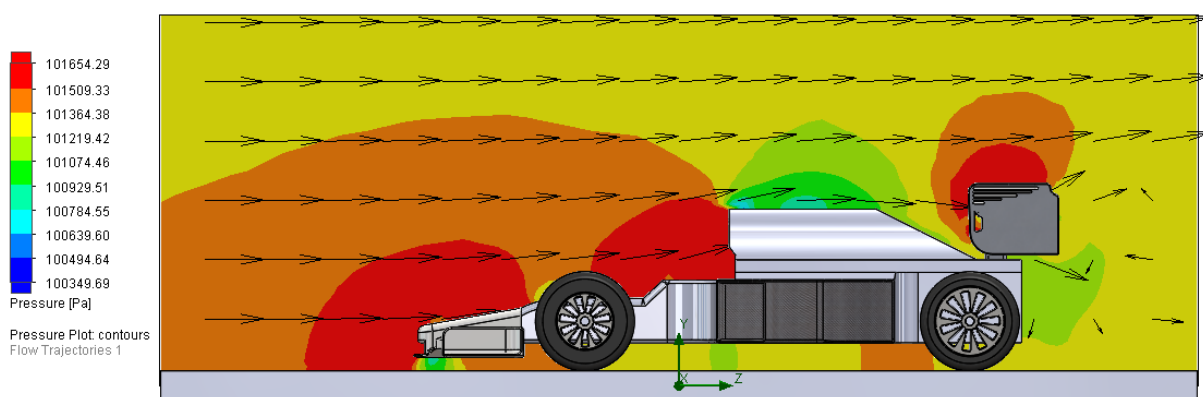


(b)



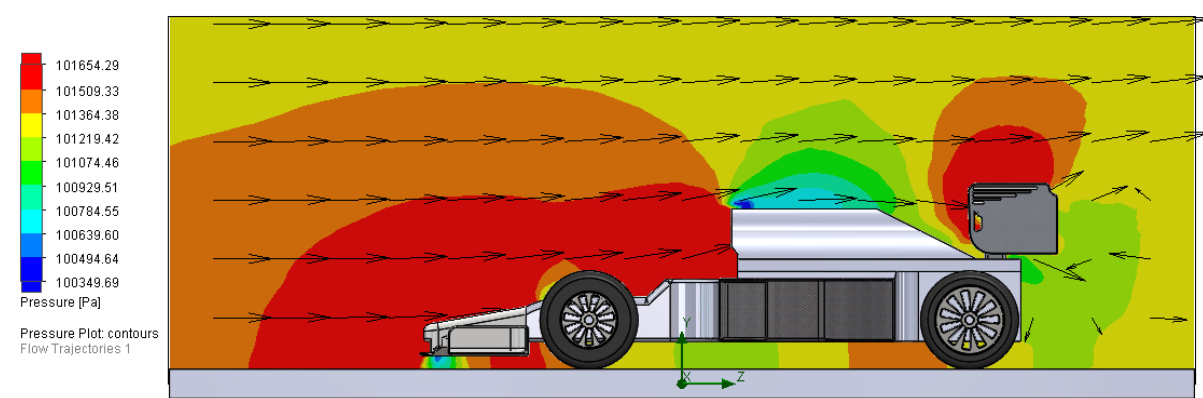
(c)

Iteration = 193



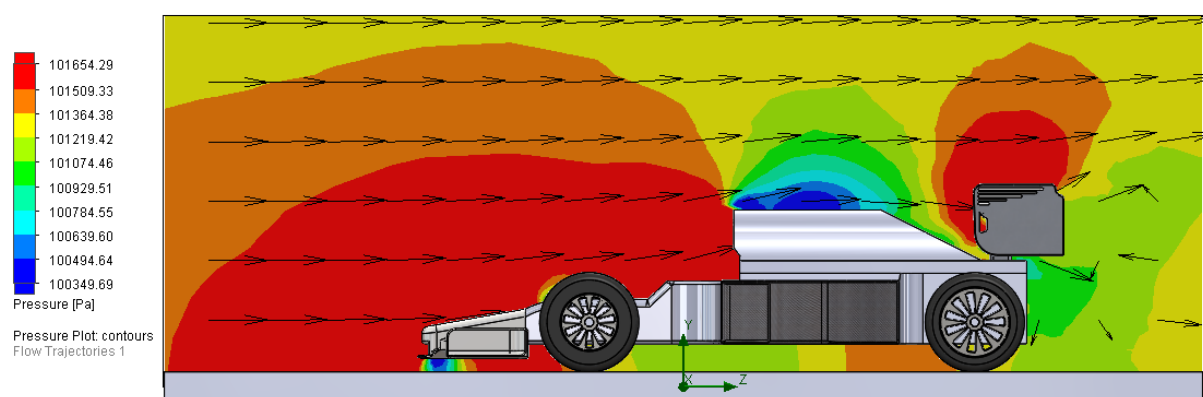
(d)

Iteration = 194



(e)

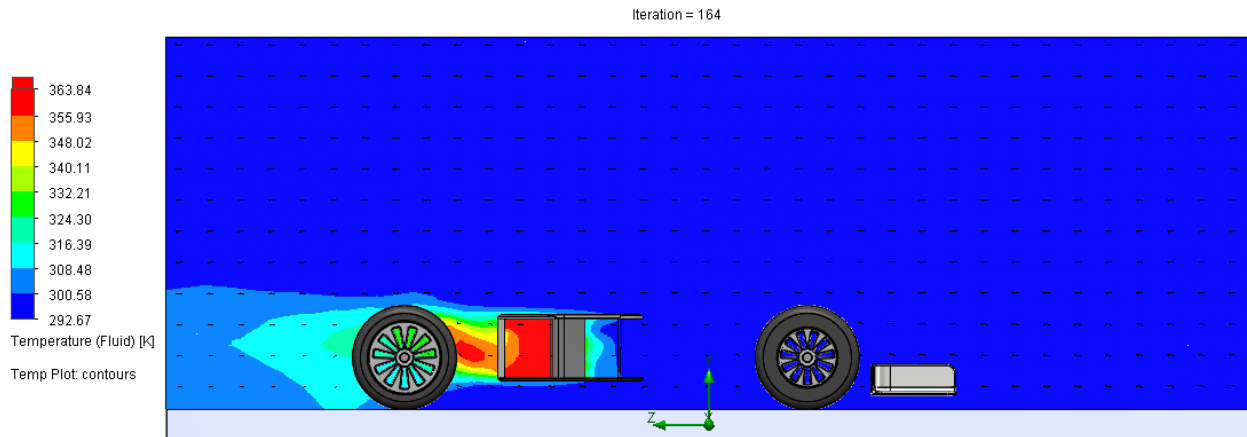
Iteration = 216



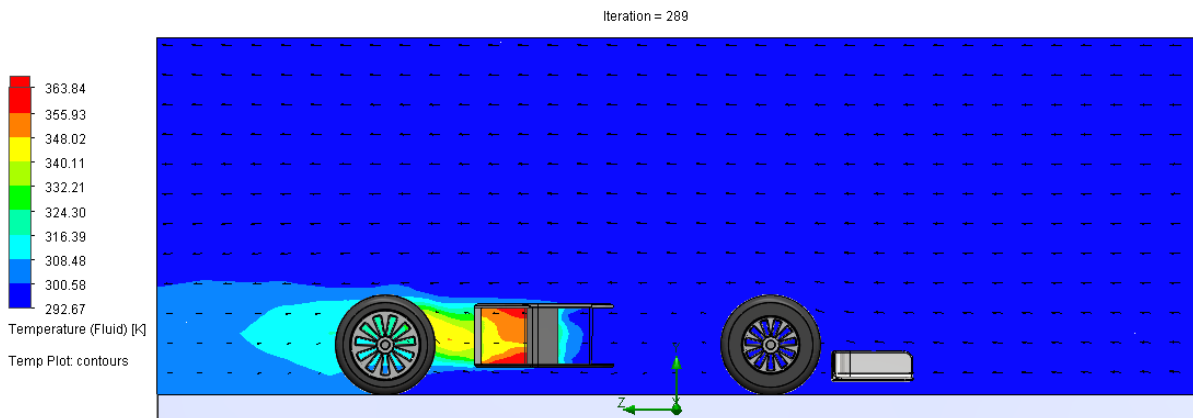
(f)

Figure F 18 Pressure plots for the vehicle moving on the road at (a) 50 km/h, (b) 100 km/h, (c) 150 km/h, (d) 200 km/h, (e) 250 km/h and (f) 300 km/h

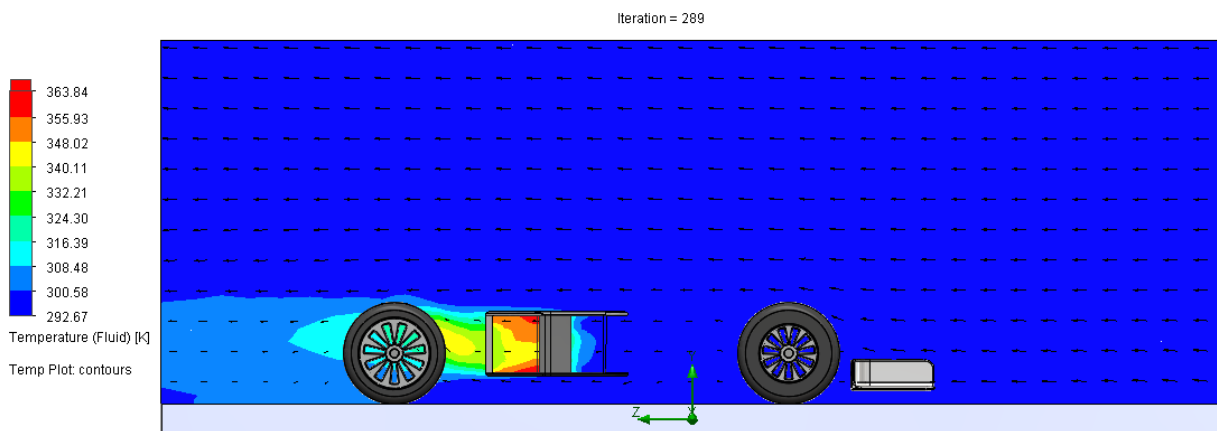
High pressure regions occur at the front of the vehicle and near the rear wing, suggesting the front and rear wings are generating enough downforce on the vehicle. The temperature plots of the side pods on the CVT are shown in Figure F 19.



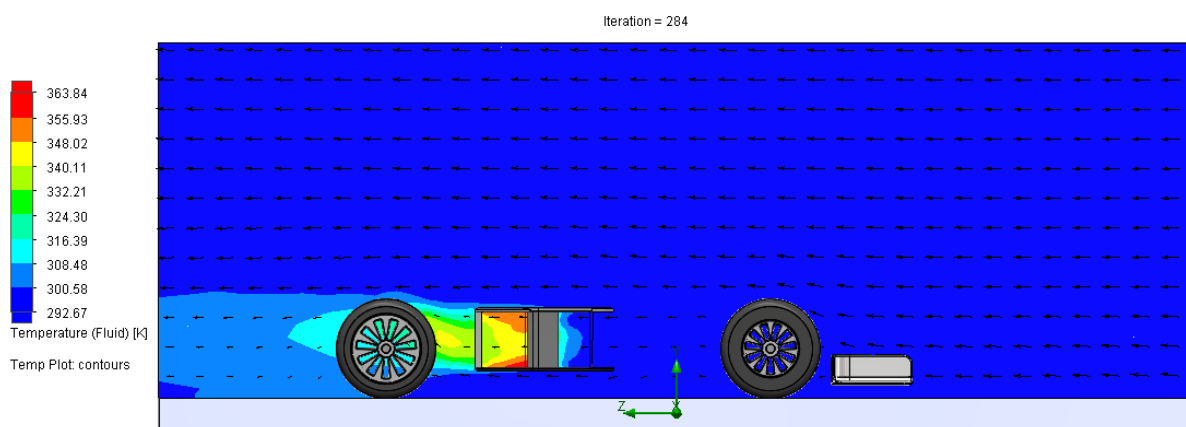
(a)



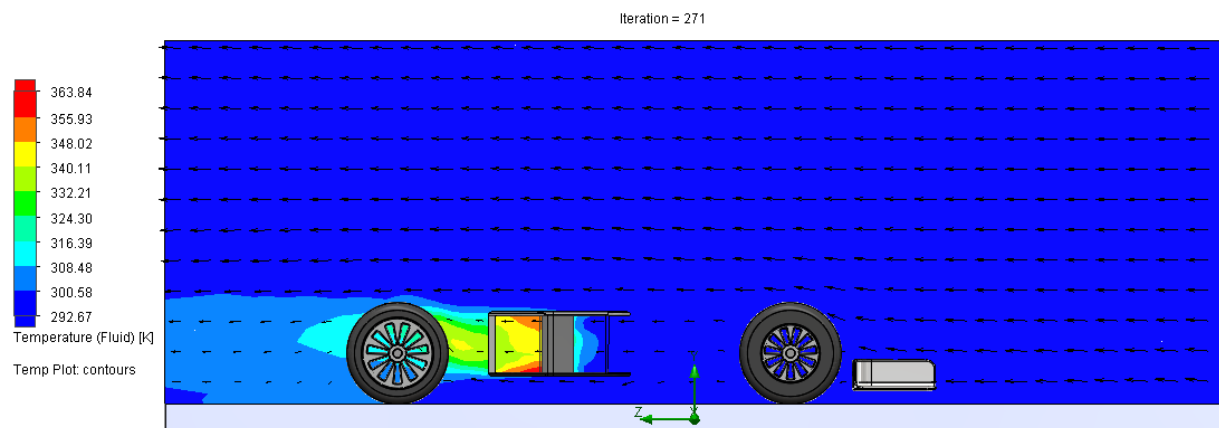
(b)



(c)

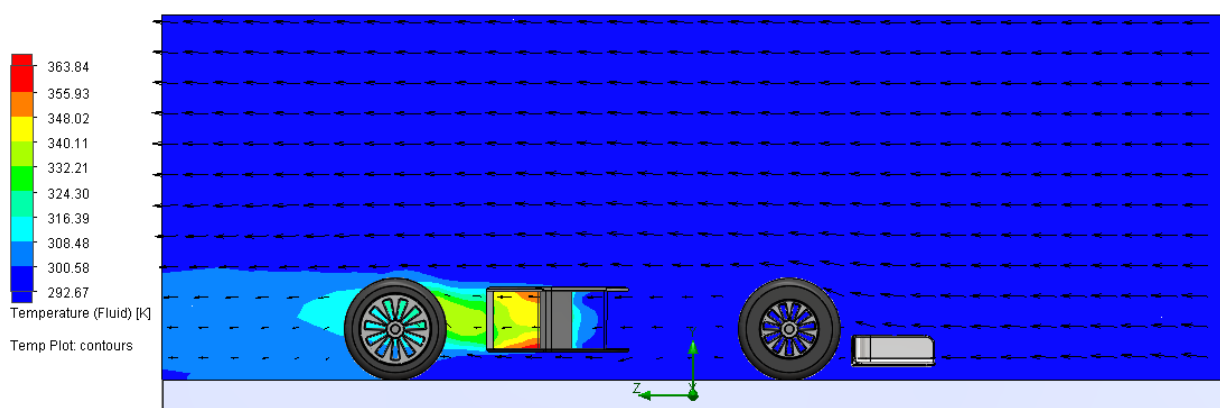


(d)



(e)

Iteration = 210

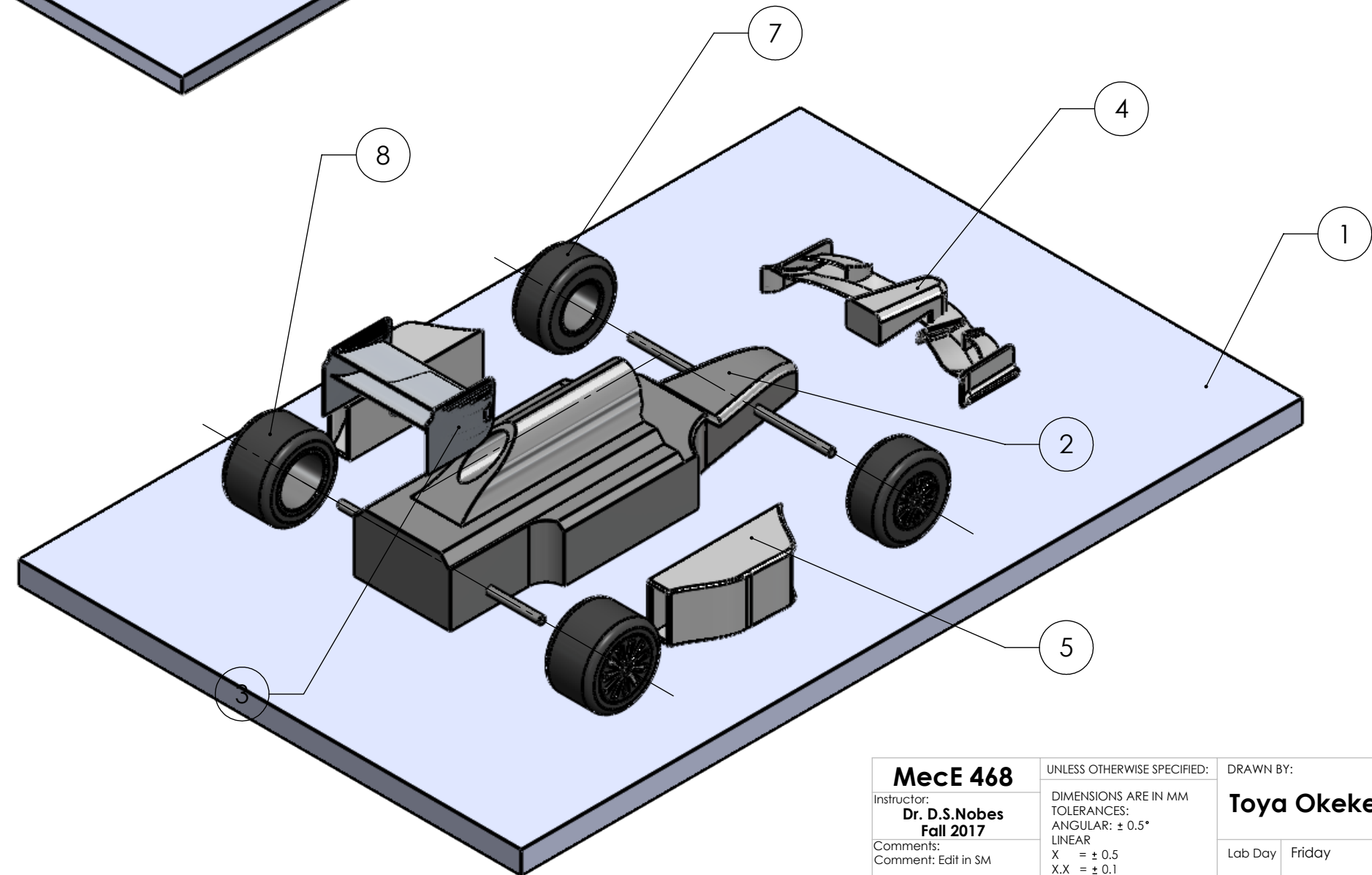
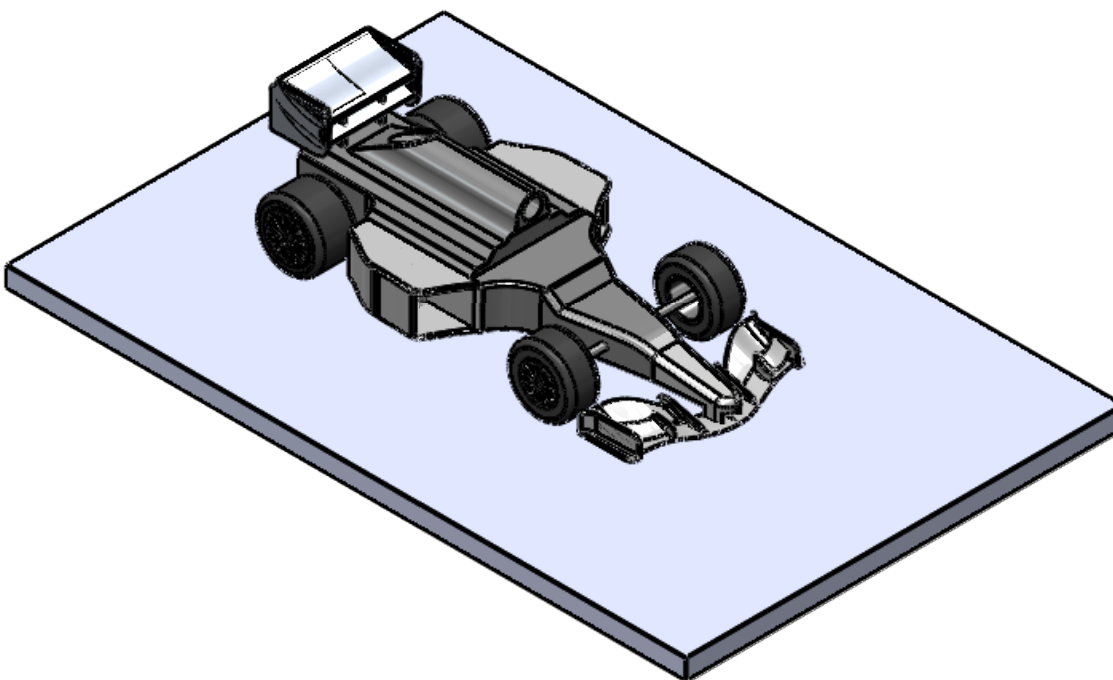


(f)

Figure F 19 Temperature plots for the vehicle moving on the road at (a) 50 km/h, (b) 100 km/h, (c) 150 km/h, (d) 200 km/h, (e) 250 km/h and (f) 300 km/h

8.7 Appendix G: Engineering Drawings

Following are the engineering drawings for the Formula 1 car designed by team 5.



ITEM NO.	PART NUMBER	Material	QTY.
1	road	Material <not specified>	1
2	Team_5_Car	Material <not specified>	1
3	P5_Iteration_3_Airfoil	HM Carbon	1
4	DI3_Assembly_2	60215.51	1
5	Simple Assembly.iteration13final	91986.28	1
6	Simple Assembly.iteration13final	91986.28	1
7	FrontWheelAssy	94603.40	2
8	RearWheelAssembly	131794.90	2

MecE 468

Instructor:
Dr. D.S.Nobes
Fall 2017

Comments:
Comment: Edit in SM

MATERIAL:
8566903.59

FILE NAME:
car_full_assembly

UNLESS OTHERWISE SPECIFIED:
DIMENSIONS ARE IN MM

TOLERANCES:
ANGULAR: $\pm 0.5^\circ$

LINEAR
 $X = \pm 0.5$

$X.X = \pm 0.1$

$X.XX = \pm 0.025$

SURFACE FINISH
 $0.6 \mu\text{m}$

DO NOT SCALE DRAWING

DRAWN BY:

Toya Okeke

Lab Day Friday

SM By Team 5

TA Initials JM

tokeke

Thursday, December 07, 2017 9:59:55 PM

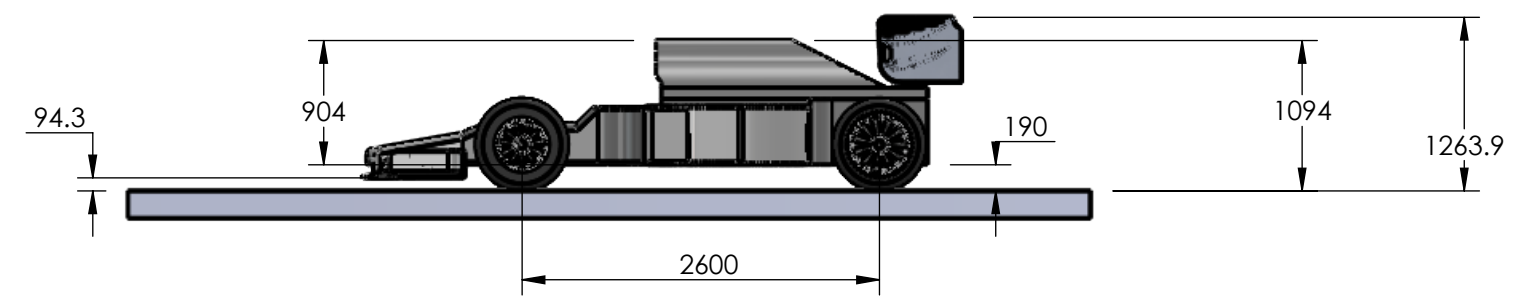
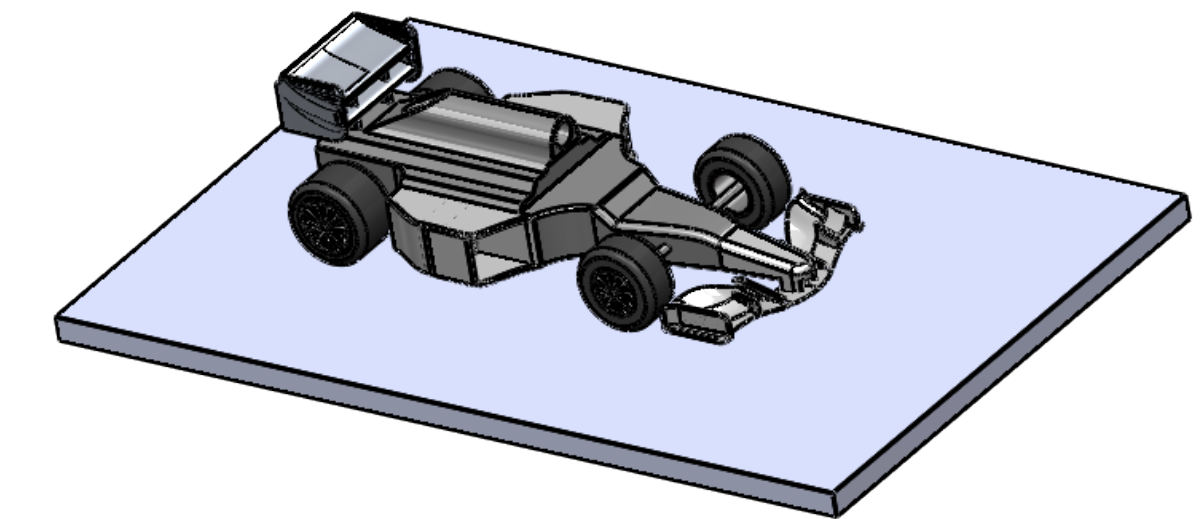
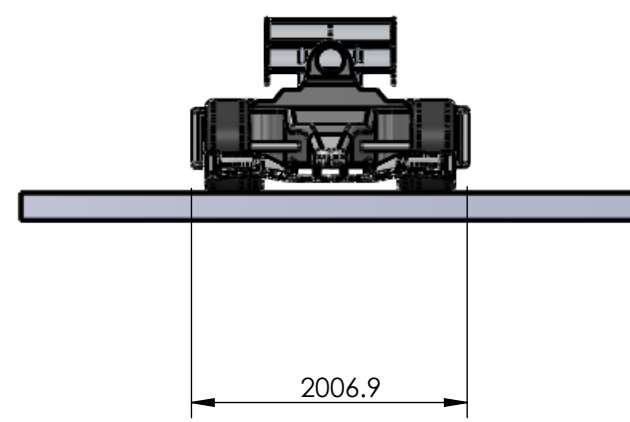
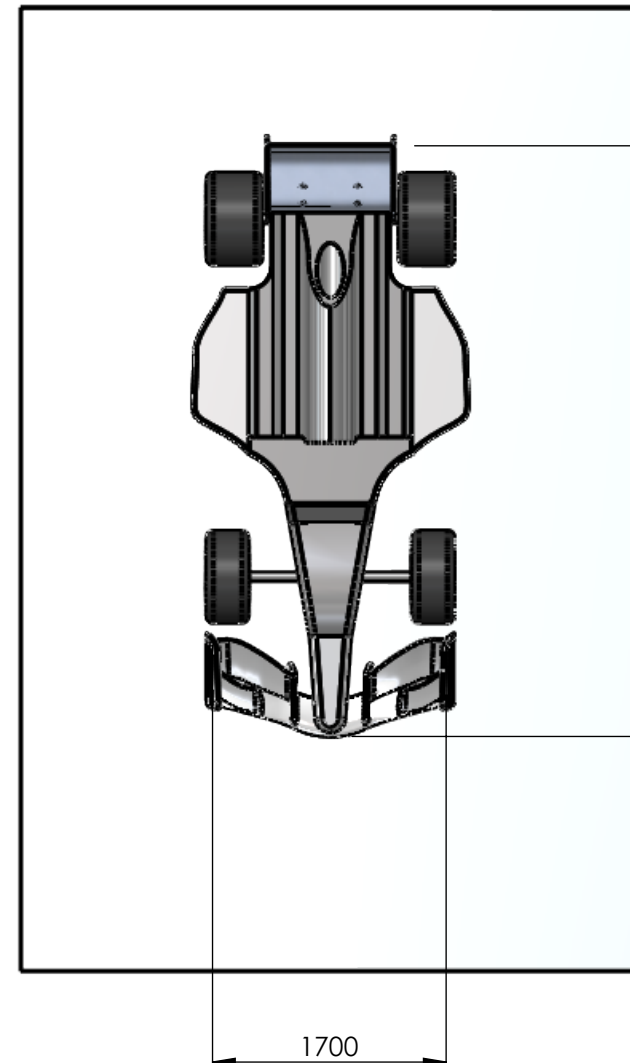
Sunday, December 03, 2017 2:56:48 PM

The Department of Mechanical Engineering
UNIVERSITY OF ALBERTA

TITLE:
Formula 1 Car Final
Design

SIZE
B Assignment Number
10 REV
1

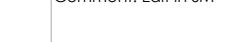
SCALE: 1:35 Mass: 8566903.59 SHEET 1 OF 3



MecE 468

Instructor:
Dr. D.S.Nobes
Fall 2017

Comments:
Comment: Edit in SM



DO NOT SCALE DRAWING

MATERIAL:
8566903.59

FILE NAME:
car_full_assembly

UNLESS OTHERWISE SPECIFIED:
DIMENSIONS ARE IN MM
TOLERANCES:
ANGULAR: $\pm 0.5^\circ$
LINEAR
 $X = \pm 0.5$
 $X.X = \pm 0.1$
 $X.XX = \pm 0.025$

SURFACE FINISH
 $0.6 \mu\text{m}$

DO NOT SCALE DRAWING

tokeke

Thursday, December 07, 2017 9:59:55 PM

Sunday, December 03, 2017 2:56:48 PM

DRAWN BY:
Toya Okeke

Lab Day Friday

SM By **Team 5**

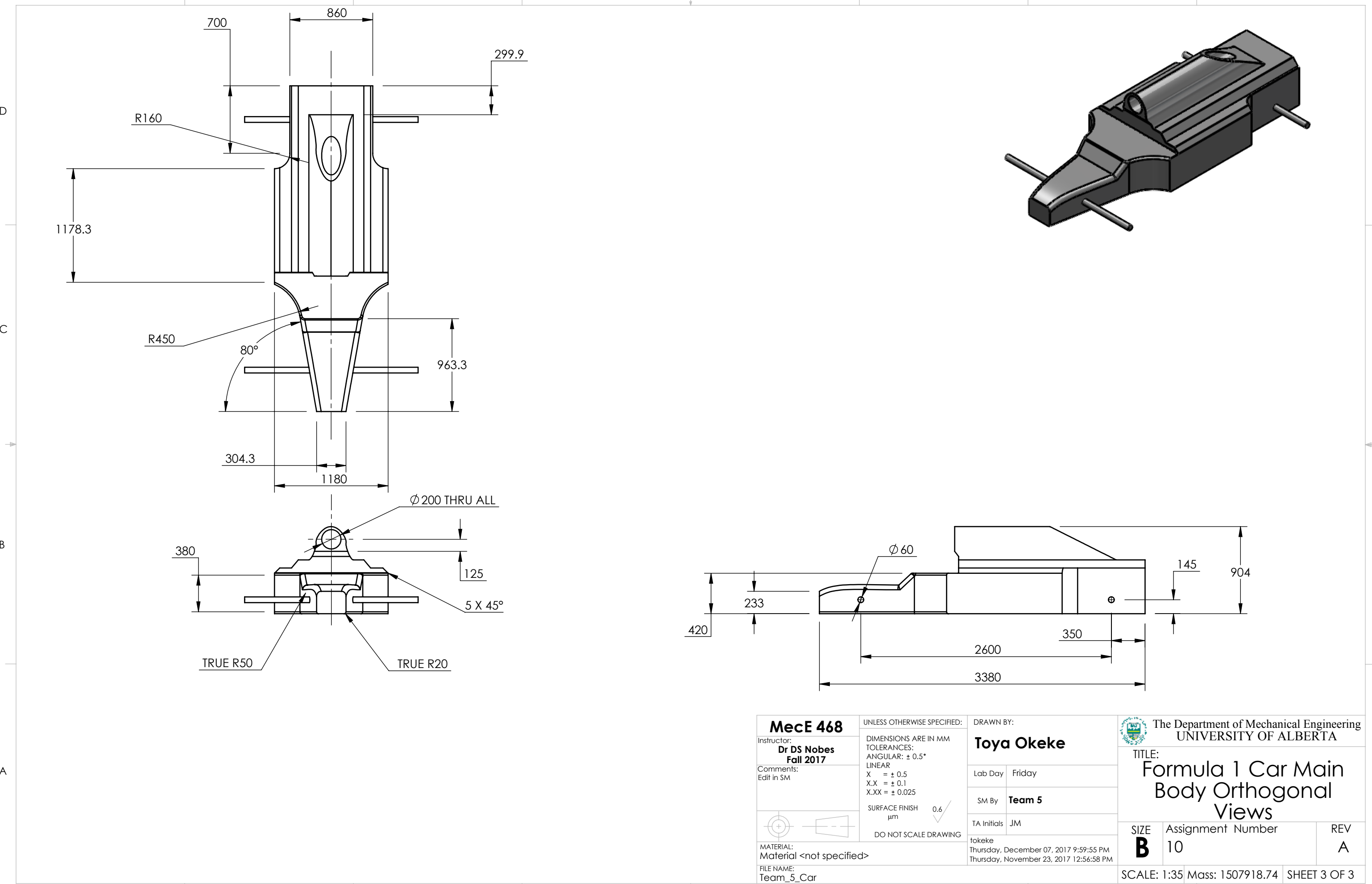
TA Initials JM

The Department of Mechanical Engineering
UNIVERSITY OF ALBERTA

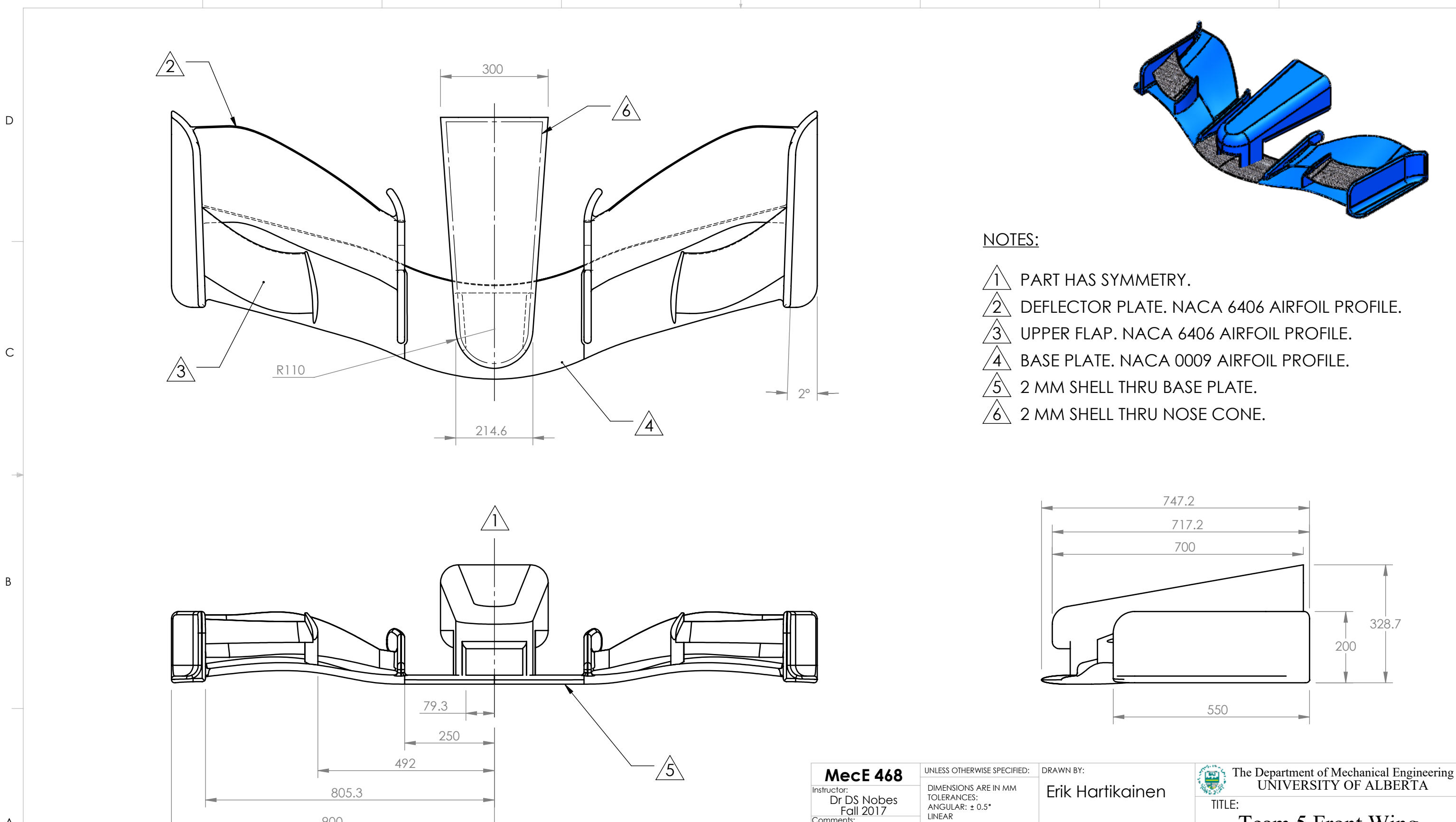
TITLE:
Formula 1 Car Final Design

SIZE **B** Assignment Number **10** **REV** **1**

SCALE: 1:55 Mass: 8566903.59 SHEET 2 OF 3

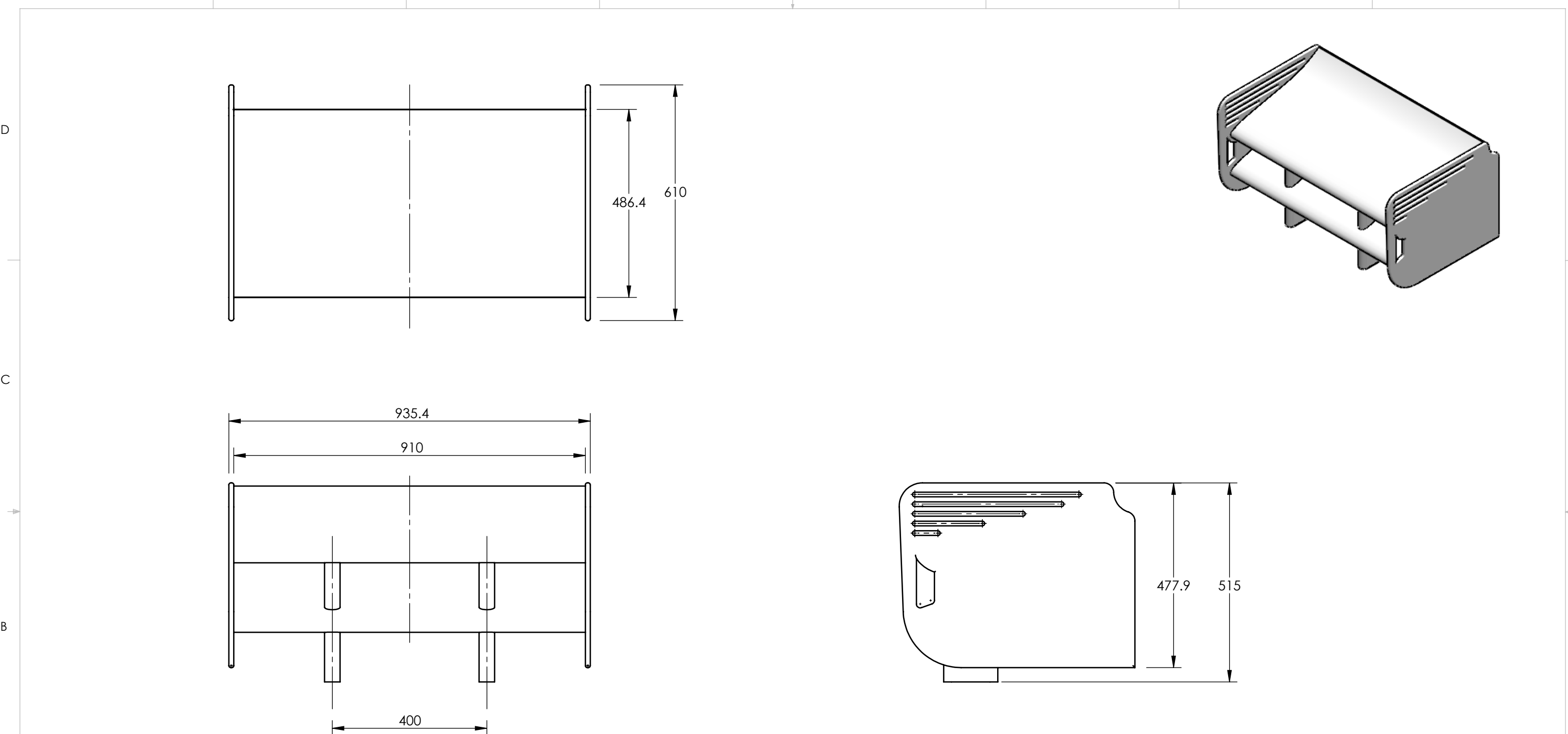


8 7 6 5 4 3 2 1



MecE 468	UNLESS OTHERWISE SPECIFIED: DIMENSIONS ARE IN MM TOLERANCES: ANGULAR: $\pm 0.5^\circ$ LINEAR $X = \pm 0.5$ $X.X = \pm 0.1$ $X.XX = \pm 0.025$	DRAWN BY: Erik Hartikainen
Instructor: Dr DS Nobes Fall 2017	SURFACE FINISH $0.6 \mu\text{m}$	Student # 1367902
Comments: Aero Configuration	DO NOT SCALE DRAWING	Lab Day Friday
		SM By Erik Hartikainen
		TA Initials J.M.
	FILE NAME: DI3_Assembly_2	December 7, 2017 10:15:59 PM December 3, 2017 8:02:40 PM
B	Assignment Number Final Project	REV B
SCALE: 1:10	Mass: 40774.72	SHEET 1 OF 1

8 7 6 5 4 3 2 1

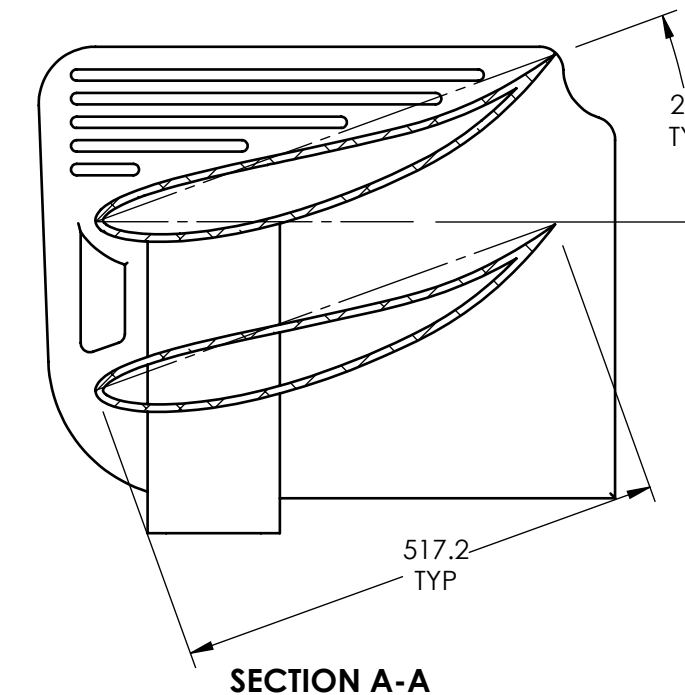
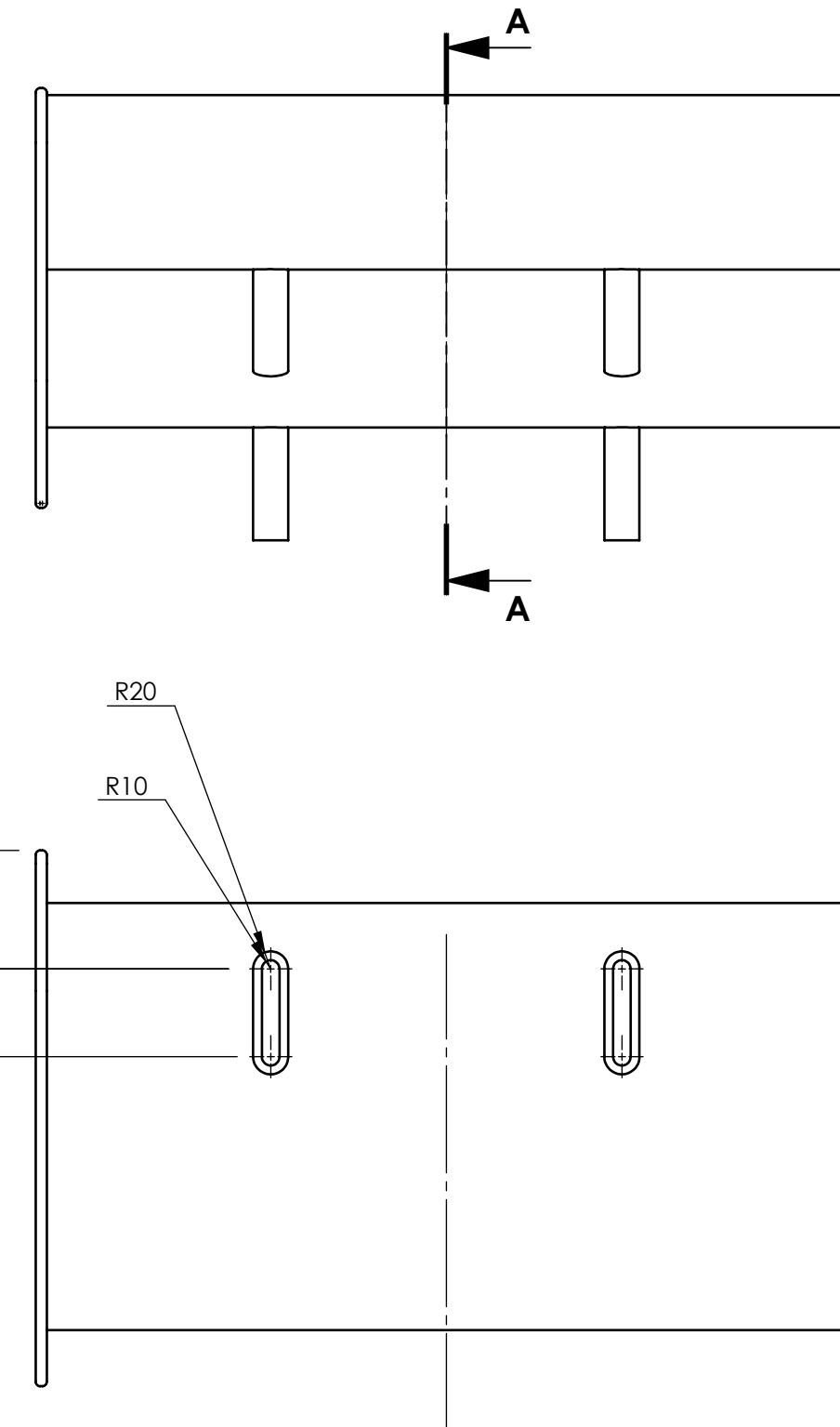


MecE 468		UNLESS OTHERWISE SPECIFIED: DIMENSIONS ARE IN MM TOLERANCES: ANGULAR: $\pm 0.5^\circ$ LINEAR $X = \pm 0.5$ $X.X = \pm 0.1$ $X.XX = \pm 0.025$	DRAWN BY: Melissa Gomez
Instructor: Dr DS Nobes Fall 2017	Comments: Edit in SM	Student # 1395350, 1381896	
		Lab Day ALL	
		SM By Anthony Tang and Melissa Gomez	
		TA Initials Jason Michaud	
FILE NAME: P5_Iteration_3_Airfoil			
DO NOT SCALE DRAWING		SURFACE FINISH $0.6 \mu\text{m}$	
MATERIAL: HM Carbon			
DATE: December 7, 2017 11:28:01 AM			
REV: A			
SIZE B		Assignment Number Final Project	
SCALE: 1:10		Mass: 62010.21	
SHEET 1 OF 2			

8 7 6 5 4 3 2 1

D

D



C

C

B

B

A

A

MecE 468

Instructor:
Dr DS Nobes
Fall 2017

Comments:
Edit in SM



MATERIAL:
HM Carbon

FILE NAME:
P5_Iteration_3_Airfoil

UNLESS OTHERWISE SPECIFIED:

DIMENSIONS ARE IN MM

TOLERANCES:

ANGULAR: $\pm 0.5^\circ$

LINEAR

X = ± 0.5

X.X = ± 0.1

X.XX = ± 0.025

SURFACE FINISH
 $0.6 \mu\text{m}$

DO NOT SCALE DRAWING

DRAWN BY:

Mellissa Gomez

Student # 1395350, 1381896

Lab Day ALL

SM By Anthony Tang and Mellissa Gomez

TA Initials Jason Michaud

December 7, 2017 11:28:01 AM
November 25, 2017 5:17:59 PM

The Department of Mechanical Engineering
UNIVERSITY OF ALBERTA

TITLE:
**Group 5: Rear Wing
Inner Dimensions**

SIZE **B** Assignment Number
Final Project

REV
A

SCALE: 1:8 Mass: 62010.21 SHEET 2 OF 2

8 7 6 5 4 3 2 1

D

D

C

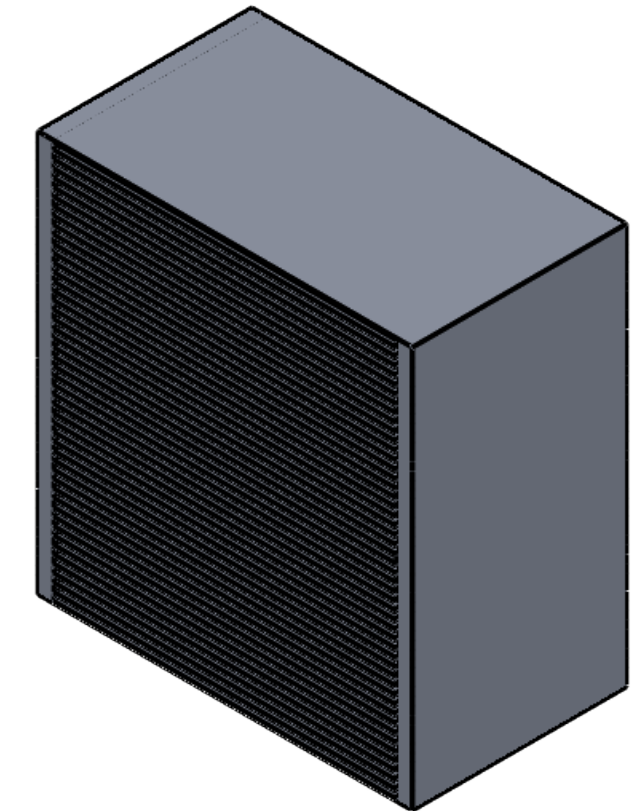
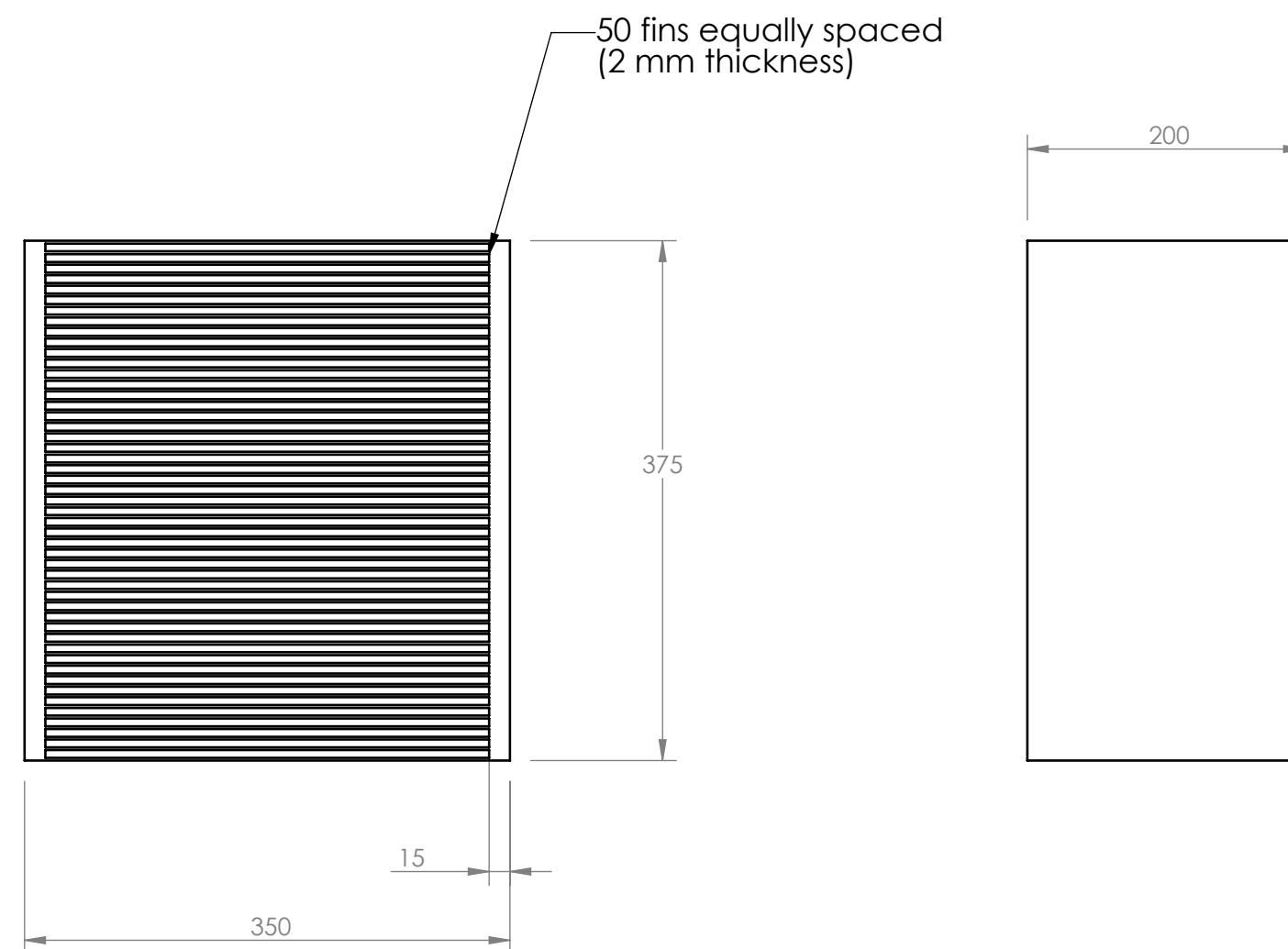
C

B

B

A

A



MecE 468	UNLESS OTHERWISE SPECIFIED:	DRAWN BY:
Instructor: Dr DS Nobes Fall 2014	DIMENSIONS ARE IN MM TOLERANCES: ANGULAR: $\pm 0.5^\circ$ LINEAR $X = \pm 0.5$ $X.X = \pm 0.1$ $X.XX = \pm 0.025$	Daniel Guenter
Comments: Edit in SM	SURFACE FINISH $0.6 \mu\text{m}$	Student # 1392989
	DO NOT SCALE DRAWING	Lab Day ALL
		SM By Daniel Guenter
		TA Initials JM
		December 8, 2017 11:14:25 AM
		November 24, 2017 2:46:38 PM
MATERIAL: 1350 Alloy	FILE NAME: Radiator final	SIZE B Assignment Number Final Project REV A
		SCALE: 1:5 Mass: 23355.00 SHEET 1 OF 1

